HEAT TRANSFER PHENOMENA IN FLOW THROUGH PACKED BEDS

T.A. Hoogenboezem

Dissertation submitted in partial fulfilment of the requirements for the degree Magister in Mechanical Engineering at the North-West University.

Promoter: Prof. P.G. Rousseau

ABSTRACT

Title	:	Heat transfer phenomena in flow through packed beds.
Author	:	T.A. Hoogenboezem.
Promoter	:	Prof. P.G. Rousseau.
School	:	Mechanical Engineering, North-West University Potchefstroom.
Degree	:	Magister in Mechanical Engineering

In order to simulate the thermal-fluid performance of a pebble bed reactor such as the PBMR, heat transfer phenomena in packed beds must be characterized. In the pseudo-heterogeneous simulation approach that is often employed, the bed is not modeled as a single lumped entity but rather is discretized into control volumes, each with a given homogeneous porosity. Therefore, the Nusselt number characteristics for pebble-to-fluid heat transfer must be investigated for homogeneous porosity packed beds.

The purpose of this study is to measure the heat transfer coefficient (Nusselt number) for pebble-to-fluid convection heat transfer for a given set of discrete homogeneous porosities and then compare it with existing correlations.

A literature study was conducted and it was found that several heat transfer phenomena exist in a packed bed and that in order to obtain useful results it is necessary to isolate convective heat transfer from conduction and radiation heat transfer. Convective heat transfer for packed beds can be divided into the following two divisions, namely:

- Pebble-to-fluid heat transfer;
- Wall-to-fluid heat transfer;

In this study the heat transfer coefficient (Nusselt number) for pebble-to-fluid convection heat transfer is measured for three discrete homogeneous porosity test sections (0.36; 0.39; 0.45) that form part of the PBMR High Pressure Test Unit (HPTU). As part of the experimental procedure the standard uncertainty due to the instrument inaccuracies were determined. Data from the physical tests was systematically processed to obtain results of Nusselt number as a function of Reynolds number. From the processed data the relevant non-dimensional

parameters could be plotted along with the standard uncertainty in each data point. Repeatability of the data as well as the comparison of the data with correlations from the literature survey is also done and graphically illustrated.

From the results it can be concluded that the HPTU test facility provides good quality results with high repeatability and relatively low uncertainty. The maximum standard uncertainty of 10.88% implies that the data measured on the HPTU is reliable. However, significant differences were found in the values measured for the homogeneous porosity test sections versus that of randomly packed beds that were employed in studies by other authors.

UITTREKSEL

Titel	:	Hitte oordrag verskynsel in vloei deur gepakte beddens.
Outeur	:	T.A. Hoogenboezem.
Promotor	:	Prof. P.G. Rousseau.
Skool	:	Meganiese Ingenieurswese, Noordwes Universiteit Potchefstroom.
Graad:	:	Meestersgraad in Meganiese Ingenieurswese.

Ten einde die termo-vloei verskynsels in reaktor modelle soos die van die PBMR te simuleer is dit nodig om die hitte-oordrag verskynsels in gepakte beddens te karakteriseer. In pseudo-heterogene simulasie modelle, wat dikwels gebruik word, word die bed nie as 'n geheel gevorm nie maar eerder opgedeel in kontrole volumes, elk met 'n homogene porositeit. Dit is dus nodig om die Nusselt getal vir konveksie hitte-oordrag in gepakte beddens vir homogene porositeit beddens te ondersoek

Hierdie studie het ten doel om die hitte-oordrag koëffisiënt (Nusselt getal) van die partikel-vloei konveksie hitte-oordrag vir 'n gegewe diskrete homogene porositeit te meet en daarna met bestaande korrelasies te vergelyk.

'n Literatuurstudie het getoon dat verskeie hitte-oordrag verskynsels in 'n gepakte bed bestaan en dat sinvolle resultate vereis dat konveksie hitte-oordrag van konduksie en radiasie hitte-oordrag isoleer word. Konveksie hitte-oordrag in 'n gepakte bed kan in die volgende afdelings verdeel word, naamlik:

- Partikel-vloeier hitte-oordrag,
- Muur-vloeier hitte-oordrag.

Drie onafhanklike homogene porositeit toets seksies (0.36; 0.39; 0.45), wat deel van die PBMR High Pressure Test Unit (HPTU) uitmaak, is gebruik om die hitte-oordrag koëffisiënt vir partikel-vloeier konveksie hitte-oordrag in die homogene porositeit gepakte beddens te meet. As deel van die navorsingsmetode is die standaard afwyking in gemete resultate wat deur onakkuraatheid van instrumentasie veroorsaak word, ondersoek. Rou data is sistematies verwerk om resultate van Nusselt getal in terme van Reynolds getal te verkry. Die relevante

nie-dimensionele getalle is geplot met die standaard onsekerheid in elke punt. Herhaalbaarheid van die data asook die vergelyking van die data met bestaande korrelasies, soos in die literatuurstudie, is gedoen en word grafies getoon.

Gevolglik kan vanuit die resultate afgelei word dat die HPTU aanleg kwaliteit data oplewer Hierdie data is hoogs herhaalbaar met relatiewe lae onsekerheid. Die maksimum onsekerheid van 10.88% toon dat die data gemeet op die HPTU betroubaar is. Tog toon studies deur ander outeurs noemenswaardige verskille tussen gemete waardes in die homogene porositeit toets seksies en waardes vir ewekansig gepakte beddens.

ACKNOWLEDGEMENTS

I would like to use this opportunity to express my gratitude towards Professor Pieter Rousseau for his time invested in order to lead me throughout this study. Through his example I grew as academic as well as person. Furthermore I would like to thank Professor Jat du Toit, my co-study leader, which also contributed a lot throughout this study.

To all my friends, family and colleagues at M-Tech Industrial for the encouragement that kept me going when things went tough.

Soli deo Gloria.

TABLE OF CONTENTS

LIST OF FIGURES

LIST OF TABLES

NOMENCLATURE

A	Area	[m^2]
Bi	Biot number	[-]
C	Discharge coefficient	[-]
D	Diameter	[m]
d_p	Particle diameter	[m]
F_{ges}	Volume force	[N/m^3]
g	Gravity constant	[m/s^2]
Gr	Grashof number = $gd^3\Delta\rho/\rho\nu^2$	[-]
h	Height	[m]
L_c	Contact length	[m]
$\dot{m}$	Mass flow	[kg/s]
Nu	Nusselt number = $\alpha\, d_p/\lambda$	[-]
P	Perimeter	[m]
p	Pressure	[Pa]
Pe	Péclet number	[-]
Pr	Prandtl number	[-]
q	Heat transfer	[kW]
R	Radius	[m]
r	Radial coordinate	[m]
Ra	Rayleigh number = Gr/Pr	[-]
Re	Reynolds number	[-]
Sc	Schmidt number	[-]
Sh	Sherwood number	[-]
T	Temperature	[K]
t	Time	[Second]
V	Volume	[m^3]
v	Velocity	[m/s]
x	Measured value	[-]
z	Axial coordinate	[m]

Greek symbols

α	Heat transfer coefficient	[W/m^{2}K]
β	Diameter ratio = d_{or}/D_{OrPipe}	[-]
ε	Porosity/Expansion coefficient	[-]
η	Viscosity	[kg/s·m]
θ	Angular coordinate	[rad]
ρ	Density	[kg/m^3]
λ	Thermal conductivity	[W/m·K]

Subscripts

$Average_{1min}$	running average calculated during the previous minute of the logged Data
$Average_{5min}$	running average calculated during the previous five minutes of the logged data
crit	Critical
cyl	Cylinder
eff	Effective
elec	Electrical
f	Fluid
fin	Fin
h	Hydraulic
∞	Infinity
l	Laminar
max	Maximum
min	Minimum
Or	Orifice
OrPipe	Orofice pipe
p	Particle
r	Radial direction
rad	Radiation
s	Surface
TC	Thermocouple

TS	Test Section
t	Turbulent
unc	Uncertainty
w	Wall
wet	Wetted
z	Axial direction

1 INTRODUCTION

1.1 Background

Today, alternative means of energy is continuously investigated. The future availability of fossil fuels combined with the polluting effect of burning carbon-based fuels has sharply increased the need for an alternative approach to produce energy. Furthermore, the need for the construction of new power plants is emphasised by South Africa's electricity demand which will soon exceed Eskom's capacity to deliver electricity. At the end of the current power plant's design-life in 2025 an additional 20 000MW of electricity will be needed. The Pebble Bed Modular Reactor (PBMR) is one of the options for providing in this need.

The PBMR has been in development by Eskom and partners in South Africa since 1994. The PBMR falls in the category of a High Temperature Reactor (HTR), with a closed-cycle, gas turbine power conversion system. The plant comprises of a reactor pressure vessel (RPV) and a power conversion unit. The RPV is lined on the inside with a thick graphite wall. This wall serves as an outer reflector and passive heat transfer medium. The fuel section is annular with a central graphite column which functions as an additional nuclear reflector. About 450,000 fuel spheres (approximately the size of a tennis ball) are assembled in the reactor. Each sphere consists of low enriched uranium triple-coated isotropic (TRISO) particles contained in a graphite matrix.

To remove the heat generated by the fuel, helium gas at an inlet temperature of 540°C and pressure of 9MPa is passed through the pebble bed and leaves the reactor at 900°C. The hot gas is expanded through a turbine and leaves the turbine at approximately 500°C and 2.6MPa. The gas is then cooled, recompressed through a compressor and reheated. The cycle is restarted by returning to the reactor. A generator is connected to the turbine through a speed-reduction gearbox.

The safety of nuclear plants has been debated thoroughly in the past, and strict safety standards are indorsed by governments. Such standards are compiled by agencies such as the Nuclear Safety Standards Commission (KTA) or in South Africa, the National Nuclear Regulator (NNR). Nuclear accidents are principally driven by surplus heat known as decay

heat, caused by radioactive decay of the fission products. In the PBMR the billions of independent fuel particles have a resistance to high temperature due to the physics of the fuel. However, this creates an inherent ceiling for temperature since indications are that in order to ensure the integrity of the TRISO-coated particles, the maximum fuel temperature must be maintained below $1600°C$ (Koster *et al.*, 2002:2).

Helium is chemically and radiologically inert. This implies that it is impossible for the cooling gas itself to become radioactive, although it may transport entrained radioactive aerosol particles. Furthermore, as long as air does not enter the high temperature reactor core, oxidation and chemical reactions should not occur.

Different heat transfer phenomena are relevant to a packed bed. It is necessary to isolate each independently. The PBMR consists of four spatially decomposed heat and mass transfer related systems. All these heat transfer mechanisms are via conduction, convection and radiation. According to Malan *et al.* (2004:2-3) these systems consist of:

- An annular fuel section, packed with the fuel spheres. The working fluid, Helium, enters the top of the bed, flows through the bed of spheres and exits at the bottom.
- Gas plenums at the top and bottom of the reactor.
- Central, side, top and bottom reflectors enclose the annular fuel section. The outer reflector contains control-rods as well as cooling channels.
- Core enclosure layers serve as insulation, structural integrity and safety. The enclosure consists of a stainless steel barrel as well as ceramic and concrete layers. Cooling pipes are situated within the outer concrete layer in which cold water is circulated.

The current study focuses on heat transfer in the annular fuel section of the PBMR reactor core. The annular fuel section system involves four non-fission types of heat transfer namely:

- Heat conduction through contact points amid pebbles, and between the pebbles and the reflector walls inside the packed bed.
- Radiation heat transfer amongst the pebble surfaces and between the pebble and reflector surfaces due to differences in temperature of radiating surfaces.
- Convection over the reflector and pebble walls inside the packed bed due to the flow of the working fluid through the packed bed.

- Fluid heat convection due to the flow dispersion between the pebbles.

With the different types of heat transfer in the annular fuel section recognized, the relevant heat transfer phenomena for this study can be identified. This study will investigate the following heat transfer phenomena:

- Convection heat transfer over the reflector wall due to the flow of the working fluid through the packed bed.
- Convection heat transfer over the pebble wall due to the flow of the working fluid through the packed bed.

For the investigation of fluid flow phenomena in packed beds a test facility was designed and developed by M-Tech Industrial (Pty) Ltd. This test facility, the High Pressure Test Unit (HPTU), was made available to the author for the purpose of this study. The HPTU was designed in such a way that different Test Sections can be installed for different flow phenomena investigations.

1.2 Purpose of this study

Heat transfer in the PBMR must be calculated for design purposes and safety case demonstrations for regulatory requirements. For the calculation of heat transfer, Greyvenstein and Van Antwerpen, (2004:3-4) and Du Toit *et al.*, (2003:3) presented a new control volume based network scheme for heat transfer in the PBMR. The discretized model allows for detail effects such as conduction, convection and radiation. In order to simulate the thermal fluid performance of the reactor in models such as these, the heat transfer phenomena in the core of the PBMR reactor must be characterized. In the past heat transfer correlations for packed beds have been investigated thoroughly. In most cases these correlations have been determined for specific bed geometries and fluid characteristics, such as cylindrical- and annular beds and different ranges of Reynolds numbers. The applicability and accuracy of these correlations are uncertain.

To clarify some terms commonly used to describe pebble bed modeling approaches, the following points need mentioning (Van Antwerpen and Greyvenstein, 2006:98):

- In a homogeneous or pseudo-homogeneous approach, particle and gas temperatures are combined in a single energy equation. Obviously, this approach is not applicable where there is a large temperature difference between the particles and the gas.
- In a pseudo-heterogeneous approach, separate energy equations are used for gas and particles. For a sphere-packed bed, this is typically done with representative spheres for control volumes larger than a single sphere.
- In a completely heterogeneous modeling approach such as used in Lattice-Boltzmann simulation or Direct Numerical Simulation (DNS), particles are treated explicitly with separate energy equations for gas and solids. Three-dimensional geometry is used.

Since the pseudo heterogeneous approach employed in these simulations do not lump the bed as a whole but rather discretize the bed into control volumes, each with a homogeneous porosity, the Nusselt number correlations for pebble-to-fluid heat transfer must be investigated for homogeneous porosity packed beds.

Thus, the purpose of this study is to measure the heat transfer coefficient (Nusselt number) for pebble-to-fluid convection heat transfer for given discrete homogeneous porosities and then compare it with existing correlations. Test Sections must be homogeneous on a macroscopic level as a microscopic homogenous porosity Test Section will be impossible to achieve. Furthermore in a macroscopic homogeneous porosity Test Section the porosity is homogeneous up to the wall.

2 LITERATURE SURVEY

2.1 Introduction

In order to fully grasp the convective heat transfer phenomena in a packed bed with specific reference to the PBMR, it is necessary to understand the key factors that have an impact on the evaluation of the Nusselt number for a packed bed. These factors are the geometry and the Reynolds number in the packed bed. Many geometrical effects exist in packed beds, but the porosity profile is the most important effect of all due to its influence on the nature of the flow field. The velocity in the bed is an important determinant in concluding the Reynolds number.

Heat transfer between the packed bed and the working fluid can be categorized as follows:

- Heat transfer between the pebbles and the fluid within the packed bed.
- Heat transfer between the bed wall, or reflector blocks as it is known in the PBMR, and the fluid.

The following sections concentrate on the porosity profiles and the bed velocity as well as the pebble-to-fluid and wall-to-fluid convective heat transfer.

2.2 Porosity profiles

Porosity and velocity profiles form the foundation of all models involving heat and mass transfer in packed beds. Porosity, ε_r, also known as voidage or void fraction, can be defined as the ratio of the void volume through which a fluid can pass to the total volume which includes the volume of the obstructions in the flow path. Marivoet *et al.*, (1974:1836) gave a summary of the porosity profile in a packed bed:

- The porosity is equal to one at the wall and decreases to about 0.4 far from the wall. The wall effect is caused by the particles' point contact with the wall.
- The transition in the wall porosity towards the constant inner bed porosity is uneven: the porosity profiles display damped oscillations around the mean value. The oscillation period closely corresponds to one particle diameter; these oscillations are

measurable for four to five particle diameters from the wall or any obstacle placed in the bed in the case of uni-sized particles. Goodling *et al.*, (1983:29) confirmed this but also reported that for the case of two-sized particles the bulk value is reached after about two to three particle diameters.

The mean radial porosity profile for a cylindrical bed is given by Vortmeyer and Schuster (1983: 1693) by the following exponential relation:

$$\varepsilon_r = \varepsilon_\infty \left[1 + C \cdot e^{\left(1-2\frac{R-r}{d_p}\right)} \right] \tag{2-1}$$

The constant C can be determined with the boundary condition of $\varepsilon_r=1$ for $r = R$, where ε_r is the porosity at the radial position r, R is the outer radius of the bed and d_p the sphere diameter. ε_∞ is the bulk porosity (i.e. the porosity of the majority of the pebble bed). For a better description of damped oscillations in the near wall region as described above, Küfner and Hofmann (1990:2142) recommended the implementation of a cosine-function into Equation 2-1:

$$\varepsilon_r = \varepsilon_\infty \left[1 + C \cdot e^{\left(1+\frac{R-r}{d_p}\right)} \cdot \cos\left(\frac{R-r}{d_p} \cdot 2\pi \right) \right] \tag{2-2}$$

Winterberg and Tsotsas (1999:569) used a similar model as that of Vortmeyer and Schuster (1983: 1693) for the radial porosity profile with a centre column taken into account for annular packed beds:

$$\varepsilon_r = \begin{cases} \varepsilon_\infty \left[1 + 1.36 \cdot e^{\left(-5.0\frac{r-r_{cyl}}{d_p}\right)} \right] & for\ r_{cyl} \le r \le \dfrac{R+r_{cyl}}{2} \\ \varepsilon_\infty \left[1 + 1.36 \cdot e^{\left(-5.0\frac{R-r}{d_p}\right)} \right] & for\ \dfrac{R+r_{cyl}}{2} \le r \le R. \end{cases} \tag{2-3}$$

with r_{cyl} the centre column radius.

2.3 Local velocity

Borkink and Westerterp (1993:863) noted that when convective heat transfer in a packed bed is investigated, one should understand the local bed velocity, also known as the interstitial velocity. The local velocity influences the calculated rate of heat transfer for packed beds through the axial convection term in the heat balance. In other words, the local velocity influences the Nusselt number through the Reynolds number and thus the convection heat transfer in the packed bed. Equation 2-4 correlates the local velocity v, with the porosity and the mean velocity (also referred to as apparent or superficial velocity), v_0, in the empty tube.

$$v = \frac{v_0}{\varepsilon} \tag{2-4}$$

Thus the relation between the Reynolds number based on the local velocity, Re, and the Reynolds number based on the mean velocity, Re_0, is given by Achenbach (1995:18) as:

$$\mathrm{Re} = \frac{d_h v \rho_f}{\mu_f} = \frac{1}{1-\varepsilon}\mathrm{Re}_0 \tag{2-5}$$

where Re_0 is calculated using the particle diameter, d_p in Equation 2-6.

$$\mathrm{Re}_0 = \frac{d_p v_0 \rho_f}{\mu_f} \tag{2-6}$$

d_h is the hydraulic diameter of the bed, ρ_f and η_f the fluid density and viscosity respectively. Many authors report their work done in terms of either Re-range or Re_0-range.

The hydraulic diameter can be calculated on a volumetric basis as follows:

$$d_h = \frac{4A}{P_{wet}} \tag{2-7}$$

Where the area, A, can be taken as the voidage volume:

$$A = \varepsilon \frac{\pi D^2}{4} \cdot h \tag{2-8}$$

and the wetted perimeter, P_{wet} as:

$$P_{wet} = \left(\frac{\pi D^2}{4} \cdot h \right) (1-\varepsilon) \left(\frac{\pi d_p^2}{\pi d_p^3 / 6} \right) \tag{2-9}$$

thus

$$d_h = \frac{2}{3} \frac{\varepsilon}{1-\varepsilon} d_p \tag{2-10}$$

Note that Achenbach (1995:18) does not include the value of $^2/_3$ in Equation 2-5, but is generally implicitly included in the constants in the relevant correlations.

The Nusselt number can be defined as a function of the Reynolds number and the Prandtl number, Equation 2-11.

$$Nu = f(\mathrm{Re}, \mathrm{Pr}) \tag{2-11}$$

The average local velocity can also be defined as:

$$v = \frac{\int_0^{2\pi} v_i \, d\theta}{2\pi} \tag{2-12}$$

and is usually measured with circular hot wire anemometers. Marivoet *et al.*, (1974:1837) noted that the local velocity is independent on θ in cylindrical beds when $r = 0$, but as r approaches R many maxima and minima velocity values are observed. This occurs as the probe passes above a void or particle. Thus the average local velocity profile $v(r)$, displays oscillations with a period approximately equal to one particle diameter. Marivoet *et al.*, (1974:1837) reported a maximum in the velocity profile at a distance of about one particle

diameter from the wall. The reason for this is because the velocity profile maxima occur in the same region as the maximum oscillating porosity where the flow would meet the least resistance.

For this reason Bey and Eigenberger (1997:1368) stated that any realistic flow model must be based on some assumptions. Generally an angular symmetry of the flow profile is assumed together with a continuous void fraction, $\varepsilon(z,r)$, in the packing. In this way a continuously distributed local velocity, $v(z,r)$, or averaged local velocity is obtained from fluid flow.

Even with the assumptions made by Bey and Eigenberger (1997:1368), this radial variation in a continuous local velocity complicates a detached evaluation of the correlation between convective heat transfer with respect to Reynolds number. An experiment with constant average local velocity will contribute to better conclusions of Nusselt number results. Equation 2-4 proves that a constant local velocity can only be obtained if the radial porosity is constant, based on the assumption that the mean velocity, v_0, is uniform at the inlet of the bed. Figure 2-1 is an attempt to illustrate the above approach.

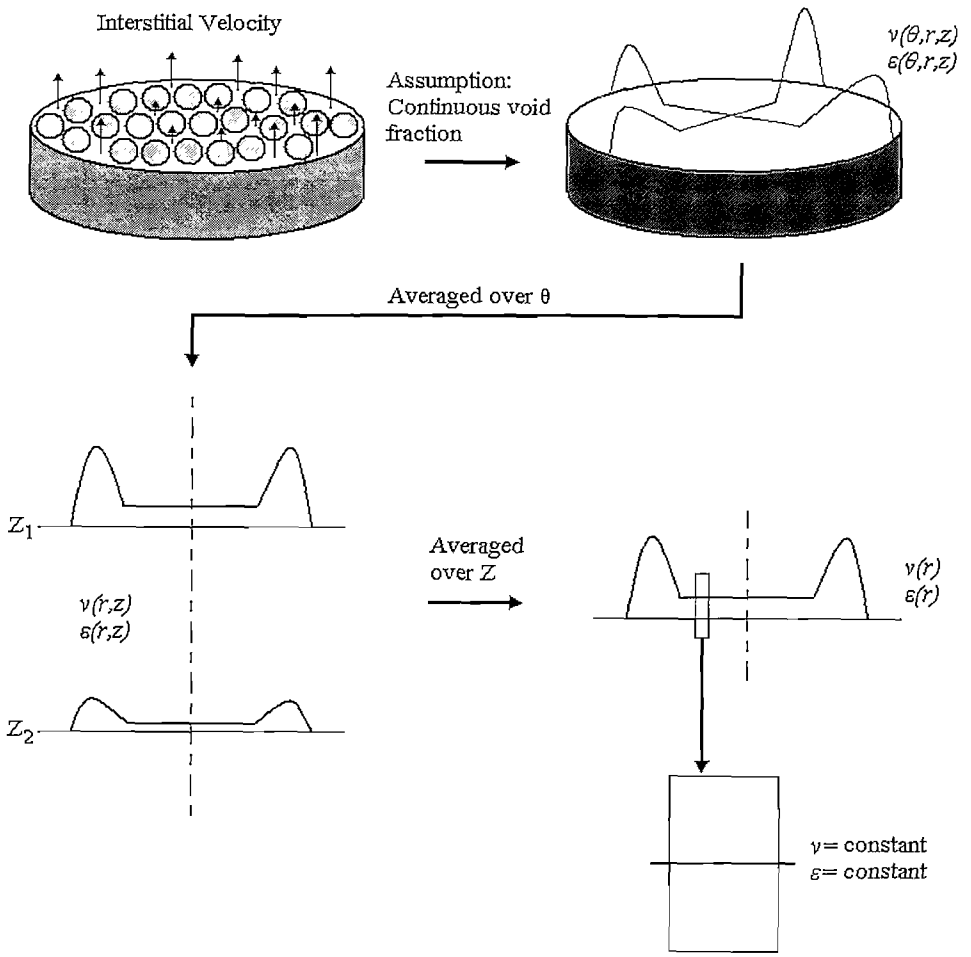

Figure 2-1: Illustration of the determination of a constant average local velocity.

2.4 Heat transfer in flow through packed beds

The heat transfer coefficient of a fluid flowing over a solid can be defined by Equation 2-13, (Romkes *et al.*, 2003:6 and Incorpera and DeWitt 2002:8). Here q is the heat input into the solid, A the heat transfer contact area, T_f the infinite or bulk fluid temperature and T_s the surface temperature of the solid.

$$\alpha = \frac{q}{A(T_f - T_s)} \tag{2-13}$$

For heat transfer calculations, dimensionless parameters such as the Nusselt-, Prandlt- and/or Reynolds numbers are used to determine fluid properties like the heat transfer coefficient. The relationship between heat transfer coefficient and the Nusselt number is given by Equation 2-14, where λ_f is the fluid conductivity.

$$Nu = \frac{\alpha d_p}{\lambda_f} \tag{2-14}$$

2.4.1 Pebble-to-fluid heat transfer

Extensive research has been done on the heat transfer between pebbles and a working fluid in a packed bed. Studies include the chilling of foodstuffs through to trickle bed reactors (Allais and Alvarez, 2000:37-47 and Boelhouwer *et al.* 2001:1181-1187). Most researchers found it difficult to conduct an accurate experimental method. Achenbach (1995:18) summarized measurement techniques applied for pebble-to-fluid heat transfer as follows:

1. Heat transfer from a single electrically heated sphere buried in an un-heated packed bed.
2. Mass transfer tests making use of the analogy between heat and mass transfer.
3. Simultaneous heat and mass transfer.
4. Regenerative heating.
5. Semi-empirical methods.

For the single heated sphere technique to be accurate, the gas mixing downstream of the particle must be nearly perfect, in other words fully developed in an axial direction with regards to turbulent flow in a packed bed. It was found in Section 2.2, that the porosity reaches the bulk porosity after four to five particle diameters from any obstacle in the bed (Marivoet *et al.*, 1974:1836). Therefore it can be concluded that the downstream mixing of the gas in an unstructured packed bed, will almost be perfect after five particle diameters from the inlet and five particle diameters before the outlet. The heating rate, the sphere wall temperature and fluid bulk temperature can easily be determined, simplifying this technique.

Allais and Alvarez (2000:41-42) and Boelhouwer *et al.*, (2001:1182) independently designed a simple, yet effective probe for the heated sphere technique, shown in Figure 2-2. A metal sphere with the same dimensions as the spheres in the bed was created. Inside the sphere was a resistance heating element and on the surface of the sphere a thermocouple was installed. This probe can then be placed in the packed bed.

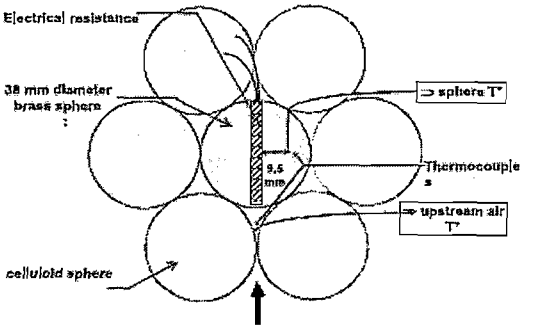

Figure 2-2: Schematic representation of probe-sphere for pebble-to-fluid heat transfer. Allais and Alvarez (2000:41).

It is important that the Biot number of the probe sphere must be as low as possible. The low Biot number ensures that the distribution of the heat conduction through the wall of the probe will be more or less isothermal. If $Bi << 1$, the resistance to conduction within the solid is much less than the resistance to convection across the fluid boundary layer (Incorpera and DeWitt, 2002:244). Hence, Equation 2-15 illustrates that with the right material selection, which is dependent of the material thermal conductivity λ, one can keep Bi as small as possible (Collier *et al.*, 2004:4615).

$$Bi = \frac{\alpha L_c}{\lambda} \tag{2-15}$$

Brass or copper can effectively be used in this manner. A further aspect to consider when implementing this technique is that radiation and heat conduction must be minimized. Highly polished surfaces will reduce the effect of radiation. However the main effect of radiation heat transfer is the difference in surface temperature between the radiating bodies since the temperature is taken to the power of four. This is an important factor that must be

incorporated in the operating ranges of an experimental facility for the measurement of heat transfer in packed beds.

Conduction through contact points of neighboring spheres can be minimized by assuring that the thermal conduction of the neighboring spheres is low in comparison with the probe-sphere. Figure 2-3 shows the effect of a copper probe-sphere when it is in contact with graphite neighboring spheres (Achenbach, 1995:20). The solid line represents the expected results while the circles illustrate the measured or total heat transfer results of Achenbach (1995:20). The difference between the expected and the measured results represents the heat conducted through the points of contact.

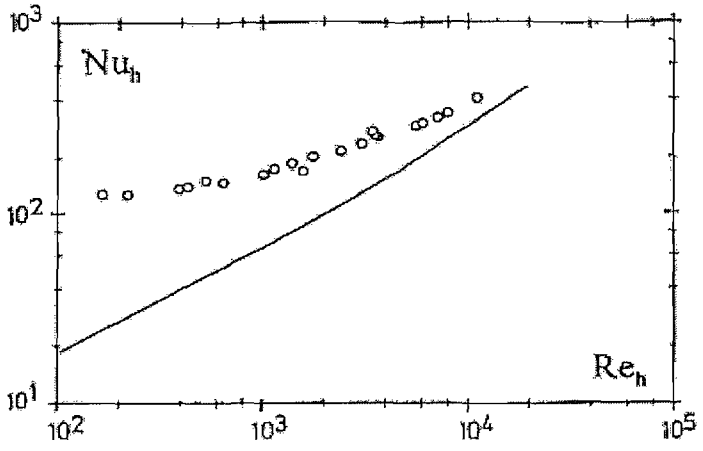

Figure 2-3: Effect of heat conduction via contact points of spheres, Achenbach (1995:20).

The effect that the radial position of the probe in the bed has on the heat transfer coefficient must also be investigated. Boelhouwer *et al.*, (2001:1185) suggests that the heat transfer is the highest at the wall and the lowest in the center of a circular bed. Boelhouwer *et al.*, (2001:1185) relates these phenomena to porosity and velocity distribution. Therefore, the elimination of the effects of porosity and velocity profiles on heat transfer is highly recommended. This can be done by ensuring a constant porosity distribution.

The mass transfer technique has a few advantages over the technique of a single heated sphere. Firstly, the effects of radiation and heat conductivity cannot occur. Given that the Grashof number can be lowered by an order of three times in comparison with the heat

transfer experiments, the effect of natural convection can be reduced. However, natural convection only plays a significant role at low Reynolds numbers.

Mass transfer experiments are preferably conducted according to the method of sublimation of naphthalene in air. The concept is to measure the weight loss of naphthalene due to sublimation in a time interval Δt. This method produces reliable results. Still, the vapor pressure of naphthalene is highly dependant on temperature. This implies that accurate surface temperatures must be taken. Achenbach (1995:18) states that an error of $1\,°C$ will result in an error of 10% in the determination of the mass transfer coefficient. However, to measure an accurate wall temperature within $\pm 1\,°C$ is not straightforward. Thus, it is challenging to obtain highly accurate results by way of the mass transfer method.

The third technique is the simultaneous heat and mass transfer method, conceptualizing that a porous sphere is saturated with a fluid that will evaporate into the working fluid throughout tests. The temperature decrease and weight loss of the sphere can be measured separately. These results can then be related to a heat transfer coefficient. A disadvantage of this technique is that difficulties arise in the exact determination of the sphere surface temperature since the temperature is also a function of the evaporation process. Another disadvantage is that this technique is a transient process with limited time for measurement. For example, if a structured bed with a constant porosity was to be used, saturating the sphere and also allowing sufficient time for the measurements will be difficult. Therefore, measurements cannot be done over an extended period of time.

The regenerative technique is based on the concept of unsteady heat transfer of a heated sphere in a packed bed through which a cooling fluid flows. When the heating and cooling of the packed bed is determined, temperature profiles can be constructed and related to a heat transfer coefficient. This technique requires a significant amount of technical and mathematical effort, which can make it an inconvenient application. This technique is also a transient process and the same difficulties arise as in the case of the simultaneous heat and mass transfer technique.

The semi-empirical technique is built on the basis of empirical relationships. This means that the pebble-to-fluid heat transfer for a sphere in a packed bed can be related to the heat transfer of a single sphere in fluid flow. This can be achieved by the use of geometrical parameters to

adjust the semi-empirical method to the experimental results. One such method was published by Gnielinski (1978) (as citied by Achenbach, 1995:19).

The method is based on the theory that the heat transfer between any body and a fluid can be related to the heat transfer between a flat plate and a fluid flowing over it. The equations for a flat plate can be made compatible by introducing a suitable length scale. In the case of spheres, the length scale equals the sphere diameter. The fluid velocity can be taken as the mean velocity between the spheres, in other words the mean interstitial velocity. These two quantities are then introduced in the asymptotic solutions for turbulent and laminar heat transfer:

$$Nu_l = 0.664\,\mathrm{Pr}^{1/3}\left(\mathrm{Re}_0/\varepsilon\right)^{1/2} \tag{2-16}$$

$$Nu_t = \frac{0.037\left(\mathrm{Re}_0/\varepsilon\right)^{0.8}\,\mathrm{Pr}}{1+2.443\left(\mathrm{Re}_0/\varepsilon\right)^{-0.1}\left(\mathrm{Pr}^{2/3}-1\right)} \tag{2-17}$$

Combining Equations 2-16 and 2-17 yields Equation 2-18 with two the asymptotic solutions for $Re_0 \rightarrow 0$.

$$Nu_{sp} = 2+\left(Nu_l^2 + Nu_t^2\right)^{1/2} \tag{2-18}$$

Applying the empirical arrangement factor, Equation 2-19, to Equation 2-18 results in Equation 2-20:

$$f(\varepsilon) = 1+1.5(1-\varepsilon) \tag{2-19}$$

$$Nu = f(\varepsilon)Nu_{sp} \tag{2-20}$$

Achenbach (1995:19) compared results from experiments of a single heated sphere and of naphthalene mass transfer with the semi-empirical method of Gnielinski (1978) described above. Mass transfer experiments were conducted with Sc = 2.53 for $1 < Re_0 < 10^4$. The heat transfer experiments conducted with a single heated sphere at various positions covered a range of Reynolds numbers of $10^4 < Re_0 < 10^5$ with $Pr = 0.7$. Achenbach (1995:20) correlated experimental results with:

$$Nu = \left[\left(1.18 \mathrm{Re}_0^{0.58}\right)^4 + \left(0.23 \mathrm{Re}_0^{0.75}\right)^4 \right]^{0.25} \tag{2-21}$$

Figure 2-4 shows a comparison by Achenbach (1995:20). It is certain that for $Re_0 > 500$ the results predicted by Gnielinski (1978) are exceptional, for $Re_0 < 500$ the deviation increases with decreasing Re_0.

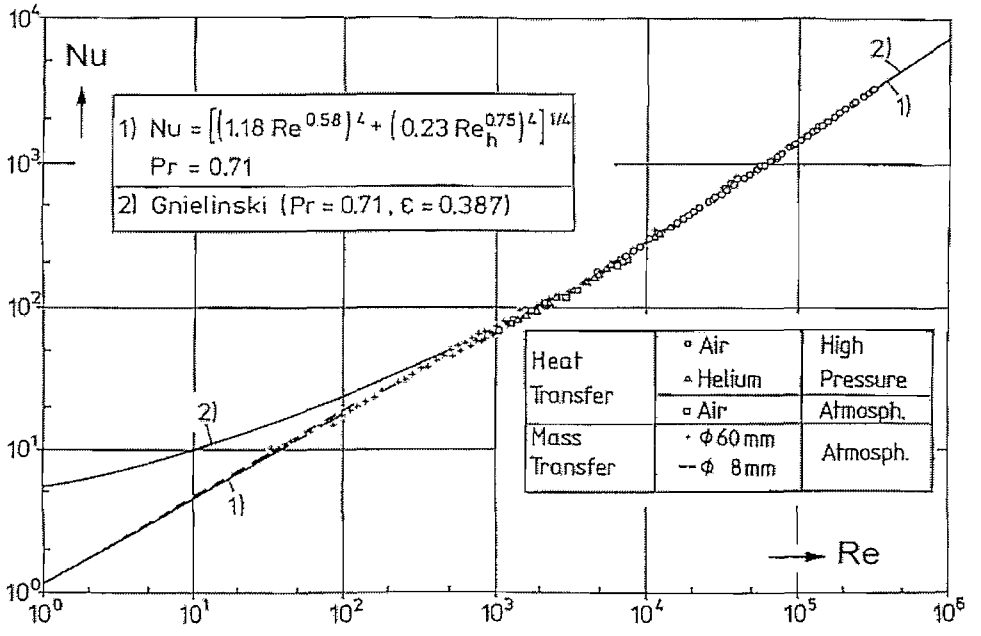

Figure 2-4: Convective pebble-to-fluid heat transfer for packed bed: (1) Achenbach (1995), (2) Eq. 2-20, Pr = 0.7, ε = 0.387. Achenbach (1995:20).

Wakao *et al* (1978:325-336) conducted a study from published heat transfer data. Steady and un-steady measurements where correlated for a range of Reynolds numbers, $15 < Re_0 < 8500$. Wakao *et al* (1978:334) recommended the use of Equation 2-22 for the design and analysis of packed bed reactors.

$$Nu = 2 + 1.1 \mathrm{Pr}^{1/3} \mathrm{Re}_0^{0.6} \tag{2-22}$$

Equation 2-22 is correlated for experimental data from various authors. The experimental setup for this data is obtained from different bed geometries and the accuracy of this correlation is uncertain.

The correlation given by the Nuclear Safety Standards Commission (KTA) (1983:2) is used by Rousseau (1999:11) to calculate the heat transfer in the PBMR. The Nusselt number for the PBMR is given by Equation 2-23 and presented in Figure 2-5. According to the Nuclear Safety Standards Commission (KTA) (1983:2) this correlation is valid for heat transfer between the pebble and the working fluid.

$$Nu = 1.27\frac{\mathrm{Pr}^{0.33}}{\varepsilon^{1.18}}\mathrm{Re}_0^{0.36} + 0.033\frac{\mathrm{Pr}^{0.5}}{\varepsilon^{1.07}}\mathrm{Re}_0^{0.86} \tag{2-23}$$

This heat transfer correlation is valid for a cylindrical bed with:

$$0.36 \le \varepsilon \le 0.42;$$
$$100 \le \mathrm{Re}_0 \le 10^5;$$
$$D/d_p \ge 20;$$
$$h/d_p \ge 4.$$

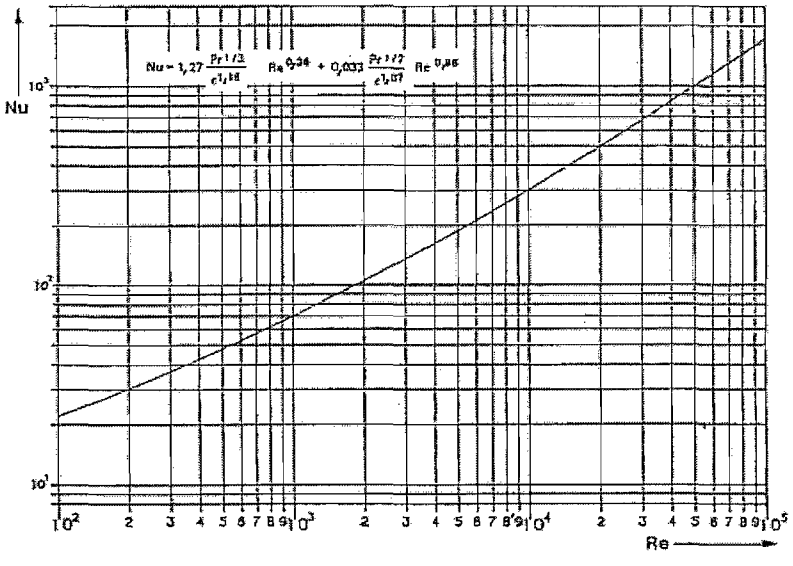

Figure 2-5: Nusselt number as function of Reynolds number for Equation 2-11. $\varepsilon = 0.39$ and $Pr = 0.7$. Nuclear Safety Standards Commission (KTA) (1983:3).

2.4.2 Wall-to-fluid heat transfer

In literature, two basic models are found for describing heat transfer at the wall (Smirnov *et al.*, 2003:243). These models are known as α_w-models and $\Lambda_r(r)$-models. The α_w-model implements two parameters namely the wall heat transfer coefficient, α_w, and the effective radial thermal conductivity, $\lambda_{eff,r}$. Smirnov *et. al.* (2003:243) states that this model predicts unrealistic fluid temperatures near the wall. To bypass this unrealistic temperature, the use of the $\Lambda_r(r)$-model is proposed. The $\Lambda_r(r)$-models implement a varying effective radial thermal conductivity, $\lambda_{eff,r}(r)$, and a first order boundary condition at the wall.

However, most authors (Vortmeyer and Haidegger, 1991:2651 and Tsotsas and Schlünder 1990:820 among others) agree that the problems encountered with the α_w-model, occurs at low Reynolds numbers. Correlations for the wall Nusselt number show considerable scatter and discrepancies in this low Reynolds number region. Vortmeyer and Haidegger (1991:2651) state that this scatter of data point occurs at Reynolds numbers below 400. Furthermore, Tsotsas and Schlünder (1990:822-824) found that for large molecular Péclet numbers ($Pe_0 > Pe_{0,crit}$) the standard α_w-model is adequate for heat transfer calculations. $Pe_{0,crit}$ is defined by Equation 2-24 and $Pe_0 > Pe_{0,crit}$ implies that the main heat transfer mechanism in the fluid is the mixing of the fluid in the voids in the bed.

$$Pe_{0,crit} = K_r \overline{\lambda}_{bed} / \lambda_f \tag{2-24}$$

Achenbach (1995:24) explains the scatter phenomena as follows: The streaming fluid establishes a wall boundary layer through which the heat has to pass. The thickness of this boundary layer depends on the Reynolds and Prandtl numbers. Similarly, a thermal boundary layer exists that causes a temperature difference.

Tsotsas and Schlünder (1990:823) proposed the use of a correlation of Dixon *et al.* (1984:1704) for the range of molecular Péclet number ($Pe_0 > Pe_{0,crit}$). The heat transfer correlation of Dixon *et al.* (1984:1711) is given by Tsotsas and Schlünder (1990:823) by Equation 2-25. Equation 2-25 and is derived for cylindrical beds, hence D. The current study focused on annulus packed beds and Equation 2-25 is thus inadequate for annulus bed design and analyses.

$$Nu_w = \left(1-1.5\left(D/d_p\right)^{-1.5}\right)\mathrm{Pr}^{1/3}\,\mathrm{Re}_0^{0.59} \tag{2-25}$$

Dixon *et al.* (1984:1703-1705) used a mass transfer experiment similar to those discussed in Section 2.4.1. The Reynolds number range covered by Dixon *et al.* (1984:1704) was $50 \leq Re_0 \leq 500$ with $2.9 \leq D/d_p \leq 11.8$. The Sherwood number of Dixon *et al.* (1984:1702,1711) is given in Equation 2-27 and the heat-mass analogy is:

$$\frac{Nu_{w,f}}{\mathrm{Re}_0\,\mathrm{Pr}^{1/3}} = \frac{Sh_{w,f}}{\mathrm{Re}_0\,\mathrm{Pr}^{1/3}} \tag{2-26}$$

$$Sh_{w,f} = \left(1.0-1.5\left(d_p/D\right)^{1.5}\right)Sc^{1/3}\,\mathrm{Re}_0^{0.59} \tag{2-27}$$

The importance of the ratio of tube-to-particle diameter, D/d_p, must also be mentioned. Demirel *et al.* (2000:327) pointed out that the importance of this quantity stems from its direct influence on the properties of the wall region. This is especially true for gas-phase systems due to the increase in porosity. When D/d_p is small, the variation of porosity and velocity may cover the significant part of the bed. Thus, with a small D/d_p ratio a homogeneous porosity bed model can be obtained without reducing the near wall effect.

$$Nu_w = 0.523\left(1-\left(D/d_p\right)^{-1}\right)\mathrm{Pr}^{1/3}\,\mathrm{Re}_0^{0.738} \tag{2-28}$$

For $D/d_p < 4$, Dixon (1997:3063) found that Equations 2-28 correlated well with measured data. Dixon (1997:3055-3056) conducted experiments for these two correlations with $1.14 < D/d_p < 4$ and a Reynolds number range of $300 < Re_0 < 3000$.

2.5 Need for further work

Despite the fact that a lot of work has already been done, there are still significant uncertainties in the field. These uncertainties are partly identified by Achenbach (1995:18)

explaining that forced convective heat transfer is influenced by a number of parameters. These parameters include for instance, Reynolds number, Prandtl number, void fraction, ratio of tube diameter to sphere diameter, ratio of bed height to sphere diameter, local flow conditions, the effects of radiation, contact conduction, natural convection and surface roughness.

Of all the abovementioned parameters, void fraction and the ratio of tube to sphere diameter, are parameters with great influence that are often not recognized. Furthermore is all the work done by previous authors on randomly packed beds and little knowledge exist on homogeneous porosity packed beds. Figure 2-6 illustrates the range of work done by previous authors.

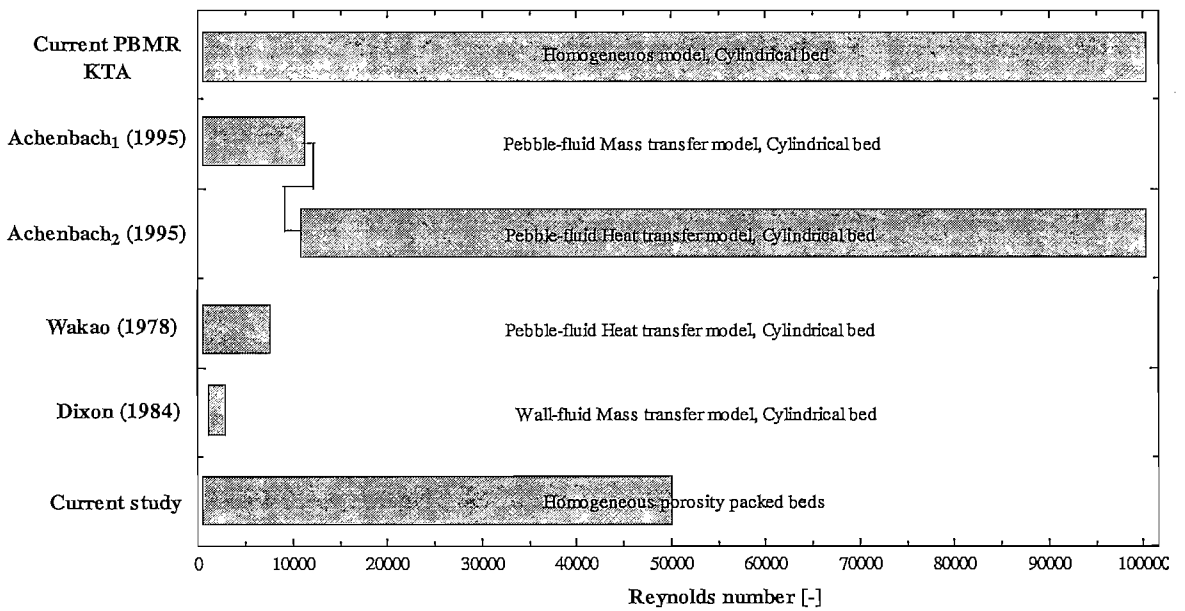

Figure 2-6: Comparisons between different authors' work.

The papers investigated in this study all report studies under certain conditions. The authors of these papers often do not report all of the necessary conditions which complicate the evaluation of their results. The correlations thus far reported can not be assumed to be representative for the convection heat transfer in any packed bed. Table 2-1 gives a summary of correlations for determining Nusselt numbers in packed beds investigated in this study.

Table 2-1: Correlations for the determining of a heat transfer coefficient, α, in packed beds.

Author	Correlation	Type	Re	Geometry
Achenbach (1995:21)	$Nu = \left[\left(1.18 \mathrm{Re}_0^{0.58}\right)^4 + \left(0.23 \mathrm{Re}_0^{0.75}\right)^4 \right]^{1/4}$	Heterogeneous pebble-to-fluid model	$1 < Re_0 < 10^5$	Cylindrical bed
Wakao *et al.* (1978:334)	$Nu = 2 + 1.1 \mathrm{Pr}^{1/3} \mathrm{Re}_0^{0.6}$	Heterogeneous pebble-to-fluid model	$15 < Re_0 < 8500$	Cylindrical bed
Dixon *et al* (1984:1704)	$Nu_w = \left(1 - 1.5 \left(D/d_p\right)^{-1.5}\right) \mathrm{Pr}^{1/3} \mathrm{Re}_0^{0.59}$	Heterogeneous wall-fluid model	$50 \leq Re_0 \leq 500$	Cylindrical bed
Dixon (1997:3063)	$Nu_w = 0.523 \left(1 - \left(D/d_p\right)^{-1}\right) \mathrm{Pr}^{1/3} \mathrm{Re}_0^{0.738}$	Heterogeneous wall-fluid model	$300 < Re_0 < 3000$	Cylindrical bed
Current PBMR (KTA) (1983:2)	$Nu = 1.27 \frac{\mathrm{Pr}^{0.33}}{\varepsilon^{1.18}} \mathrm{Re}_0^{0.36} + 0.033 \frac{\mathrm{Pr}^{0.5}}{\varepsilon^{1.07}} \mathrm{Re}_0^{0.86}$	Homogeneous	$100 \leq Re_0 \leq 10^5$	Cylindrical bed

The parameter, ratio of tube diameter to sphere diameter, D/d_p, leads to a further more important distinction between this study and others like those of Achenbach (1995:17-27), Wakao *et al* (1978:325-336), Dixon *et al* (1984:1701-1713) as well as the current correlation that is used in the PBMR (Nuclear Safety Standards Commission – KTA, 1983:2). All the above-mentioned studies used cylindrical beds in their experimental setup, whereas the PBMR for example is an annular bed. Some uncertainties about the applicability of these correlations to annular beds arise. A homogeneous porosity eliminates the effect of D/d_p and can lead to a better delineated study.

A homogeneous bed (ε = constant) will eliminate velocity variations due to a porosity profile. With controlled velocity (Reynolds number) the only effects on the Nusselt number will be geometrical and since the bed is homogeneous, parameters such as D/d_p will also be eliminated. The only remaining parameter that can be adjusted, besides Reynolds number, is the porosity. Thus, different porosities between $0.36 \leq \varepsilon < 1$ must be investigated. Furthermore, other heat transfer phenomena such as radiation and conduction must be eliminated or minimized to obtain reliable convection heat transfer results. The ideal is to have an experiment that addresses these requirements.

2.6 Summary

In this chapter the literature applicable to convective heat transfer phenomena in packed beds was investigated. It was found that several heat transfer phenomena exist in a packed bed and that it is necessary to isolate convective heat transfer from conduction and radiation heat transfer in a packed bed. Furthermore, convective heat transfer for packed beds can be divided into the following two divisions, namely:

- Pebble-to-fluid heat transfer;
- Wall-fluid heat transfer;

It was found that previous authors studied the same phenomena of convective heat transfer through the basic use of Equation 2-13. Some authors pointed out some restrictions for their correlations for Nusselt numbers. The major restrictions that have an effect on the Nusselt number correlation is geometry and Reynolds number. Since the purpose of this study is to measure the heat transfer coefficient for given discrete homogeneous porosities it would be feasible to control these two parameters. The Reynolds number can be controlled through the fluid velocity and geometry through the use of different homogeneous porosity beds.

3 EXPERIMENTAL FACILITY

3.1 Introduction

The detail design of the HPTU experimental facility falls outside the scope of this study. However, one can appreciate the importance of such a facility for the measurement of the heat transfer coefficient for given discrete homogeneous porosities. Thus, for completeness a discussion of the facility used for measurement is included.

The facility applicable to this study, the High Pressure Test Unit (HPTU) was made available to the author. The HPTU was designed and developed by M-Tech Industrial (Pty) Ltd. The company gave the author access to the HPTU and several of the design documents for the purpose of this study. The HPTU is used for the following:

- Steady-state separate effects tests to validate the correlations used for the pebble-to-fluid heat transfer coefficients at different porosities.
- Steady-state separate effects tests to validate the correlations used for the wall-to-fluid heat transfer coefficient.

In order to create a separate effects test, structured porosity packed beds is used as opposed to randomly packed beds. The only way to practically control the porosity is through the use of structured packed beds. Furthermore, in a structured bed the flow around the spheres are the same over all the spheres. With a flow pattern that is the same through the entire bed only one test sphere is needed, otherwise a number of spheres must be situated at different positions in the packed bed. The difference between structured beds and randomly packed beds in terms of pebble-to-fluid heat transfer is uncertain and can be investigated in this manner.

Most of the information in this section was disclosed by the document of Labuschagne (2005:1-101). In order to keep this document well-organized, this source will not be referred to again in the applicable sections.

3.2 Experimental set-up

The HPTU was designed to accommodate different experiments in one unit. Only three types of experiments were conducted on the HPTU as part of the current study to investigate the pebble-to-fluid heat transfer phenomena in homogeneous packed beds. These experiments are summarized in Table 3-1.

Table 3-1: Experiments for conduction on the HPTU.

	Experiment 1	Experiment 2	Experiment 3
Fluid	N_2	N_2	N_2
Porosity (Homogeneous)	0.36	0.39	0.45
Steady-state	✓	✓	✓
Separate effects	✓	✓	✓
Forced convection	✓	✓	✓
$1000 < Re < 50\ 000$	✓	✓	✓
$100<p_{out}<50000$	✓	✓	✓
Inlet fluid temperature ($T_{f,i}$)	Ambient	Ambient	Ambient
Test sphere elevated temperature (ΔT_s)	50°C	50°C	50°C

3.2.1 HPTU system layout

The HPTU system was designed to incorporate various bed geometries known as Test Sections. These Test Sections can fit into the Test Section Pressure Vessel (TSPV) and can thus be used to conduct different experiments such as those in Table 3-1. The HPTU is also designed to incorporate other types of experiments. However this Section will only focuses on the part of the HPTU that is applicable to the experiments referred to in Table 3-1.

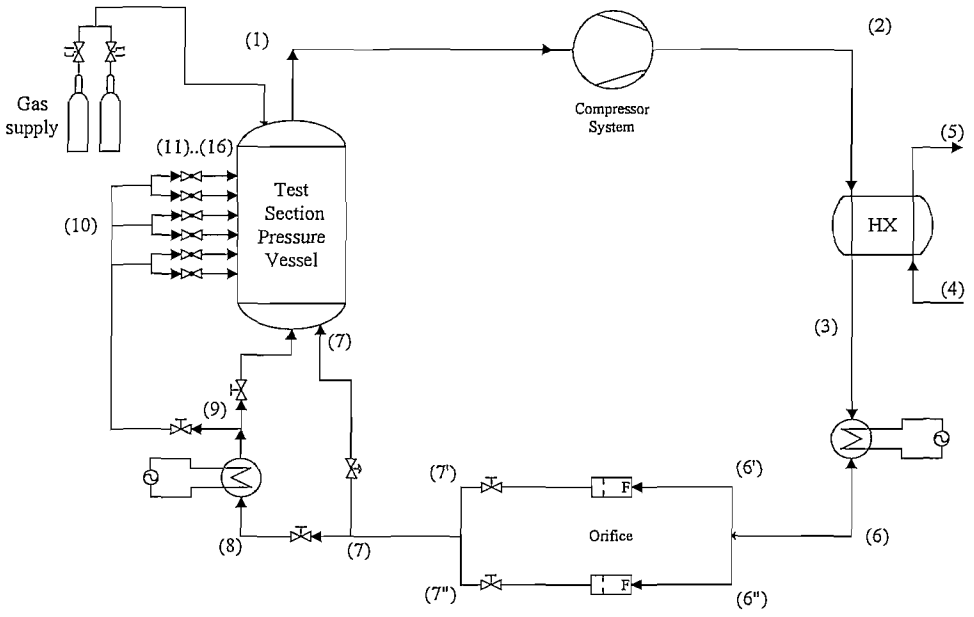

Figure 3-1: Basic schematic layout of the HPTU.

The pressure in the TSPV can be controlled by a gas supply and extraction system in order to maintain the correct pressure in the Test Section. The HPTU system cycle (Figure 3-1) starts off with a blower subsystem that compresses the working fluid, Nitrogen, from point (1) to (2). The blower subsystem produces a pressure ratio of 1.004 with two blowers in series.

Figure 3-2 illustrates the blower subsystem layout. The blowers were placed in a pressure vessel since the maximum working pressure of the system is $5MPa$. This is to reduce the pressure difference over the blower wall and to enable the use of less expensive blowers. The inlet of the blower subsystem (1) is open to the inside of the pressure vessel as well as the inlet to the first blower. The second blower is connected in series to the first blowers' outlet. The second blower outlet leads out of the pressure vessel, point (2).

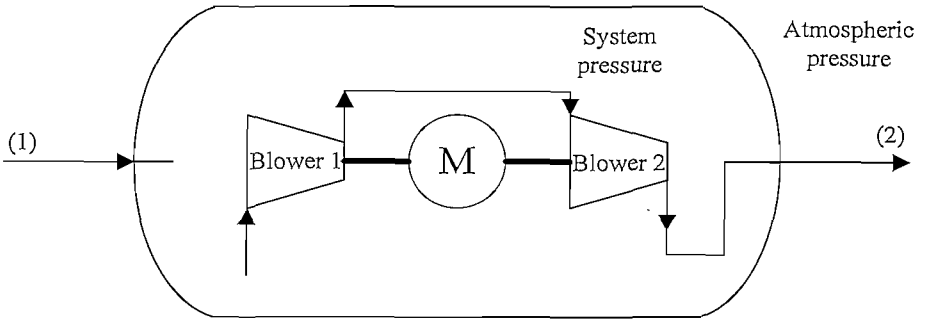

Figure 3-2: Schematic layout of the blower subsystem.

The Nitrogen temperature will rise gradually throughout the cycle. This is due to the compression through the blower subsystem and the heating elements in the gas stream. It is thus necessary to attain the correct temperature before measurements are made on the Nitrogen for experimental purposes. The gas temperature at the inlet of the Test Section is controlled at ambient temperatures.

With the above named addition of extra heat the Nitrogen must be cooled in order to obtain steady state. Therefore the Nitrogen is cooled through the exchange of heat with cooling water by means of a shell-and-tube heat exchanger, points (2) to (3). The designed heat transfer duty of the heat exchanger is $34kW$. In order for the heat exchanger not to extract too much heat from the Nitrogen, a bypass temperature-controlled system is used in the cooling water cycle. Figure 3-3 illustrates the heat exchanger cooling water cycle. The three-way control valve is controlled by the Nitrogen outlet temperature at point (3). The controller maintains the Nitrogen outlet temperature (3) to the set ambient temperatures through bypassing a certain fraction of the heated water from point (5) to the cooled water at point (5"). Thus the water entering the heat exchanger is not all cooled in the cooling tower and as a result the water temperature entering the heat exchanger (4) can be controlled. To further help with temperature control a $20kW$ inline flanged heater is installed between points (3) and (6).

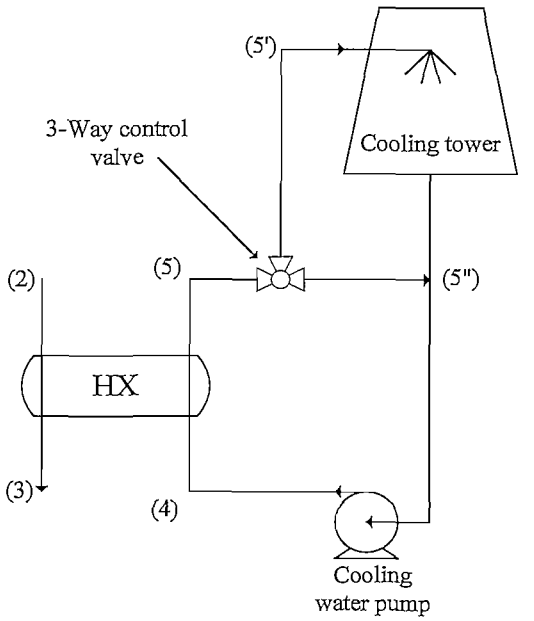

Figure 3-3: Schematic layout of the heat exchanger cooling water cycle.

Between points (6) and (7) a subsystem is implemented to measure the fluid mass flow rate. This subsystem consists of two 4" pipe channels that can be opened or closed independently of each other. Each pipe channel consists of a valve to open or close the channel, an orifice plate and the necessary pressure and temperature instrumentation. From measurements of these instrumentation, the flow rate can be determined.

The reason for implementation of two independent orifice measuring stations is because of the wide range in mass flows to be measured. As a result, different orifice plates are necessary to cover an upper and lower Reynolds number range. Hence, the pipe system combined with closing valves makes it easy to measure different flow rates.

From the orifice subsystem the flow can be split into two, depending on the experiment type. Firstly the main flow line runs through a two-way control valve directly into the TSPV. All types of experiments have flow through this line.

Secondly flow can be diverted from the main line for all braiding experiments, (8). The braiding experiments fall outside the scope of this study and experiments for this study will exclude these elements of the HPTU. The braiding distribution network can be isolated with a valve.

The outlet of the TSPV is directly connected to the blower subsystem inlet (1) from where the system pressure is once again increased to complete the cycle.

3.2.2 HPTU Test sections

The different Test Sections to be used in the HPTU are designed so that one can be exchanged with relative ease with another in the TSPV, Figure 3-4. The TSPV is divided into two cavities, the inlet cavity and the outlet cavity. The Test Section connects the two cavities in such a way that the flow of Nitrogen continues through the TSPV from the inlet cavity all the way through the Test Section in the direction of the outlet cavity towards the outside of the TSPV (1). This ensures that the measured flow can be directed through a particular Test Section. The inlet to the bottom cavity was specifically designed to ensure a near-perfect plug flow distribution at the inlet of the pebble bed.

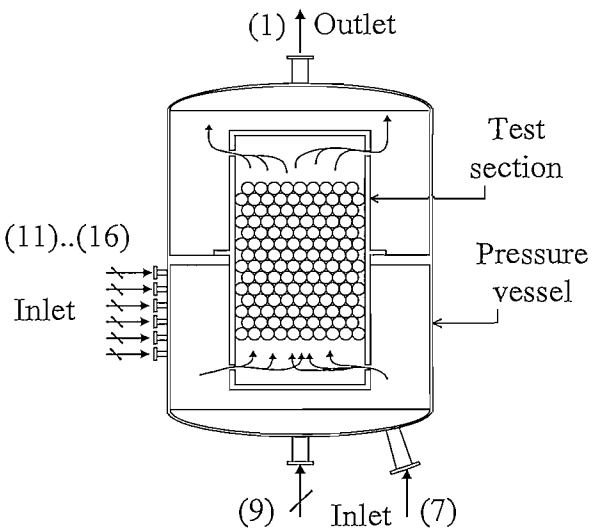

Figure 3-4: Concept of implementation of Test section into the Test Section Pressure Vessel.

In order to measure the pebble-to-fluid heat transfer coefficient the Convection Coefficient Test Sections (CCTS) will be used.

4.2.2.1 Convection Coefficient Test Section

Three CCTS's were developed, each with a different porosity. The porosities are as follows:

- $\varepsilon = 0.36$
- $\varepsilon = 0.39$
- $\varepsilon = 0.45$

The CCTS is a square bed with a geometry given in Table 3-2. The CCTS is a homogeneous porosity Test Section. All three porosities use 60*mm* acrylic spheres. To obtain different porosities with the same sphere and bed dimensions the spaces between spheres were altered. The spheres are held in position by a thin cable that runs through the spheres. The cable is fixed between the top and bottom of the Test Section and then tensioned. The calculated porosity of each Test Section includes the volume of the cables.

Table 3-2: CCTS geometry.

Specification		
Pebble diameter	60	*[mm]*
Width	300	*[mm]*
Depth	300	*[mm]*
Length	720	*[mm]*
Number of pebbles (Total for 3 different porosities)	1266	*[-]*

To obtain a homogeneous porosity in the CCTS from wall to wall the spheres intersecting with the wall of the Test Section were machined to flatten the surface in order to place it on level pegging on the wall. Thus the porosity at the wall is equal to the porosity at the centre of the bed and thus homogeneous.

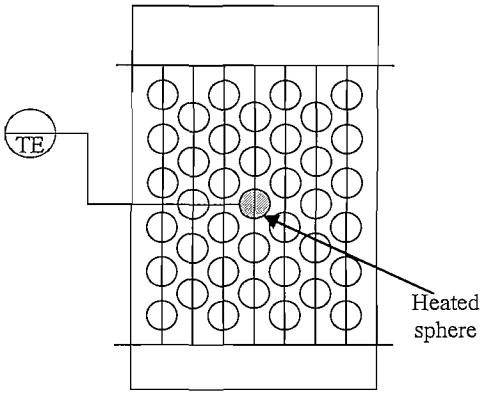

(a)

Figure 3-5: Schematic layout of single heated ball in CCTS.

A special heated sphere was developed for use in the CCTS experiments. The heated sphere (d_p = 60mm) is placed inside the CCTS to represents any other sphere in the Test Section, Figure 3-5. The sphere consists basically of a copper casing, a resistance element and thermocouples attached on its outer surface with an adhesive, Figure 3-6.

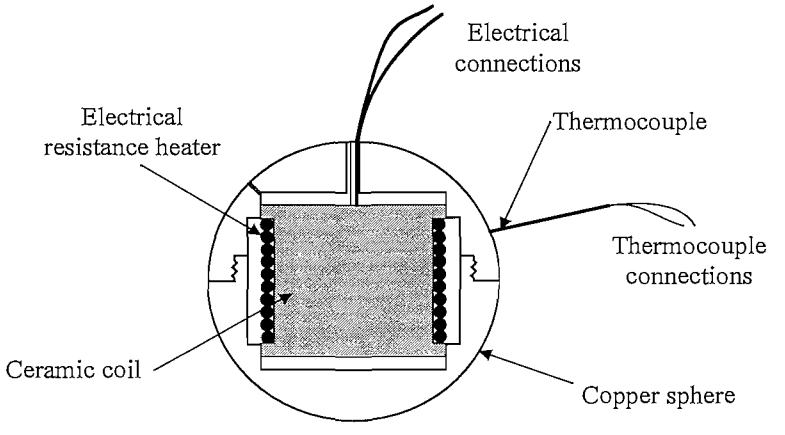

Figure 3-6: Illustration of electrical heated sphere for implementation in CCTS.

Six thermocouples are attached to the heated sphere, five of which is for measuring the surface temperature and one is connected to the Equipment Protection System (EPS). The up-stream hemisphere of the heated sphere houses three of the six thermocouples with the relative position of each illustrated in Figure 3-7. The thermocouple positions on the down-stream hemisphere is the same as the positions on the up-stream hemisphere

In order to lower the effect of radiation heat transfer from the heated sphere to the neighbouring spheres, the heated sphere is chrome-plated and the neighbouring spheres are made of acrylic materials.

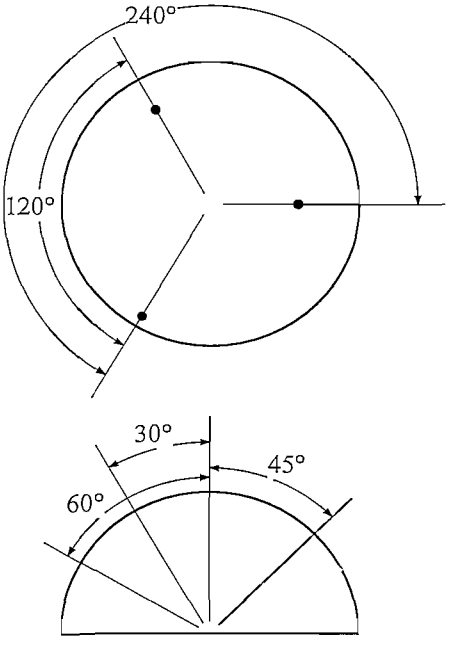

Figure 3-7: Illustration of thermocouple positions on CCTS hemisphere.

3.3 Summary

In this chapter the experimental facility was discussed. The facility known as the HPTU was developed for experiments such as steady state separate effects tests to investigate correlations being used for pebble-to-fluid heat transfer coefficients. The HPTU cycle consist basically of the following:

- System pipes
- Blower subsystem
- Heat exchanger
- System heater
- Shut-off valves
- Flow measuring devices

- System control valve
- Braiding subsystem
- Test Section Pressure Vessel.

For this study three different porosities with the CCTS (ε = 0.36; 0.39; 0.45) were used to measure the heat transfer coefficient (Nusselt number) for pebble-to-fluid convection heat transfer for given discrete homogeneous porosities.

4 INSTRUMENTATION UNCERTAINTY ANALYSIS

4.1 Introduction

Since measurement of a certain unknown is the purpose of this study it is necessary to be familiar with the associated uncertainties or errors that could be involved in these measurements. Two basic types of errors exist that may cause uncertainty in an experimental measurement (Holman 1994:49-57). Firstly there may be certain fixed errors which will cause repeated readings to be in error by roughly the same amount but for some unknown reason. Secondly there are random errors which may be caused by random electronic fluctuations in the apparatus or instruments, various influences of friction etc.

In many instances it is difficult to distinguish between fixed errors and random errors. In order to get a idea of random errors involved in the HPTU it is necessary to conduct a uncertainty analysis on the applicable instruments.

4.2 Instrumentation

The instrumentation of the HPTU was designed and developed along with the HPTU by the M-Tech Industrial (Pty)Ltd design team. A representation of the instrumentation of the HPTU can be found in Appendix A.

All instruments as well as measurement loops are calibrated before an experiment commences. Measurement loops are calibrated by subjecting the instrument to a known process condition. The readout of the instrument is compared to the readout of a secondary standard at the same conditions. All secondary standard instruments are calibrated by a SANAS accredited laboratory. Using regression, a slope and intercept can be determined in order to adjust the field instrument to reflect the same readout as the secondary standard.

4.3 Uncertainty analysis

The uncertainty in a calculated value, for example in the Nusselt number, can be determined by a procedure described by Holman (1994:49-57) with the uncertainty given by Equation 4-1.

$$w_R = \sqrt{\left(\frac{\partial R}{\partial x_1} w_1\right)^2 + \left(\frac{\partial R}{\partial x_2} w_2\right)^2 + \ldots + \left(\frac{\partial R}{\partial x_n} w_n\right)^2} \tag{4-1}$$

where R is the result for a given function of the independent variables x_1, x_2, x_3, ..., x_n:

$$R = R(x_1, x_2, x_3, \ldots, x_n) \tag{4-2}$$

and w_r is the uncertainty in the result and w_1, w_2, ..., w_n are the uncertainties in the independent variables.

The pebble-to-fluid convection heat transfer coefficient α is calculated as follows:

$$\alpha = \frac{q_{conv}}{A(T_s - T_f)} \tag{4-3}$$

with q_{conv} the convection heat transfer rate, A the surface area that is in contact with the fluid and T_s and T_f the surface and fluid temperatures respectively. The Nusselt number is calculated from the convection heat transfer coefficient as follows:

$$Nu = \frac{\alpha d_p}{\lambda_f} \tag{4-4}$$

with d_p the relevant hydraulic diameter and λ_f the thermal conductivity of the fluid. These two equations may be combined to obtain

$$Nu = \frac{q_{conv}}{A(T_s - T_f)} \frac{d_p}{\lambda_f} \tag{4-5}$$

The uncertainty associated with the resultant Nusselt number is therefore determined by the combined uncertainties of the measured parameters on the right-hand side of Equation 4-5. These parameters will therefore be considered in the following sections.

4.3.1 Hydraulic diameter

In the case of the heated sphere the hydraulic diameter will be equal to the sphere diameter, i.e. $60mm$. For the purpose of this analysis there will be no uncertainty associated with the hydraulic diameter since it is a theoretical property allocated to the specific geometry.

4.3.2 Surface area

The sphere was machined accurately with the diameter to within $200\mu m$ i.e. $60 \pm 0.2mm$. We assume that since the uncertainty is given without an associated confidence level that the extreme values are just as likely to occur as those close to the actual measured value. Therefore a rectangular distribution is assumed, with a standard uncertainty of:

$$\Delta d_p = \frac{0.0002}{\sqrt{3}} = 1.1547E-4 \text{ m}$$

Through Equation 4-1 the uncertainty in the area can be calculated as follows:

$$\Delta A = \sqrt{\left(\frac{\partial A}{\partial d_p}\right)^2 \Delta d_p{}^2} \tag{4-6}$$

with

$$A = \pi d_p^2 \tag{4-7}$$

and

$$\frac{\delta A}{\delta d_p} = 2\pi d_p \tag{4-8}$$

The standard uncertainty for the measured ball surface area is therefore 0.38%.

4.3.3 Test section cross section area

The test section has the following general dimensions (Hoogenboezem 2006:10):

- $D_1 = 779.83 \pm 0.025mm$
- $D_2 = 299.975 \pm 0.025mm$
- $D_3 = 299.925 \pm 0.025mm$

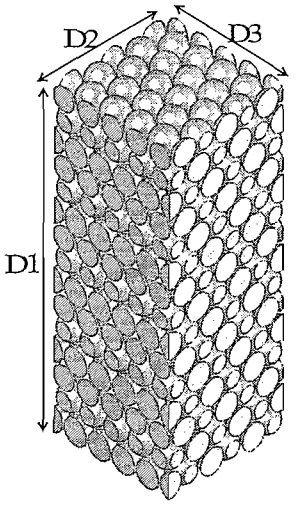

Figure 4-1: CCTS geometry

Thus the flow cross-sectional area is $0.08997m^2$. We assume that since the uncertainty is given without an associated confidence level that the extreme values are just as likely to occur as those close to the actual measured value. Therefore a rectangular distribution is assumed, with a standard uncertainty of:

$$\Delta D_2 = \frac{0.000025}{\sqrt{3}} = 1.443E-5 \text{ m}$$

The height (D_3) was calculated as follows:

$$D_3 = D_3' - 2 \cdot d_1 \tag{4-9}$$

Where

D_3' $= 302.975 \pm 0.025mm$. The back plate length

d_1 = 1.525 ±0.025*mm*. The width of the two plates placed perpendicular on the back plate.

The standard uncertainty for the height (D_3) is calculated as follows when a rectangular distribution is assumed:

$$\begin{aligned}\Delta D_3 &= \sqrt{\left(\frac{\partial D_3}{\partial D_3'}\cdot \Delta D_3'\right)^2 + \left(\frac{\partial D_3}{\partial d_1}\cdot \Delta d_1\right)^2} \\ &= \sqrt{\left((1)\cdot\left(\frac{0.025}{\sqrt{3}}\right)\right)^2 + \left((-2)\cdot\left(\frac{0.025}{\sqrt{3}}\right)\right)^2} \\ &= 3.228E-5 \text{ m}\end{aligned} \tag{4-10}$$

Through Equation 4-1 the uncertainty in the flow cross sectional area can be calculated as follows:

$$\Delta A_{TS} = \sqrt{\left(\frac{\partial A_{TS}}{\partial D_2}\right)^2 \Delta D_2^{\,2} + \left(\frac{\partial A_{TS}}{\partial D_3}\right)^2 \Delta D_3^{\,2}} \tag{4-11}$$

The standard uncertainty for the measured cross sectional area is 0.0118%.

4.3.4 Fluid temperature

The temperature at the inlet to the test sections is controlled at atmospheric temperature and measured with PT100 sensors with uncertainty of ±0.25 ℃. However, the PT100 sensors were calibrated with a Secondary standard with an uncertainty of ±0.1 ℃. The uncertainties of measurement were estimated for a coverage factor of two, which approximates a 95% confidence level. This leads to a standard uncertainty of the instrumentation calculated as:

$$\Delta T_{PT100} = \frac{0.1}{2} = 0.05^{\circ} C \tag{4-12}$$

The fluid temperature is measured with the following sensors: TT-200, TT-201 (Figure A 1), from which the fluid temperature, T_s, can be obtained by:

$$T_f = \frac{1}{2}(T_{200} + T_{201}) \tag{4-13}$$

Through Equation 4-1 the uncertainty in the surface temperature can be calculated as follows:

$$\Delta T_f = \sqrt{\left(\frac{\partial T_f}{\partial T_{200}} \cdot \Delta T_{PT100}\right)^2 + \left(\frac{\partial T_f}{\partial T_{201}} \cdot \Delta T_{PT100}\right)^2} \tag{4-14}$$

Where

$$\frac{\partial T_f}{\partial T_{200}} = \frac{\partial T_f}{\partial T_{201}} = \frac{1}{2}$$

This leads to a standard uncertainty of the instrumentation calculated as 0.04 ℃.

4.3.5 Surface temperature

In the CCTS the aim is to maintain the average surface temperature at atmospheric temperature plus 50 ℃ by varying the rate of heat input via the electrical resistance coil inside of the heated pebble. The average surface temperature is determined by measuring the temperatures at five points on the surface and taking the average of the five values.

The surface temperature measurement is conducted with thermocouples for which the measurement uncertainty is given as ±0.4 ℃. The uncertainties of measurement were estimated for a coverage factor of two, which approximates a 95% confidence level. This leads to a standard uncertainty of the instrumentation as:

$$\Delta T_{tc} = \frac{0.4}{2} = 0.2°C \tag{4-15}$$

The surface temperature is measured with the following thermocouples: TE-250, TE-251, TE-252, TE-253 and TE-254 (Figure A 2), from which the surface temperature, T_s, can be obtained as:

$$T_s = \frac{1}{5}(T_{250} + T_{251} + T_{252} + T_{253} + T_{254}) \tag{4-16}$$

Through Equation 4-1 the uncertainty in the surface temperature can be calculated as follows:

$$\Delta T_s = \sqrt{\left(\frac{\partial T_s}{\partial T_{250}} \cdot \Delta T_{tc}\right)^2 + \left(\frac{\partial T_s}{\partial T_{251}} \cdot \Delta T_{tc}\right)^2 + \left(\frac{\partial T_s}{\partial T_{252}} \cdot \Delta T_{tc}\right)^2 + \left(\frac{\partial T_s}{\partial T_{253}} \cdot \Delta T_{tc}\right)^2 + \left(\frac{\partial T_s}{\partial T_{254}} \cdot \Delta T_{tc}\right)^2} \tag{4-17}$$

Where

$$\frac{\partial T_s}{\partial T_{250}} = \frac{\partial T_s}{\partial T_{251}} = \frac{\partial T_s}{\partial T_{252}} = \frac{\partial T_s}{\partial T_{253}} = \frac{\partial T_s}{\partial T_{254}} = \frac{1}{5}$$

This leads to a standard uncertainty of the instrumentation calculated as 0.1 °C.

However, a CFD analysis of the pebble surface temperature was conducted by Viljoen (Rousseau 2006:24). Figure 4-2 illustrates the surface temperature distribution at 80°C ranging from 83.24°C to 84.43°C. The 1.19°C temperature difference implicates an additional uncertainty upon the surface temperature. Thus it is safe to assume a standard uncertainty in the surface temperature as follows:

$$\Delta T_s = \frac{1.19}{2} + 0.1 = 0.7\ ^\circ C$$

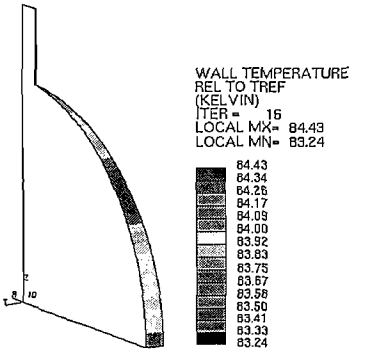

Figure 4-2: CFD analysis results of the heated pebble surface temperature. (Rousseau 2006:24)

4.3.6 Fluid properties

Three fluid properties will be calculated for this analysis: thermal conductivity, viscosity and density. The fluid properties will be calculated with the aid of Engineering Equation Solver (EES).

With the fluid temperature known the fluid pressure remains to be determined in order to determine the fluid properties. Two absolute pressure transducers are installed to measure the absolute fluid pressure in the test sections namely:

- $0 < p \leq 1600\,kPa \qquad \pm 1.6kPa$
- $0 < p \leq 6000\,kPa \qquad \pm 30kPa$

These two pressure transducers were calibrated with secondary standards that have the following claimed uncertainties.

- $0 < p \leq 400\,kPa \qquad \pm 1kPa$
- $400 < p \leq 6000\,kPa \qquad \pm 2kPa$

The uncertainties of measurement were estimated for a coverage factor of two, which approximates a 95% confidence level. This leads to a standard uncertainty of the instrumentation as calculated below.

- $0 < p \leq 400\,kPa \qquad \Delta p_f = \frac{1}{2} = 0.5kPa$
- $400 < p \leq 6000\,kPa \qquad \Delta p_f = \frac{2}{2} = 1kPa$

Table 4-1 presents the pressure levels and associated standard instrument uncertainties. All fluid properties are taken at $25°C$ as an approximation of atmospheric temperature.

Table 4-1: Instrument standard uncertainty for TSPV fluid pressure.

p_f [kPa]	Instrument standard uncertainty [kPa]
100	0.5
200	0.5
300	0.5
400	0.5
500	1
600	1
700	1
800	1
900	1
1000	1
2000	1
3000	1
4000	1
5000	1

In Section 4.3.4 the standard uncertainty in the fluid temperature was found to be $0.04°C$.

Through Equation 4-1 the uncertainty in the fluid thermal conductivity can be calculated with Equation 4-18, the uncertainty in the fluid viscosity with Equation 4-19 and the uncertainty in the fluid density with Equation 4-20.

$$\Delta\lambda_f = \sqrt{\left(\frac{\partial\lambda_f}{\partial T_f}\right)^2 \Delta T_f{}^2 + \left(\frac{\partial\lambda_f}{\partial p_f}\right)^2 \Delta p_f{}^2} \tag{4-18}$$

$$\Delta\mu_f = \sqrt{\left(\frac{\partial\mu_f}{\partial T_f}\right)^2 \Delta T_f{}^2 + \left(\frac{\partial\mu_f}{\partial p_f}\right)^2 \Delta p_f{}^2} \tag{4-19}$$

$$\Delta\rho_f = \sqrt{\left(\frac{\partial\rho_f}{\partial T_f}\right)^2 \Delta T_f^{\,2} + \left(\frac{\partial\rho_f}{\partial p_f}\right)^2 \Delta p_f^{\,2}} \tag{4-20}$$

The partial derivatives is calculated numerically in EES. The partial derivatives in the case of fluid thermal conductivity are given in Table 4-2 along with the standard uncertainty of the thermal conductivity. The viscosity cases are represented in Table 4-3 and the density in Table 4-4.

Table 4-2: Partial derivatives and standard uncertainty in thermal fluid conductivity.

p_f [kPa]	$\partial\lambda_f/\partial T_f$	$\partial\lambda_f/\partial p_f$	$\Delta\lambda_f$ [W/m K]
100	0.000069	4.91E-07	2.46E-06
200	0.000069	4.93E-07	2.46E-06
300	0.000069	4.94E-07	2.45E-06
400	0.000069	4.95E-07	2.45E-06
500	0.000069	4.96E-07	2.48E-06
600	0.000068	4.97E-07	2.47E-06
700	0.000068	4.98E-07	2.47E-06
800	0.000068	4.99E-07	2.46E-06
900	0.000068	5.00E-07	2.45E-06
1000	0.000068	5.02E-07	2.45E-06
2000	0.000066	5.12E-07	2.39E-06
3000	0.000064	5.22E-07	2.32E-06
4000	0.000062	5.32E-07	2.25E-06
5000	0.000059	5.41E-07	2.17E-06

Table 4-3: Partial derivatives and standard uncertainty in viscosity.

p_f [kPa]	$\partial\mu_f/\partial T_f$	$\partial\mu_f/\partial p_f$	$\Delta\mu_f$ [kg/m s]
100	4.73E-08	9.14E-11	1.67E-09
200	4.73E-08	9.33E-11	1.67E-09
300	4.73E-08	9.52E-11	1.67E-09

400	4.72E-08	9.71E-11	1.67E-09
500	4.72E-08	9.89E-11	1.67E-09
600	4.72E-08	1.01E-10	1.67E-09
700	4.71E-08	1.03E-10	1.67E-09
800	4.71E-08	1.05E-10	1.67E-09
900	4.71E-08	1.06E-10	1.67E-09
1000	4.70E-08	1.08E-10	1.67E-09
2000	4.65E-08	1.27E-10	1.65E-09
3000	4.58E-08	1.47E-10	1.63E-09
4000	4.49E-08	1.66E-10	1.60E-09
5000	4.39E-08	1.85E-10	1.56E-09

Table 4-4: Partial derivatives and standard uncertainty in density.

p_f [kPa]	$\partial\rho_f/\partial T_f$	$\partial\rho_f/\partial p_f$	$\Delta\rho_f$ [kg/m^3]
100	-0.003801	1.13E-02	5.66E-03
200	-0.007622	1.13E-02	5.66E-03
300	-0.011460	1.13E-02	5.67E-03
400	-0.015330	1.13E-02	5.69E-03
500	-0.019210	1.13E-02	1.13E-02
600	-0.023110	1.13E-02	1.14E-02
700	-0.027030	1.13E-02	1.14E-02
800	-0.030980	1.13E-02	1.14E-02
900	-0.034940	1.13E-02	1.14E-02
1000	-0.038920	1.13E-02	1.14E-02
2000	-0.079750	1.14E-02	1.17E-02
3000	-0.122300	1.14E-02	1.22E-02
4000	-0.166400	1.14E-02	1.28E-02
5000	-0.211700	1.13E-02	1.36E-02

4.3.7 Heat transfer

The heat supplied by the resistance element is not all lost through convection heat transfer. The energy conservation, Equation 4-21, is used to calculate the convection heat transfer, q_{conv}.

$$q_{conv} = q_{elec} - q_{rad} - q_{TC\,fin} \tag{4-21}$$

where q_{elec} is the electrical input kilowatts through the resistance heater; q_{rad} radiation heat loss and $q_{TC\,fin}$ a heat loss through conduction through the thermocouples attached to the heated sphere.

The oscilloscope used for the power measurement was calibrated with secondary standards. The maximum difference between the Oscilloscope and the secondary standards were 1.9% of the measured value. This is taken as the uncertainty of the measurement and not the secondary standard calibration certificate uncertainty, since the secondary standard uncertainty is in the order of 0.1%. We assume that since the uncertainty is given without an associated confidence level that the extreme values are just as likely to occur as those close to the actual measured value. Therefore a rectangular distribution is assumed, with a standard uncertainty of:

$$\Delta q_{elec} = \frac{1.9}{\sqrt{3}} = 1.097\ \%$$

The radiation heat loss can be calculated with:

$$q_{rad} = \varepsilon_{chrome} A_{sphere} \sigma_{SB} \left(T_s^4 - T_f^4\right) \tag{4-22}$$

with $\sigma_{SB} = 5.670\text{x}10^{-8} W/m^2K^4$ the Stefan-Boltzmann constant, ε_{chrome} the surface emissivity of the pebble and T_f the temperature of the surroundings, which at steady-state should be equal to the fluid temperature.

The emissivity of the pebble surface should be similar to a highly polished metal, foil or film surface since it will be chromed and polished specifically to minimise the radiation heat loss.

This means that the surface emissivity should be somewhere between 0.02 and 0.07 (Incorpera and DeWitt, 2002:929), i.e. ε_{chrome} = 0.045±0.025. We assume that since the uncertainty is given without an associated confidence level that the extreme values are just as likely to occur as those close to the actual measured value. Therefore a rectangular distribution is assumed, with a standard uncertainty of:

$$\Delta\varepsilon_{chrome} = \frac{0.025}{\sqrt{3}} = 0.0144 \tag{4-23}$$

The standard uncertainty for the radiation heat transfer is calculated as follows:

$$\Delta q_{rad} = \sqrt{\left(\frac{\partial q_{rad}}{\partial A}\cdot\Delta A\right)^2 + \left(\frac{\partial q_{rad}}{\partial \varepsilon_{rad}}\cdot\Delta\varepsilon_{chrome}\right)^2 + \left(\frac{\partial q_{rad}}{\partial T_s}\cdot\Delta T_s\right)^2 + \left(\frac{\partial q_{rad}}{\partial T_f}\cdot\Delta T_f\right)^2} \tag{4-24}$$

Where

$$\frac{\partial q_{rad}}{\partial A} = \sigma\varepsilon_{chrome}\left(T_s^4 - T_f^4\right) \tag{4-25}$$

$$\frac{\partial q_{rad}}{\partial \varepsilon_{chrome}} = \sigma A\left(T_s^4 - T_f^4\right) \tag{4-26}$$

$$\frac{\partial q_{rad}}{\partial T_s} = 4\sigma A\varepsilon_{chrome}\left(T_s^3\right) \tag{4-27}$$

$$\frac{\partial q_{rad}}{\partial T_f} = -4\sigma A\varepsilon_{chrome}\left(T_f^3\right) \tag{4-28}$$

This leads to a standard uncertainty of the radiation heat loss of 0.063 W.

The thermocouples act as fins on the sphere and a simple CFD-code was compiled to calculate $q_{TC\ fin}$. This CFD-code is summarized in Appendix B. Table 4-5 gives the calculated heat loss due to the thermocouples attached to the sphere. $\Delta q_{TC,fin}$ is assumed for the surface temperature range of the sphere calculated in Section 4.3.5.

Table 4-5: Table of predicted heat loss through thermocouples.

Re [-]	$q_{TC,fin}$ [W]	$\Delta q_{TC,fin}$ [W]
1000	0.52	0.006
2000	0.52	0.006
3000	0.53	0.006
4000	0.53	0.006
5000	0.53	0.006
6000	0.53	0.006
7000	0.53	0.006
8000	0.53	0.006
9000	0.53	0.006
10000	0.53	0.006
20000	0.53	0.006
30000	0.53	0.006
40000	0.53	0.006
50000	0.53	0.006

In order to estimate the required power input, the Nusselt number may be calculated based on Equation 4-29. Table 4-6 represents the calculated power requirement.

$$Nu = 1.27\frac{\mathrm{Pr}^{0.33}}{\varepsilon^{1.18}}\mathrm{Re}_0^{0.36} + 0.033\frac{\mathrm{Pr}^{0.5}}{\varepsilon^{1.07}}\mathrm{Re}_0^{0.86} \tag{4-29}$$

Table 4-6: Calculated power requirement.

Re [-]	q_{conv} [W]	q_{elec} [W]
1000	17.08	17.79
2000	25.72	26.44
3000	33.17	33.89
4000	39.99	40.71

5000	46.42	47.14
6000	52.57	53.29
7000	58.50	59.23
8000	64.27	65.00
9000	69.91	70.63
10000	75.43	76.16
20000	127.15	127.88
30000	175.99	176.72
40000	224.06	224.79
50000	272.19	272.92

Through Equation 4-1 the uncertainty in the convective heat transfer can be calculated as follows:

$$\Delta q_{conv} = \sqrt{\left(\frac{\partial q_{conv}}{\partial q_{elec}}\Delta q_{elec}\right)^2 + \left(\frac{\partial q_{conv}}{\partial q_{rad}}\Delta q_{rad}\right)^2 + \left(\frac{\partial q_{conv}}{\partial q_{TC,fin}}\Delta q_{TC,fin}\right)^2} \quad (4\text{-}30)$$

Where:

$$\frac{\partial q_{conv}}{\partial q_{elec}} = 1 \quad (4\text{-}31)$$

$$\frac{\partial q_{conv}}{\partial q_{rad}} = -1 \quad (4\text{-}32)$$

$$\frac{\partial q_{conv}}{\partial q_{TC,fin}} = -1 \quad (4\text{-}33)$$

Table 4-7 presents the sphere convective heat transfer instrument standard uncertainty.

Table 4-7: Convective heat transfer instrument standard uncertainty.

Re [-]	Δq_{conv} [W]	[%]
1000	0.21	1.20
2000	0.30	1.15
3000	0.38	1.14
4000	0.45	1.13
5000	0.52	1.12
6000	0.59	1.12
7000	0.65	1.12
8000	0.72	1.11
9000	0.78	1.11
10000	0.84	1.11
20000	1.40	1.10
30000	1.94	1.10
40000	2.47	1.10
50000	2.99	1.10

4.3.8 Heat transfer coefficient

The standard uncertainty for the heat transfer coefficient is calculated as follows through the use of Equation 4-1:

$$\Delta\alpha = \sqrt{\left(\frac{\partial\alpha}{\partial q_{conv}}\cdot\Delta q_{conv}\right)^2 + \left(\frac{\partial\alpha}{\partial A}\cdot\Delta A\right)^2 + \left(\frac{\partial\alpha}{\partial T_s}\cdot\Delta T_s\right)^2 + \left(\frac{\partial\alpha}{\partial T_f}\cdot\Delta T_f\right)^2} \quad (4\text{-}34)$$

Where

$$\frac{\partial\alpha}{\partial q_{conv}} = \frac{1}{A(T_s - T_f)} \quad (4\text{-}35)$$

$$\frac{\partial\alpha}{\partial A} = \frac{-q_{conv}}{A^2(T_s - T_f)} \quad (4\text{-}36)$$

$$\frac{\partial \alpha}{\partial T_s} = \frac{-q_{conv}}{A(T_s - T_f)^2} \tag{4-37}$$

$$\frac{\partial \alpha}{\partial T_f} = \frac{q_{conv}}{A(T_s - T_f)^2} \tag{4-38}$$

Table 4-8 presents the heat transfer coefficient instrument standard uncertainty.

Table 4-8: Heat transfer coefficient instrument standard uncertainty.

Re [-]	$\Delta\alpha$ [W/m K]	[%]
1000	0.563	1.86
2000	0.834	1.83
3000	1.069	1.82
4000	1.284	1.82
5000	1.488	1.81
6000	1.683	1.81
7000	1.871	1.81
8000	2.055	1.81
9000	2.233	1.81
10000	2.409	1.81
20000	4.051	1.80
30000	5.603	1.80
40000	7.131	1.80
50000	8.661	1.80

4.3.9 Nusselt number

The standard uncertainty for the Nusselt number is calculated as follows through the use of Equation 4-1:

$$\Delta Nu = \sqrt{\left(\frac{\partial Nu}{\partial \alpha}\cdot \Delta\alpha\right)^2 + \left(\frac{\partial Nu}{\partial d_p}\cdot \Delta d_p\right)^2 + \left(\frac{\partial Nu}{\partial \lambda_f}\cdot \Delta\lambda_f\right)^2} \tag{4-39}$$

Where

$$\frac{\partial Nu}{\partial \alpha} = \frac{d_p}{\lambda_f} \tag{4-40}$$

$$\frac{\partial Nu}{\partial d_p} = \frac{\alpha}{\lambda_f} \tag{4-41}$$

$$\frac{\partial Nu}{\partial \lambda_f} = \frac{-\alpha d_p}{\lambda_f^2} \tag{4-42}$$

Table 4-9 presents the heat transfer coefficient instrument standard uncertainty, with a graphical illustration presented in Figure 4-3.

Table 4-9: Heat transfer coefficient instrument standard uncertainty.

Re [-]	ΔNu [W/m K]	[%]
1000	1.32	1.87
2000	1.95	1.84
3000	2.49	1.83
4000	2.99	1.83
5000	3.46	1.82
6000	3.91	1.82
7000	4.34	1.82
8000	4.75	1.82
9000	5.16	1.82
10000	5.55	1.82
20000	9.16	1.81
30000	12.42	1.81
40000	15.51	1.81
50000	18.48	1.81

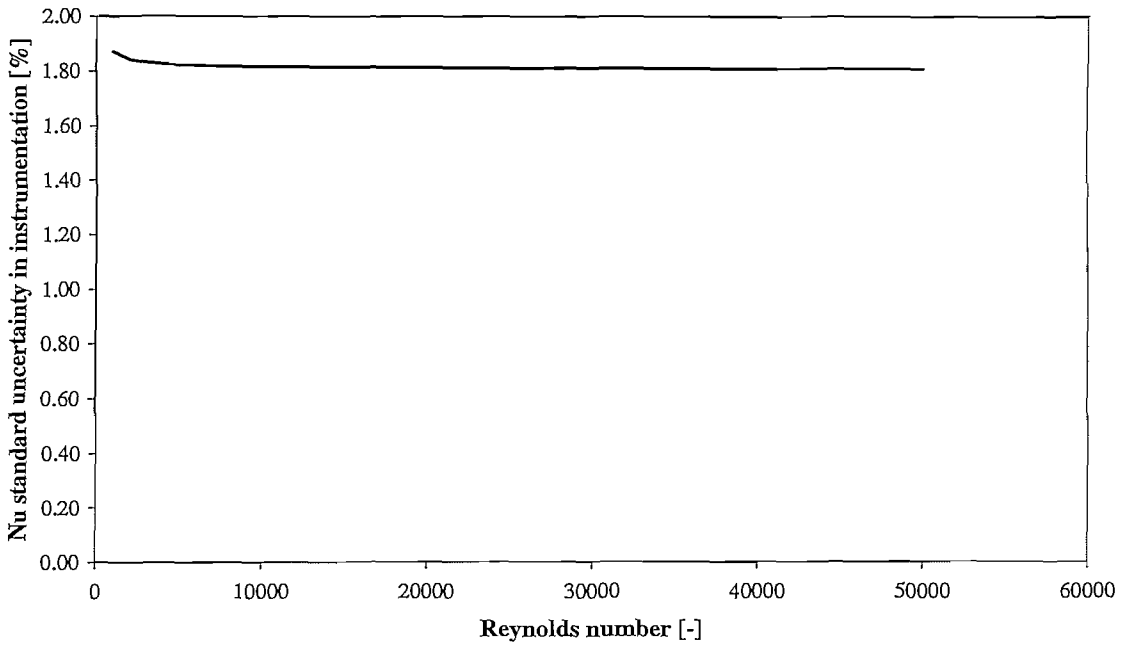

Figure 4-3: Graph of Nu number standard uncertainty in instrumentation against Reynolds number.

4.3.10 Mass flow

The system mass flow rate is measured with orifice plates (Section 3.2.1). The calculation of the uncertainty in the measurement of the mass flow rate is given by Van der Walt (2006:10-14) as follows:

$$\frac{\Delta \dot{m}}{\dot{m}} = \sqrt{\left(\frac{\Delta C}{C}\right)^2 + \left(\frac{\Delta \varepsilon}{\varepsilon}\right)^2 + \left(\frac{2\beta^4}{1-\beta^4}\right)^2 \cdot \left(\frac{\Delta D_{OrPipe}}{D_{OrPipe}}\right)^2 + \left(\frac{2}{1-\beta^4}\right)^2 \left(\frac{\Delta d_{or}}{d_{or}}\right)^2 + \frac{1}{4}\left(\frac{\Delta p_{unc}}{\Delta p}\right)^2 + \frac{1}{4}\left(\frac{\Delta \rho_1}{\rho_1}\right)^2} \quad (4\text{-}43)$$

With:

$\frac{\Delta C}{C}$ $= 1\%$

$\frac{\Delta \varepsilon}{\varepsilon}$ $= 3.5\frac{\Delta p}{\kappa \cdot p_1}\%$ (The uncertainty of the expansion factor)

$\frac{\Delta D_{OrPipe}}{D_{OrPipe}}$ $= 0.00027$. The pipe diameter uncertainty percentage

$\frac{\Delta d_{or}}{d_{or}}$ $= 0.000597$. The orifice diameter uncertainty percentage

$\frac{\Delta p_{Unc}}{\Delta p}$ = the pressure drop across the orifice plate uncertainty percentage.

$\frac{\Delta \rho_1}{\rho_1}$ = the density uncertainty percentage

Based on the Reynolds number required in the Test section Equation 4-38 can be implemented to calculate the pressure drop over the orifice plate.

$$\dot{m} = \frac{C\varepsilon}{\sqrt{1-\beta^4}} \frac{\pi}{4} d_{or}^2 \sqrt{2\rho_f \Delta p_{or}} \tag{4-44}$$

with the discharge coefficient C as:

$$C = 0.5961 + 0.0261 \cdot \beta^2 - 0.216 \cdot \beta^8 + 0.000521 \cdot \left(\frac{10^6 \cdot \beta}{\mathrm{Re}_D} \right)^{0.7} + \left(0.0188 + 0.0063A'\right) \cdot \beta^{3.5} \cdot \left(\frac{10^6}{\mathrm{Re}_D} \right)^{0.3} \tag{4-45}$$

and:

$$A' = \left(\frac{19000 \cdot \beta}{\mathrm{Re}_D} \right)^{0.8} \tag{4-46}$$

$$\beta = \frac{d_{or}}{D_{OrPipe}} \tag{4-47}$$

The expansion factor ε is calculated as:

$$\varepsilon = 1 - \left(0.351 + 0.256 \cdot \beta^4 + 0.93 \cdot \beta^8\right) \cdot \left[1 - \left(\frac{p_2}{p_1} \right)^{1/\kappa} \right] \tag{4-48}$$

Table 4-10 presents the pressure drop over the orifice plate. Only one orifice plate was used since over the whole range of Reynolds numbers the mass flow remains below 1.44*kg/s*.

Table 4-10: Calculated mass flow and orifice plate pressure drop.

Re_0	$\dot{m}$ [kg/s]	Δp_{or} [Pa]
1000	0.027	69.3
2000	0.054	236.9
3000	0.082	441.6
4000	0.109	663.1
5000	0.136	893.6
6000	0.164	1129.9
7000	0.191	1369.8
8000	0.218	1612.4
9000	0.246	1856.7
10000	0.273	2103.8
20000	0.550	4635.3
30000	0.831	7258.0
40000	1.118	9992.0
50000	1.411	12852.2

Now Equation 4-43 can be implemented to calculate the theoretical standard uncertainty in the mass flow due to instrument uncertainty. The results of the calculation are presented in Table 4-11 with the maximum standard uncertainty in the mass flow 1.04%.

Table 4-11: Results in the calculation of the standard uncertainty in the mass flow.

Re0	$\frac{\Delta\varepsilon}{\varepsilon}$	$\frac{\Delta p_{Unc}}{\Delta p}$	$\frac{\Delta\rho_1}{\rho_1}$	$\frac{\Delta\dot{m}}{\dot{m}}$ [%]
1000	1.73E-05	0.002	5.01E-03	1.04
2000	2.96E-05	0.002	2.50E-03	1.02
3000	3.67E-05	0.002	1.67E-03	1.02
4000	4.14E-05	0.002	1.26E-03	1.01
5000	4.46E-05	0.002	2.01E-03	1.02
6000	4.70E-05	0.002	1.67E-03	1.02

7000	4.88E-05	0.002	1.44E-03	1.02
8000	5.03E-05	0.002	1.26E-03	1.01
9000	5.15E-05	0.002	1.12E-03	1.01
10000	5.25E-05	0.002	1.01E-03	1.01
20000	5.78E-05	0.002	5.16E-04	1.01
30000	6.03E-05	0.002	3.57E-04	1.01
40000	6.23E-05	0.002	2.82E-04	1.01
50000	6.41E-05	0.002	2.39E-04	1.01

4.3.11 Reynolds number

The Reynolds number through the bed can be calculated as follows:

$$\mathrm{Re}_0 = \frac{\dot{m} d_p}{\mu_f A_{TS}} \tag{4-49}$$

with $\dot{m}$ the system mass flow, d_p the pebble diameter, μ_f the fluid viscosity and A_{TS} the cross sectional flow area through the bed. The uncertainty associated with the Reynolds number is therefore determined by implementing of Equation 4-1 for the parameters on the right hand side of Equation 4-49.

$$\Delta \mathrm{Re}_0 = \sqrt{\left(\frac{\partial \mathrm{Re}_0}{\partial \dot{m}} \cdot \Delta \dot{m}\right)^2 + \left(\frac{\partial \mathrm{Re}_0}{\partial d_p} \cdot \Delta d_p\right)^2 + \left(\frac{\partial \mathrm{Re}_0}{\partial \mu_f} \cdot \Delta \mu_f\right)^2 + \left(\frac{\partial \mathrm{Re}_0}{\partial A_{TS}} \cdot \Delta A_{TS}\right)^2} \tag{4-50}$$

with:

$$\frac{\partial \mathrm{Re}_0}{\partial \dot{m}} = \frac{d_p}{\mu_f A_{TS}} \tag{4-51}$$

$$\frac{\partial \mathrm{Re}_0}{\partial d_p} = \frac{\dot{m}}{\mu_f A_{TS}} \tag{4-52}$$

$$\frac{\partial \mathrm{Re}_0}{\partial \mu_f} = -\frac{\dot{m} d_p}{\mu_f^2 A_{TS}} \tag{4-53}$$

$$\frac{\partial \mathrm{Re}_0}{\partial A_{TS}} = -\frac{\dot{m} d_p}{\mu_f A_{TS}^2} \tag{4-54}$$

Table 4-12 presents the Reynolds number instrument standard uncertainty, with a graphical illustration presented in Figure 4-4.

Table 4-12: Reynolds number instrument standard uncertainty.

Re_0 [-]	ΔRe_0 [-]	[%]
1000	10.61	1.06
2000	20.78	1.04
3000	31.04	1.03
4000	41.33	1.03
5000	51.81	1.04
6000	62.08	1.03
7000	72.36	1.03
8000	82.65	1.03
9000	92.95	1.03
10000	103.25	1.03
20000	206.32	1.03
30000	309.42	1.03
40000	412.54	1.03
50000	515.66	1.03

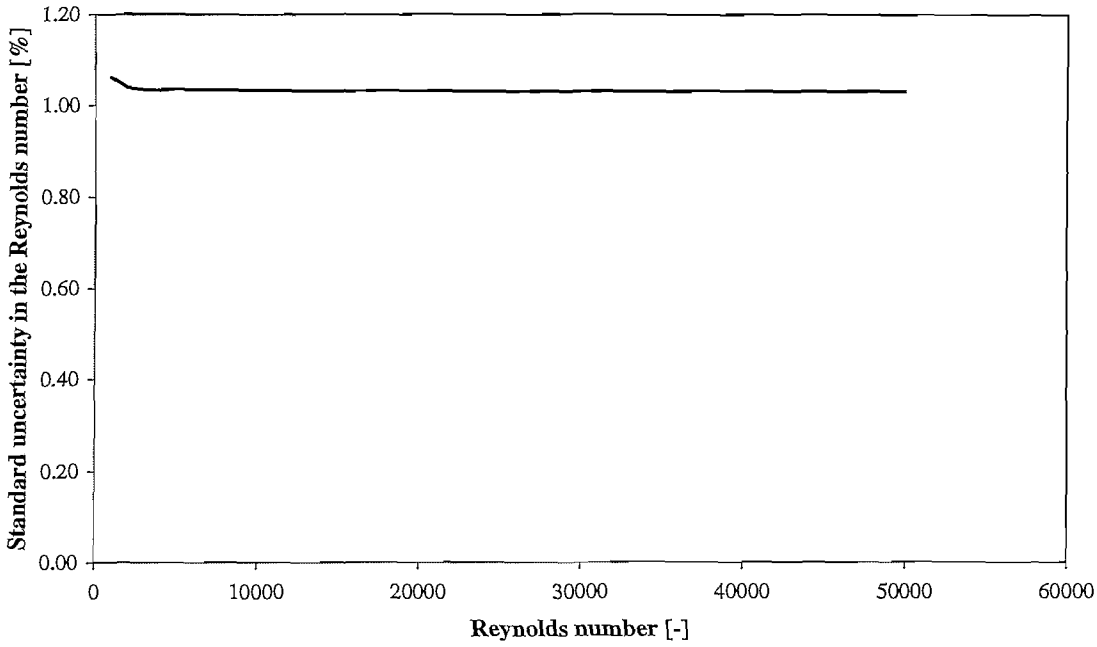

Figure 4-4: Graph of Reynolds number standard uncertainty in instrumentation against Reynolds number.

4.4 Summary

The standard uncertainty in the instruments was investigated. The standard uncertainty in the Nusselt number is illustrated in Figure 4-3 and that of the Reynolds number in Figure 4-4. The uncertainty in the Nusselt number for the CCTS due to instrumentation is less than 2.0% and the uncertainty in the Reynolds number is less than 1.2%. The uncertainties due to instrumentation are kept as low as possible by calibrating necessary instrumentation.

5 RESEARCH METHODOLOGY

5.1 Introduction

In order to obtain meaningful resultants through measurement one must understands the measurement procedure followed. The following sections describe the experimental methodology that was followed.

5.2 Range of measurement

In order to determine the range of measurements that must be covered by this study it is helpful to get a picture of the operating range of the PBMR. In the PBMR the following fluid flow conditions exist:

- Fluid: Helium
- $300 \leq T_f \leq 1130$ *[°C]*
- $100 \leq p_f \leq 9000$ *[kPa]*
- $\dot{m} \leq 186$ *[kg/s]*

From the above conditions a Reynolds number of $Re \leq 46\ 800$ was obtained at the maximum mass flow, $\dot{m}$. At low Reynolds numbers ($Re \rightarrow 0$) natural convection flow conditions may be encountered. To avoid this situation and also cover the upper Reynolds number in the PBMR the experimental Reynolds number range was set as:

$$1000 \leq Re_0 \leq 50000.$$

The Prandtl number for Helium varies between 0.65 and 0.69 for the operating range of the PBMR. However in the case of the HPTU the following operating ranges will be implemented in order to achieve the Reynolds number range:

- Fluid: Nitrogen
- $100 \leq p_f \leq 5000$ *[kPa]*

- Atmospheric temperature, $T_f = \pm 25°C$

This will result in a Prandtl number range of 0.7 to 0.85, depending on the actual fluid temperature.

The operating temperature of the HPTU is at atmospheric temperature. In order to obtain a largely homogeneous surface temperature for the heated sphere as well as a large enough temperature difference between the surface and the fluid, the sphere shall be heated to at least $50°C$ above the fluid temperature.

Combining the known operating range of the HPTU and desired measurement range, the feasible experimental range can be set. Table 5-1 represent the range of experiments that will be covered in this study. Tests shall be conducted under steady-state conditions with fully developed flow in the axial coordinate direction.

Table 5-1: Measurement ranges for the current study.

$1000 \leq Re_0 \leq 50\,000$
$\varepsilon = 0.36$, 0.39 and 0.45
$0.7 \leq \mathrm{Pr} \leq 0.85$
$100 \leq p_f \leq 5000$
T_f – atmospheric
$T_s = T_f + 50°C$

5.3 Measurement frequency

In order to cover the Reynolds number range, 14 tests were specified for each test section in the HPTU test plan (Labuschagne 2006:14-15). Table 5-2 gives the Reynolds number for each of the 14 tests. Each test run is conducted twice, this way two sets of data are obtained through which a measure of the repeatability of the experiment can be determined. Figure 5-1 illustrates the conduction of an experiment in order to obtain two separate sets of data.

Table 5-2: Reynolds number intervals.

Reynolds number
1 000
2 000
3 000
4 000
5 000
6 000
7 000
8 000
9 000
10 000
20 000
30 000
40 000
50 000

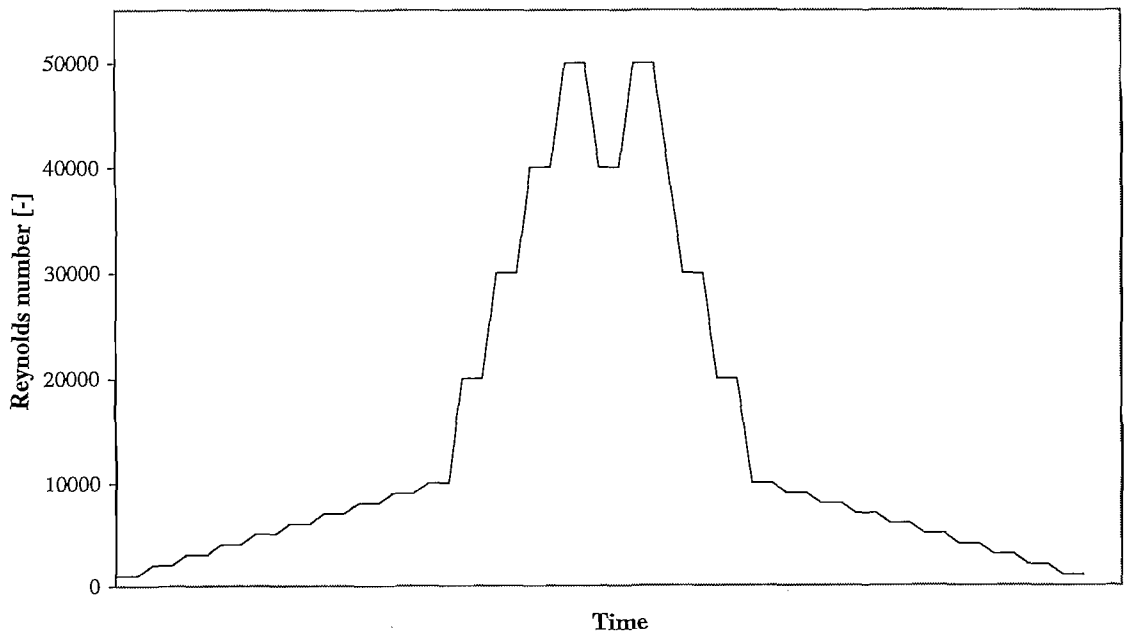

Figure 5-1: Graph illustrating the conduction of an experiment in order to obtain two separate sets of data for a single experiment.

For each test five minutes worth of steady-state data will be used to calculate the applicable averages and standard deviations at that test point. Since data is captured at $2Hz$, five minutes of data will result in 600 data points per test. This should be enough data to calculate a good average as well as a good standard deviation. Table 5-3 represents the test matrix for the tests conducted.

Table 5-3: Test matrix.

Re_0	$\varepsilon = 0.36$		$\varepsilon = 0.39$		$\varepsilon = 0.45$	
	Run 1	Run 2	Run 1	Run 2	Run 1	Run 2
1 000	1.1.1	1.2.1	2.1.1	2.2.1	3.1.1	3.2.1
2 000	1.1.2	1.2.2	2.1.2	2.2.2	3.1.2	3.2.2
3 000	1.1.3	1.2.3	2.1.3	2.2.3	3.1.3	3.2.3
4 000	1.1.4	1.2.4	2.1.4	2.2.4	3.1.4	3.2.4
5 000	1.1.5	1.2.5	2.1.5	2.2.5	3.1.5	3.2.5
6 000	1.1.6	1.2.6	2.1.6	2.2.6	3.1.6	3.2.6
7 000	1.1.7	1.2.7	2.1.7	2.2.7	3.1.7	3.2.7
8 000	1.1.8	1.2.8	2.1.8	2.2.8	3.1.8	3.2.8
9 000	1.1.9	1.2.9	2.1.9	2.2.9	3.1.9	3.2.9
10 000	1.1.10	1.2.10	2.1.10	2.2.10	3.1.10	3.2.10
20 000	1.1.11	1.2.11	2.1.11	2.2.11	3.1.11	3.2.11
30 000	1.1.12	1.2.12	2.1.12	2.2.12	3.1.12	3.2.12
40 000	1.1.13	1.2.13	2.1.13	2.2.13	3.1.13	3.2.13
50 000	1.1.14	1.2.14	2.1.14	2.2.14	3.1.14	3.2.14

5.4 Steady-state determination

Since the adjustment between two different Reynolds numbers entail a transient process it is necessary to determine the steady-state portion from the data captured in order to do data analysis. The author was part of a M-Tech Industrial (Pty.) Ltd. team that developed a criteria system to help with steady-state determination. The criteria system consists of two sub-criteria (Van der Merwe 2006:11-15):

- Criteria 1: Long and short term average convergence.
- Criteria 2: Normalized slope.

5.4.1 Criteria 1: Long and short term average convergence

Criteria 1 is described by Equation 5-1 and is based on the difference between the average of the measured data during the previous five minutes and the average of the measured data during the previous minute. This difference is normalized and then averaged over the previous five minutes. It was found that steady-state is reached if Criteria 1 is less than 5%.

$$Average_{5\min}\left|\left(\frac{x_{Average_{5\min}}(t)-x_{Average_{1\min}}(t)}{x_{max}-x_{min}}\right)\times 100\right|<5\% \qquad (5\text{-}1)$$

where

$Average_{5\min}$ = running average calculated during the previous 5 minutes.

$x_{Average_{1\min}}(t)$ = running average calculated during the previous minute of the logged data at time step *t*.

$x_{Average_{5\min}}(t)$ = running average calculated during the previous 5 minutes of the logged data at time step *t*.

x_{max} = maximum measured value from the beginning of the specific test.

x_{min} = minimum measured value from the beginning of the specific test.

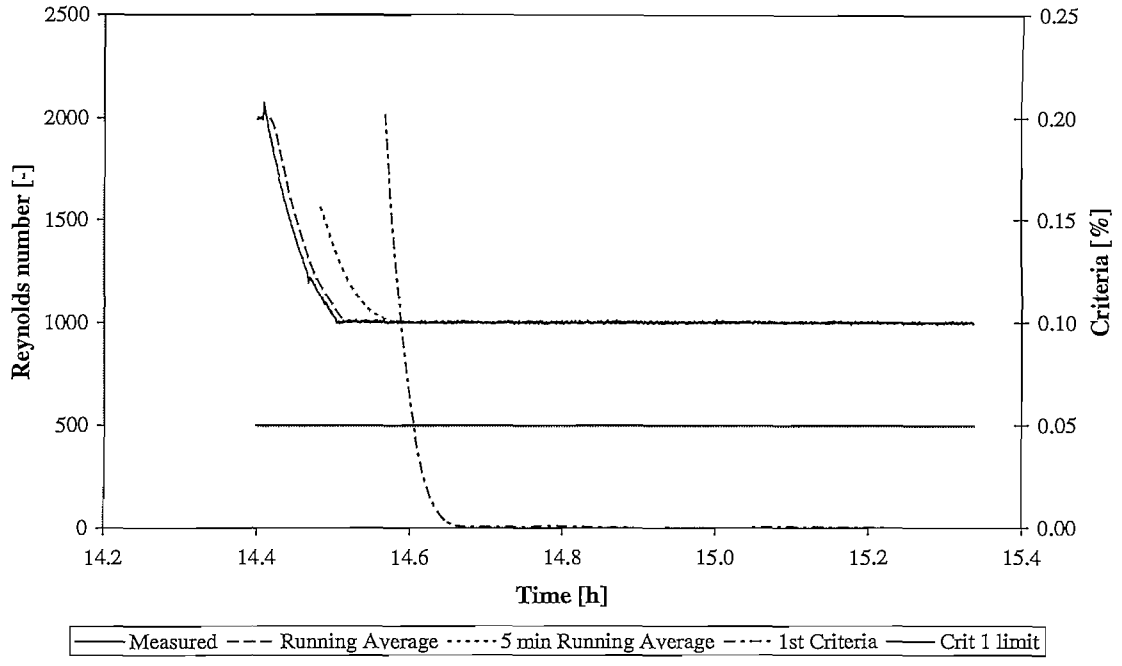

Figure 5-2: Illustration of Criteria 1 for a case with a fast transition between experiments.

Criteria 1 preformed very well when the transition from one experiment to another is relatively quick, Figure 5-2. However when for slow transitions, Criteria 1 can fail, as shown in Figure 5-3. Thus a second criterion is needed to avoid this.

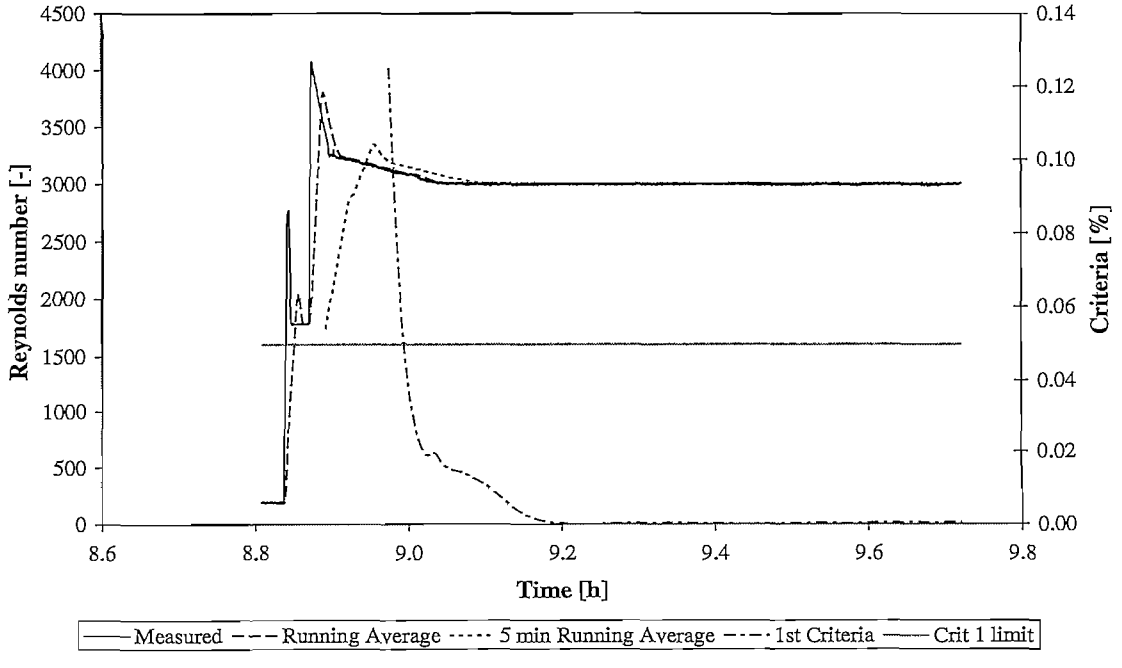

Figure 5-3: Illustration of Criteria 1 for a case with relative slow transition between experiments.

5.4.2 Criteria 2: Normalized slope

Criteria 2 is described by Equation 5-2 and is based on the normalized slope of the one minute running average. The difference of the one minute running average at time t_1 and t_2 is normalized with the average between the values taken at t_1 and t_2, with t_1 and t_2 sixty seconds apart. The calculated slope is then averaged over five minutes. It was found that when the averaged value is less than 0.004% the system has reached steady-state, Figure 5-4.

$$\left| Average_{5\min} \left(\frac{\frac{x_{Average_{1\min}}(t_2) - x_{Average_{1\min}}(t_1)}{(x_{Average_{1\min}}(t_2) + x_{Average_{1\min}}(t_1))/2}}{t_2 - t_1} \times 100 \right) \right| < 0.004\% \qquad (5\text{-}2)$$

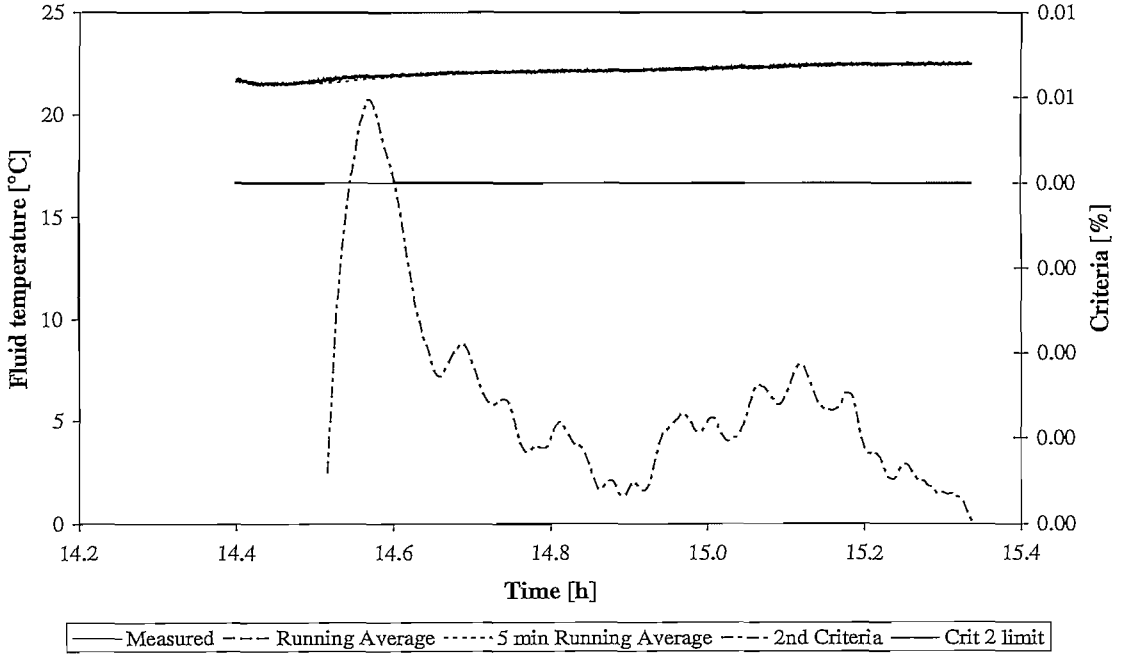

Figure 5-4: Illustration of the use of Criteria 2.

Following from the above discussion a variable can be deemed steady-state if both Criteria 1 and Criteria 2 are adhered to. All data logged as steady-state by the SCADA system adhere to

these two criteria and can thus be accepted as such. The following variables were used to determine steady-state:

- TSPV fluid inlet temperature, T_f.
- TSPV pressure, p_f.
- Reynolds number in test section, Re_0.
- Average surface temperature of the heated sphere, T_s.

Once all of the above four variables have reached steady-state the test can be said to have reached steady-state. Both Criteria 1 and Criteria 2 must be kept for five minutes in order to keep the data valid as steady-state for those five minutes. The five minute worth of data can then be used for further calculations.

5.5 Data processing

From the five minutes of steady-state data logged for each test the desired non-dimensional parameters can be calculated. The aim is to extract a heat transfer coefficient (Nusselt number) as well as a corresponding Reynolds number from the data. A thorough uncertainty analysis is also required in order to validate the data integrity. The data processing procedure will be discussed for test 1.1.1 as defined in Table 5-3 through the following sections. The processed data for the remainder of the tests can be found in Appendix C.

5.5.1 Geometrical

In Section 4.3 the geometrical features relevant to this calculation were discussed along with the uncertainty in these values, they are as follows:

- Hydraulic diameter, $d_p = 0.06m$
- Heated sphere heat transfer area, $A = 0.0113 \pm 0.000044 m^2$
- Cross sectional flow area in Test section, $A_{TS} = 0.08997 \pm 0.000011 m^2$

5.5.2 Fluid Temperature

The temperature at the inlet to the test sections was controlled at atmospheric temperature and measured with PT100 sensors. The instrument standard uncertainty calculated in Section 4.3.4 was found to be 0.04°C. The measured values of TT-200 and TT-201 (Figure A 1) resulted in an average fluid temperature of 23.48°C with a standard deviation in the measurement of 0.0365°C.

Since the instrument standard uncertainty is the largest of the two uncertainty values this value, 0.04°C, will be used as the standard uncertainty in calculations following. Thus $T_f = 23.48 \pm 0.04°C$. Fluid temperature data for all test conducted is presented in Table C 1.

5.5.3 Surface temperature

The average surface temperature is determined by measuring the temperatures at five points on the surface and taking the average of the five values. Table 5-4 compares the measured standard deviation with the instrument standard uncertainty.

Table 5-4: Comparison between thermocouple measured standard deviation and instrument standard uncertainty.

Thermocouple	Temperature [°C]	Measured standard deviation [°C]	Instrument standard uncertainty [°C]
TE-250	75.65	0.1406	0.2
TE-251	75.14	0.1770	0.2
TE-252	77.75	0.1208	0.2
TE-253	72.94	0.0266	0.2
TE-254	79.36	0.1338	0.2

For each thermocouple the largest of the two uncertainty values are used and implemented in Equation 4-17. The resultant average surface temperature is 76.17°C with an standard uncertainty of 0.08°C. Thus $T_s = 76.17 \pm 0.08°C$.

A variation in the measured thermocouple temperature values can be seen in Table 5-4. The maximum variation between the average temperature of the different thermocouples and the average surface temperature observed during the experiments is $3.23\,°C$. This variation could be due to the fact that the down-stream thermocouples might be situated in an eddy and thus experience different heat transfer compared to the up-stream thermocouples. Surface temperature data for all test conducted is presented in Table C 2.

5.5.4 Fluid properties

Fluid properties are calculated with a function of absolute pressure p_f and temperature T_f with the aid of a suitable real gas model for pure Nitrogen. Van der Merwe (2006:29) developed these functions for the HPTU SCADA system and is discussed in Appendix D. Three fluid properties are calculated:

- Fluid thermal conductivity, λ_f.
- Fluid viscosity, μ_f.
- Fluid density, ρ_f.

With T_f known, only p_f remains to be determined in order to determine the fluid properties with the above named functions. The average pressure at the inlet of the Test Section is found to be $101.60kPa$ with a standard deviation of $0.40kPa$. However in Section 4.3.6 the standard instrument uncertainty at $100kPa$ was found to be $0.5kPa$, thus the pressure will be taken as: $p_f = 101.60 \pm 0.5kPa$. Fluid pressure data for all test conducted is presented in Table C 3.

The partial derivatives of the fluid properties with respect to T_f and p_f for test 1.1.1 are calculated numerically with the aid of the functions in Appendix D. Below is the calculated partial derivates for test 1.1.1 as well as the standard uncertainty of the fluid properties obtained through the use of Equations 4-18, 4-19 and 4-20. These values differ slightly from the values in Table 4-2, Table 4-3 and Table 4-4 due to the fact that the values below is calculated for the specific test fluid temperature ($23.48\,°C$) and pressure ($101.60kPa$).

$$\frac{\partial \lambda_f}{\partial T_f} = 6.72\times10^{-5} \left[W/m\cdot K^2\right]; \qquad \frac{\partial \lambda_f}{\partial p_f} = 3.40\times10^{-7} \left[W/m\cdot K\cdot kPa\right]$$

$$\Delta\lambda_f = 3.36\times10^{-6} \quad \left[W/m\cdot K\right]$$

$$\frac{\partial\mu_f}{\partial T_f} = 4.63\times10^{-8} \quad \left[kg/m\cdot s\cdot K\right]; \qquad \frac{\partial\mu_f}{\partial p_f} = 1.56\times10^{-10} \quad \left[kg/m\cdot s\cdot kPa\right]$$

$$\Delta\mu_f = 2.31\times10^{-9} \quad \left[kg/m\cdot s\right]$$

$$\frac{\partial\rho_f}{\partial T_f} = -0.004 \quad \left[kg/m^3\cdot K\right]; \qquad \frac{\partial\rho_f}{\partial p_f} = 0.011 \quad \left[kg/m^3\cdot kPa\right]$$

$$\Delta\rho_f = 0.006 \quad \left[kg/m^3\right]$$

Thus the three fluid properties for test 1.1.1 are as follows:

- $\lambda_f = 0.0256 \pm 3.36\times10^{-6} \quad \left[W/m\cdot K\right]$
- $\mu_f = 0.000018 \pm 2.31\times10^{-9} \quad \left[kg/m\cdot s\right]$
- $\rho_f = 1.14 \pm 0.006 \quad \left[kg/m^3\right]$

Fluid property data for all test conducted is presented in Table C 4.

5.5.5 Heat transfer

Referring to Section 4.3.7 the convection heat transfer can be calculated with Equation 5-3. The heat loss via the thermocouples, $q_{TC,fin}$, is difficult to quantify. Many factors that plays a role in this heat transfer is not measurable in the current experimental setup. For example the CFD-code (Appendix B) assumes flow perpendicular to the thermocouple wire were as in reality it is not possible to determine the exact flow direction across the wire. Furthermore is the uncertainty in the heat transfer correlation for flow over a tube used in the CFD-code at least 20% in the calculated value (Incropera and De Witt, 2002:411). In order to obtain a analytical value to perform an valid data analyses the thermocouple heat loss will be ignored

$$q_{conv} = q_{elec} - q_{rad} - q_{TC\,fin} \tag{5-3}$$

Radiation heat transfer plays a major role in the heat losses. Recalling that the radiation heat transfer can be calculated with Equation 4-22 and the uncertainty in the radiation heat transfer with Equation 4-24 one obtains: $q_{rad} = 0.21 \pm 0.07 W$ for test case 1.1.1.

The average electrical power input is measured as $47.44 W$, which results in an instrument standard uncertainty of $0.52 W$. The measured standard deviation is calculated as $1.91 W$. With the measured standard deviation the largest the electrical power input can be taken as $q_{elec} = 47.44 \pm 1.91 W$. It can be easily seen that the resultant convection heat transfer coefficient is as follows:

with:

$$\Delta q_{conv} = \sqrt{\left(\frac{\partial q_{conv}}{\partial q_{rad}} \cdot \Delta q_{rad}\right)^2 + \left(\frac{\partial q_{conv}}{\partial q_{elec}} \cdot \Delta q_{elec}\right)^2} \tag{5-4}$$

$$q_{conv} = 45.38 \pm 1.91 W.$$

Heat transfer data for all test conducted is presented in Table C 5.

5.5.6 Heat transfer coefficient

With all the data calculated up to now the heat transfer coefficient can be calculated with Equations 4-1 and 4-34 and the partial derivatives is calculated as in Section 4.3.8. The resultant heat transfer for the single heated pebble in a homogeneous packed bed is calculated as:

$$\alpha = 79.62 \pm 3.22 \text{ [W/m}^2 \text{ K]}$$

Heat transfer coefficient data for all test conducted is presented in Table C 5.

5.5.7 Nusselt number

The non-dimensional parameter, Nusselt number, resulting from the heat transfer coefficient can be calculated with Equation 4-5 and the resulting standard uncertainty with Equation 4-39. The resulting Nusselt number is:

$$Nu = 186.43 \pm 15.10\ [-]$$

The standard uncertainty in the Nusselt number can also be given as 8.10%. Nusselt number data for all test conducted is presented in Table C 5.

5.5.8 Mass flow

The system mass flow as calculated with the help of Equation 4-44 and the average value is $0.03 kg/s$ with the measured standard deviation calculated as $0.0001 kg/s$. The calculation of the standard uncertainty in the mass flow due to the instrumentation is done with the same procedure as discussed in Section 4.3.10. Table 5-5 presents the calculated parameters in order to calculate the standard uncertainty in the mass flow.

Table 5-5: Parameters in the calculation of the standard uncertainty in the mass flow.

$\frac{\Delta C}{C}$	0.01	[-]
$\frac{\Delta \varepsilon}{\varepsilon}$	5.71×10^{-5}	[-]
$\frac{\Delta D_{OrPipe}}{D_{OrPipe}}$	0.00027	[-]
$\frac{\Delta d_{or}}{d_{or}}$	0.00060	[-]
$\frac{\Delta p_{Unc}}{\Delta p}$	0.0029	[-]
$\frac{\Delta \rho}{\rho}$	0.005	[-]

$\Delta \dot{m} / \dot{m}$	0.0105	[-]
$\Delta \dot{m}$	0.00028	[kg/s]

Since the calculated standard uncertainty is larger than the measured standard deviation, the mass flow through the Test section can be taken as $\dot{m} = 0.03 \pm 0.00028 kg/s$. Mass flow data for all test conducted is presented in Table C 6.

5.5.9 Reynolds number

Referring to the calculations for the Reynolds number in Section 4.3.11 the calculated Reynolds number is: Re_D = 999.95 with the measured standard deviation in the Reynolds number given as 2.35. Following from the standard uncertainty calculation in the Reynolds number as conducted in Section 4.3.11, the standard uncertainty is 21.06. Once again taking the more conservative value as the standard uncertainty the Reynolds number can be given as:

$$Re_D = 999.95 \pm 21.06$$

This results in an uncertainty of 2.11% in the Reynolds number measurement. Reynolds number data for all test conducted is presented in Table C 6.

5.6 Summary

This section took a closer look at the measurement technique used to obtain data for the calculation of a heat transfer coefficient (Nusselt number) for pebble-to-fluid convection heat transfer for given discrete homogeneous porosities. The heat transfer coefficient was measured for three homogeneous porosity packed beds in a Reynolds number range of 1000 to 50 000. Tests was conducted at 1000 Reynolds numbers intervals up to Re_D = 10 000 from where it was conducted in intervals of 10 000. In order to compare data for repeatability two sets of test were done for each homogeneous porosity Test section (28 x 3 = 84).

Two steady-state criteria were defined that help with the data capturing. The steady-state data was then processed to obtain two relevant non-dimensional numbers, Nusselt and Reynolds

number. Also included in the data process the determination of the standard uncertainty was illustrated. The maximum standard uncertainty in the Nusselt number resulted in 10.88% with the maximum standard uncertainty in the Reynolds number was found to be 2.11%.

The six sets of data (two per Test Section) were compared with each other in order to get an implication of the repeatability of the tests. The difference between the Nusselt numbers for each set was found to be less than 6.5%. It can be seen from Figure 6-1 that all data measured follows the same trend in the measured Nusselt number.

6 RESULTS

6.1 Measurement results

All applicable data measured for tests as in the test matrix, Table 5-3, were reduced in the process described in Section 5.5. Figure 6-1 provides a summary of test results for the pebble-to-fluid heat transfer in homogeneous porosity packed beds. The results of each homogeneous porosity Test Section is presented in two sets of measurements. Figure 6-1 presents the repeatability of the tests conducted. The maximum difference between Nusselt numbers measured for test run one and two is in the case of the 0.36 porosity test section. Table 6-1 presents these differences where the maximum of 6.42% can be found at Re_0 = 1000 for porosity $\varepsilon = 0.36$.

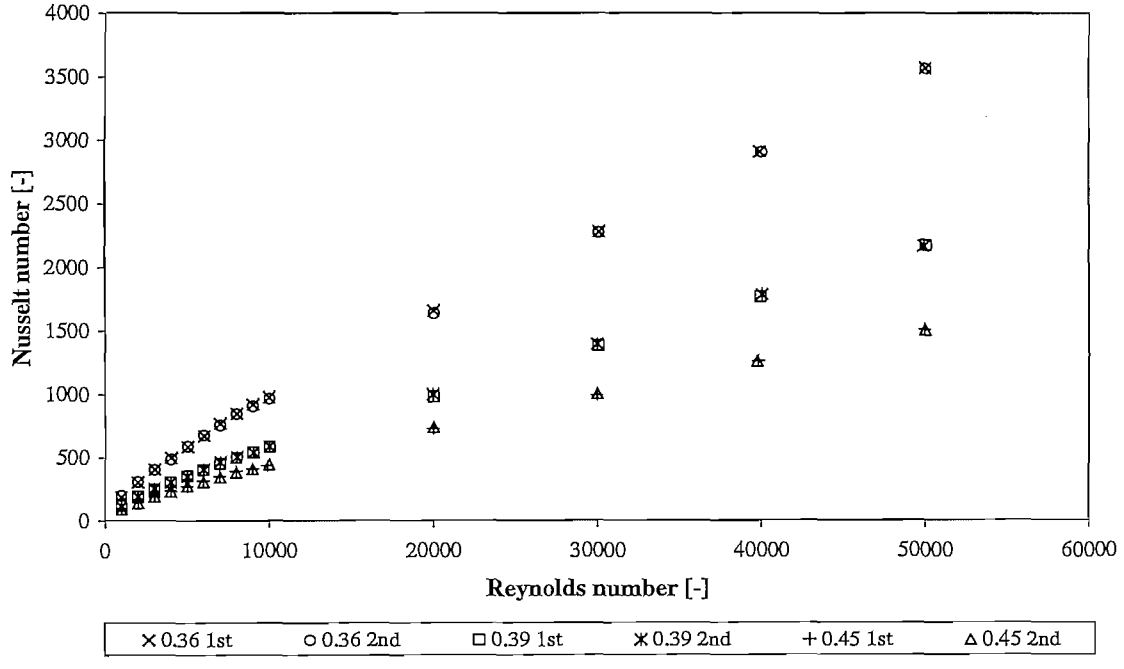

Figure 6-1: Graph of Nusselt number vs. Reynolds number indicating repeatability of data measured.

Table 6-1: Percentage difference between Nusselt numbers measured for test runs one and two.

Re_0	$\varepsilon = 0.36$ $\Delta Nu/Nu$ [%]	$\varepsilon = 0.39$ $\Delta Nu/Nu$ [%]	$\varepsilon = 0.45$ $\Delta Nu/Nu$ [%]
1 000	6.42	2.93	4.29
2 000	1.44	0.27	4.98
3 000	0.10	2.70	1.81
4 000	2.94	0.37	1.33
5 000	0.33	0.45	0.73
6 000	0.79	1.34	3.25
7 000	1.72	2.46	1.89
8 000	0.13	1.23	3.17
9 000	1.44	0.16	0.47
10 000	1.05	0.48	2.05
20 000	1.17	1.82	1.35
30 000	0.31	0.85	1.36
40 000	0.07	0.97	0.27
50 000	0.08	0.28	0.26

Figure 6-2 presents the summary of data standard uncertainty. Each data set has its own uncertainty range bars associated with it. The uncertainties are in all cases symmetrical around the data points. The largest uncertainty in the Nusselt number is 10.88% for the 0.36 porosity case at Reynolds number Re_0 = 4000. The largest uncertainty in the Reynolds number is 2.11% for the 0.36 and 0.39 porosity cases at Reynolds number Re_0 = 1000 for both cases.

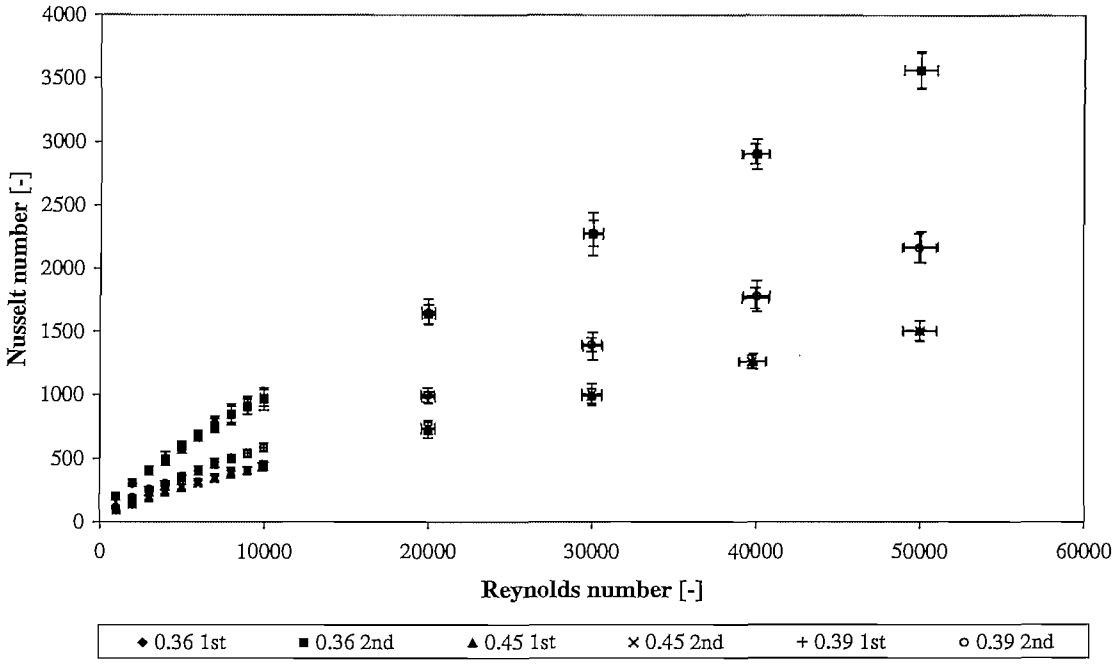

Figure 6-2: Summary of tests results for CCTS in terms of Nusselt number versus Reynolds number indicating the standard uncertainties.

6.2 Comparison with previous authors

Figure 6-3 compares results obtained in this study with pebble-to-fluid heat transfer correlations from authors as discussed in Section 2. At low Reynolds numbers, the experimental data and the correlations tend to converge to the same point. However with an increase in Reynolds number this difference increases drastically. The difference is at such a scale that even when the 20% uncertainty associated with the KTA (1983:2) correlation and the uncertainty of the measured data are taken into account, the values do not overlap. The difference is thus not a result of the uncertainty in measured values.

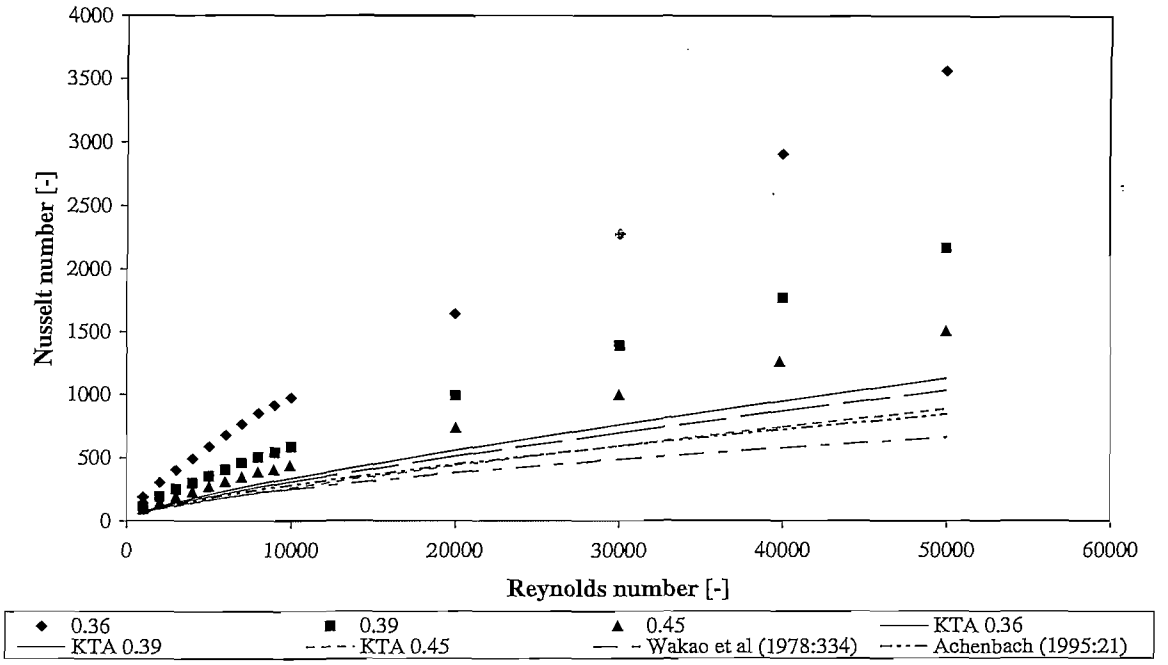

Figure 6-3: Comparison between the current study results and relevant authors work as mentioned in Section 2.

Graphically, the experimental HPTU data and correlations in Figure 6-3 exhibit the same trend in terms of the Reynolds number but not for porosity. This can be shown by comparing the relative values between the different porosities for the two sets of data, namely if:

$$\frac{Nu_{0.36\,KTA}}{Nu_{0.39\,KTA}} = \frac{Nu_{0.36\,HPTU}}{Nu_{0.39\,HPTU}} \tag{6-1}$$

$$\frac{Nu_{0.39\,KTA}}{Nu_{0.45\,KTA}} = \frac{Nu_{0.39\,HPTU}}{Nu_{0.45\,HPTU}} \tag{6-2}$$

The values for Equations 6-1 and 6-2 is given in Table 6-2 and illustrated by Figure 6-4. From Figure 6-4 it can be seen that Equations 6-1 and 6-2 are not valid for the data and thus there exists a difference in the data trends with regard to porosity. Furthermore, the error in Equation 6-1 is greater than the error in Equation 6-2:

$$\frac{Nu_{0.36\,KTA}}{Nu_{0.39\,KTA}} - \frac{Nu_{0.36\,HPTU}}{Nu_{0.39\,HPTU}} > \frac{Nu_{0.39\,KTA}}{Nu_{0.45\,KTA}} - \frac{Nu_{0.39\,HPTU}}{Nu_{0.45\,HPTU}} \tag{6-3}$$

which indicates the importance of the porosity in such tests.

Table 6-2: Relation between data sets at different porosity.

Re_0	$NU_{0.36KTA}$: $Nu_{0.39KTA}$	$Nu_{0.36HPTU}$: $Nu_{0.39HPTU}$	*Delta*	$NU_{0.39KTA}$: $Nu_{0.45KTA}$	$Nu_{0.39HPTU}$: $Nu_{0.45HPTU}$	*Delta*
1 000	1.09	1.66	0.57	1.177	1.232	0.055
2 000	1.10	1.59	0.49	1.174	1.355	0.180
3 000	1.09	1.61	0.52	1.174	1.316	0.143
4 000	1.10	1.63	0.53	1.171	1.297	0.126
5 000	1.09	1.66	0.57	1.174	1.297	0.124
6 000	1.09	1.67	0.58	1.173	1.297	0.125
7 000	1.09	1.67	0.57	1.172	1.327	0.155
8 000	1.09	1.69	0.60	1.173	1.303	0.130
9 000	1.09	1.69	0.60	1.171	1.328	0.157
10 000	1.09	1.66	0.57	1.176	1.333	0.157
20 000	1.09	1.66	0.57	1.169	1.348	0.179
30 000	1.09	1.64	0.55	1.170	1.392	0.222
40 000	1.09	1.64	0.55	1.174	1.406	0.232
50 000	1.09	1.64	0.55	1.168	1.440	0.272
Average	1.09	1.65	0.56	1.17	1.33	0.16

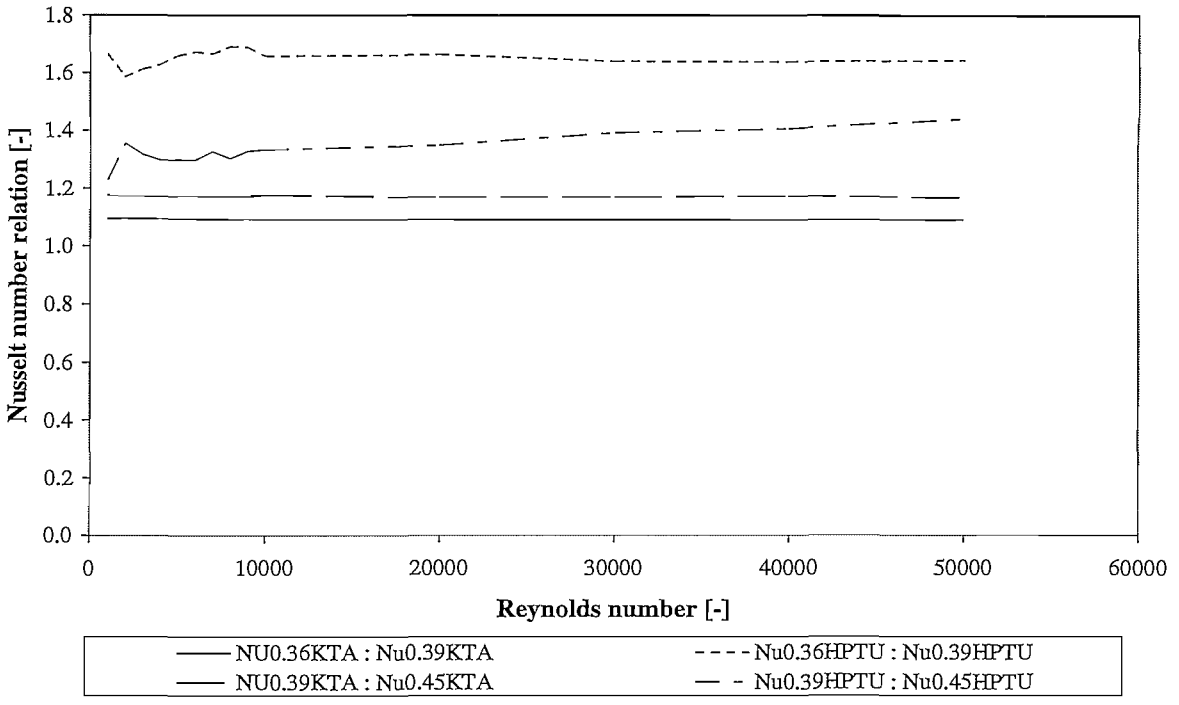

Figure 6-4: Graphical results from Table 6-2.

Since the porosities for the homogeneous test section and that of the KTA (1983:2) correlation is the same, the difference in the Nusselt numbers could be a result of the difference in the structure of the beds. The current study used homogeneous porosity test sections versus that of randomly packed beds that were employed in studies by other authors. This reason could not be confirmed through the literature survey (Section 2) and indicates that an unknown and very interesting phenomenon is uncovered. This porosity phenomenon will have to be investigated further in order to obtain a better conclusion with regards to the Nusselt number variations mentioned earlier and unfortunately falls outside the scope of this study.

7 CONCLUSIONS AND RECOMMENDATIONS

7.1 Summary of work

A literature survey provided the necessary background to the convective heat transfer phenomena in packed beds. In the literature survey the aspects that play a role in the convective heat transfer in packed beds were identified. Correlations for convective heat transfer in packed beds were also identified and investigated.

Since the purpose of this study is the measurement of heat transfer coefficients for pebble-to-fluid convection heat transfer for discrete homogeneous porosities, the necessary instrumentation was investigated. The role of instrument uncertainty can greatly influence measurements and an instrumentation uncertainty analysis was conducted.

The theoretical knowledge obtained in the literature survey ensured that the experiment could be conducted in a structured fashion. The experiment was conducted on the HPTU, a test facility designed and developed by M-Tech Industrial (Pty.) Ltd. for the PBMR (Pty) Ltd and made available by the company in order to conduct the experiment. The experiment was divided into 84 different tests (Table 5-3).

Data captured during tests was systematically processed as described in Section 5.5. From the processed data the relevant non-dimensional parameters were plotted, see Figure 6-2, along with the standard uncertainty for each data point. Repeatability of the data (Figure 6-1) as well as the comparison of the data with correlations from the literature survey were performed and graphically illustrated (Figure 6-3).

7.2 Conclusion

The instrumentation uncertainty in the calculated Nusselt number for the cases under investigation was found to be less than 2% and in the Reynolds number case less than 1.2%. Based on the 25% acceptable uncertainty levels in the design criteria used for the complete

HPTU test facility design (Rousseau, 2005:39), the maximum instrumentation standard uncertainty implies that the data measured is reliable.

From the results presented it can be concluded that the test sections used in HPTU test facility provided results with good repeatability and relatively low uncertainty values (maximum 10.88%). This uncertainty compares well with the uncertainty of the correlation of the Nuclear Safety Standards Commission (KTA) (1983:2) which is +20% with a confidence level of 95%.

Although the measured data from the HPTU exhibited the same trends as the correlation of the Nuclear Safety Standards Commission (KTA) (1983:2) in terms of the Reynolds number it was found that there is a difference in the trends with regard to porosity, Figure 6-4. Equation 6-3 indicates the importance of the porosity in such type of tests. With a decrease in porosity, where the spheres are closer to each other, the deviation between the correlation and measured data trend increases.

Furthermore the difference between the measured data and existing correlations indicates a deviation from previous researchers' findings. One possible reason for the difference is, that for this study structured homogeneous porosity beds were used where as previous researchers work was mainly conducted on randomly packed beds. Furthermore, the porosity for the HPTU Test Sections is homogeneous by design but the porosity for an infinitely small radial section in the bed could differ in the axial direction. This may result in a different flow field compared to a randomly packed bed with the same average porosity. This reason could not be confirmed through the literature survey (Section 2) and indicates that an unknown and very interesting phenomenon is uncovered in the structure of packed beds.

7.3 Recommendations for further work

7.3.1 Effect of bed structure at constant porosity

It could be feasible to investigate the porosity in homogeneous structured beds in order to get an even better understanding of heat transfer characteristics measured in this study and the factors influencing it. It should be investigated if the structured beds implemented in the HPTU, is homogeneous for every discretized section of the bed perpendicular to the flow direction. Comparison between different types of structured homogeneous porosity packed beds with the same porosity can reveal interesting convection heat transfer results.

7.3.2 Pebble-to-fluid heat transfer in randomly packed beds

A Test Section for pebble-to-fluid heat transfer measurements in a randomly packed bed could also be designed, implemented and tested in the HPTU. Results from such a test could also provide a link between the convective heat transfer observed in such beds and the current structured bed test sections. Furthermore results of a randomly packed bed in the HPTU can be compared with existing correlations.

7.3.3 Effect of pebble surface roughness

Test Sections implemented in the HPTU is constructed with smooth surfaced Acrylic spheres. Incorpera and De Witt (2002:329) note the effect of boundary layers on convection heat transfer. The change in boundary layers due to a change in surface roughness should be investigated since pebbles implemented in the PBMR is manufactured of graphite with a greater surface roughness.

7.3.4 Wall-to-fluid convective heat transfer

Although this study covered a large part of convective heat transfer in packed beds, it focussed on the convective heat transfer between a pebble and the gas for a homogeneous bed. The wall-to-fluid convective heat transfer experiment was not done in this study. The wall-to-fluid convective heat transfer could differ significantly from the pebble-to-fluid convective heat transfer due to the enormous porosity gradient close to the wall. The wall-to-fluid convective heat transfer plays a significant role in the heat removal from a pebble bed reactor, through the cooling channels such as those in the PBMR, as described in Section 1.1. This is an important safety aspect when designing packed bed reactors for excess heat removal from the core.

REFERENCES

Achenbach, E., Heat and flow characteristics of packed beds, Experimental Thermal and Fluid Science, vol. 10, pp. 17-27, 1995.

Allais, I., Alvarez, G., Analysis of heat transfer during mist chilling of a packed bed of spheres simulating foodstuffs, Journal of Food Engineering, vol. 49, pp. 37-47, 2000.

Boelhouwer, J.G., Piepers, H.W., Drinkenburg, A.A.H., Particle-liquid heat transfer in trickle-bed reactors, Chemical Engineering Science, vol. 56, pp. 1181-1187, 2001.

Bey, O., Eigenberger, G., Fluid flow through catalyst filled tubes, Chemical Engineering Science, vol. 52, pp. 1365-1376, 1997.

Borkink, J.G.H., Westerterp, K.R., Significance of the radial porosity profile for the description of heat transport in wall-cooled packed beds, Chemical Engineering Science, vol. 49, pp. 863-876, 1994.

Collier, A.P., Hayhurst, A.N., Richardson, J.L., Scott, S.A., The heat transfer coefficient between a particle and a bed (packed or fluidised) of much larger particles, Chemical Engineering Science, vol. 59, pp. 4613–4620, 2004.

Demirel, Y., Sharma, R.N., Al-Ali, H.H., On the effective heat transfer parameters in a packed bed, International Journal of Heat and Mass Transfer, vol. 43, pp. 327-332, 2000.

Dixon, A.G., DiCostanzo, M.A., Soucy, B.A., Fluid-phase radial transport in packed beds of low tube-to-particle diameter ratio, International Journal of Heat and Mass Transfer, vol. 27, pp. 1701-1713, 1984.

Dixon, A.G., Heat transfer in fixed beds at very low (<4) tube-to-particle diameter ratio, Industrial Engineering & Chemical Research, vol. 36, pp. 3053-3064, 1997.

Du Toit, C.G., Greyvenstein, G.P., Rousseau, P.G., A comprehensive reactor model for the integrated network simulation of the PBMR power plant, North West University, Potchefstroom, South Africa, 2003.

Gnielinski, V., Gleichungen zur Berechnung des Wärme- und Stoffaustausches in durchströmten ruhenden Kugelschüttungen bei mittleren und grossen Pecletzahlen, Verfahrenstechnik, vol. 12, pp. 63-366, 1978.

Goodling, J.S., Vachon, R.I., Stelpflug, W.S., Ying, S.J., Radial porosity distribution in cylindrical beds packed with spheres, Powder Technology, vol. 35, pp. 23-29, 1983.

Greyvenstein, G.P., Van Antwerpen, H.J., A finite volume-based network method for prediction of heat, mass and momentum transfer in a pebble bed reactor, 2nd Int. Topical meeting on high temperature reactor technology, Beijing, China, 2004.

Holman, J.P., Experimental methods for engineers, 6th. Ed., pp. 49-57, McGraw-Hill, Inc., ISBN 0-07-029666-9, 1994.

Hoogenboezem, T.A., High Pressure Test Unit CCTS 0.36 Test report, M-Tech rep. HPTU002-CCTS036, rev. A, 2006.

Incropera, F.P., DeWitt, D.P., Fundamentals of heat and mass transfer, 5th ed., pp. 244-245, Wiley, ISBN 0-471-38650-2, 2002.

Koster, A., Matzner, H.D., Nicholsi, D.R., PBMR design for the future, Nuclear Engineering and Design, vol. 222, pp. 231-245, 2002.

Küfner, R., Hofman, H., Implementation of radial and velocity distribution in a reactor model for heterogeneous catalytic gas phase reactions (TORUS-model), Chemical Engineering Science, vol. 45, no.8, pp. 2141-2146, 1990.

Labuschagne, J.T., High pressure test unit thermal-fluid design report, M-Tech rep. HTTF001-0009.2, rev. 3, 2005.

Labuschagne, J.T., High pressure test unit test plan, M-Tech rep. HTTF001-0003, rev. 3, 2006.

Malan, A.G., Visser, C., Meyer, J.P., Continuum thermodynamic modelling of a Pebble-bed Modular Reactor, University of Pretoria, South Africa, 2004.

Marivoet, J., Teodoroiu, P., Wajc, S.J., Porosity, velocity and temperature profiles in cylindrical packed beds, Chemical Engineering Science, vol. 29, pp. 1836-1840, 1974.

Nuclear Safety Standards Commission, Reactor core design of high-temperature gas-cooled reactors, Part 2: Heat transfer in spherical fuel elements, KTA 3102.2, 1983.

Romkes, S.J.P., Dautzenberg, F.M., Van den Bleek, C.M., Calis, H.P.A., CFD modelling and experimental validation of particle-to-fluid mass and heat transfer in a packed bed at very low channel to particle diameter ratio, Chemical Engineering Journal, vol. 96, pp. 3-13, 2003.

Rousseau, P.G., Equations and input parameters for the PBMR pebble bed reactor simulation model, M-Tech mechanical, Potchefstroom, South Africa, 1999.

Rousseau, P.G., Uncertainty analysis of expected results from the HTTF plant design, M-Tech rep. HTTF001-0031.1, rev. 2, 2006.

Rousseau, P.G., Heat transfer test facility test specification, M-Tech rep. HTTF001-0008.1, rev. 3, 2005.

Smirnov, E.I., Muzykantov, A.V., Kuzmin, V.A., Kronberg, A.E., Zolotarskii, I.A., Radial heat transfer in packed beds of spheres, cylinders and Rashig rings. Verification of model with linear variation of λ_{er} in the vicinity of the wall, Chemical Engineering Journal, vol. 91, pp. 243-248, 2003.

Tsotsas, E., Schlünder, E.U., Heat transfer in packed beds with fluid flow: Remarks on the meaning and the calculation of a heat transfer coefficient at the wall, Chemical Engineering Science, vol. 45, pp. 819-837, 1990.

Van Antwerpen, H.J., Greyvenstein, G.P., HTGR Thermal-Fluid Analysis – Part 1, Lecture Notes, North West University, Potchefstroom Campus, Postgraduate School for Nuclear Engineering, 2006.

Van der Merwe, J., HPTU PDTS 0.36 Test Report, M-Tech rep. HPTU001-PDTS036, rev. 1, 2006.

Van der Walt, A.J.K., Orifice flow meter instalation review, M-Tech rep. HPTU001-0034, rev. 1, 2006.

Vortmeyer, D., Haidegger, E., Discrimination of three approaches to evaluate heat fluxes for wall-cooled fixed bed chemical reactors, Chemical Engineering Science, vol. 46, pp. 2651-2660, 1991.

Vortmeyer, D., Shuster, J., Evaluation of steady flow profiles in rectangular and circular packed beds by a variational method, Chemical Engineering Science, vol. 38, pp. 1691-1699, 1983.

Wakao, N., Kaguei, S., Funazkri, T., Effect of fluid dispersion coefficients on particle-to-fluid heat transfer coefficients in packed beds, Chemical Engineering Science, vol. 34, pp. 325-336, 1978.

Winterberg, M., Tsotsas., E., Modelling of heat transport in beds with spherical particles for various bed geometries and/or thermal boundary conditions, International Journal of Thermal Science, vol. 39, pp. 556-570, 1999.

APPENDIXES

Appendix A

Instrumentation of HPTU

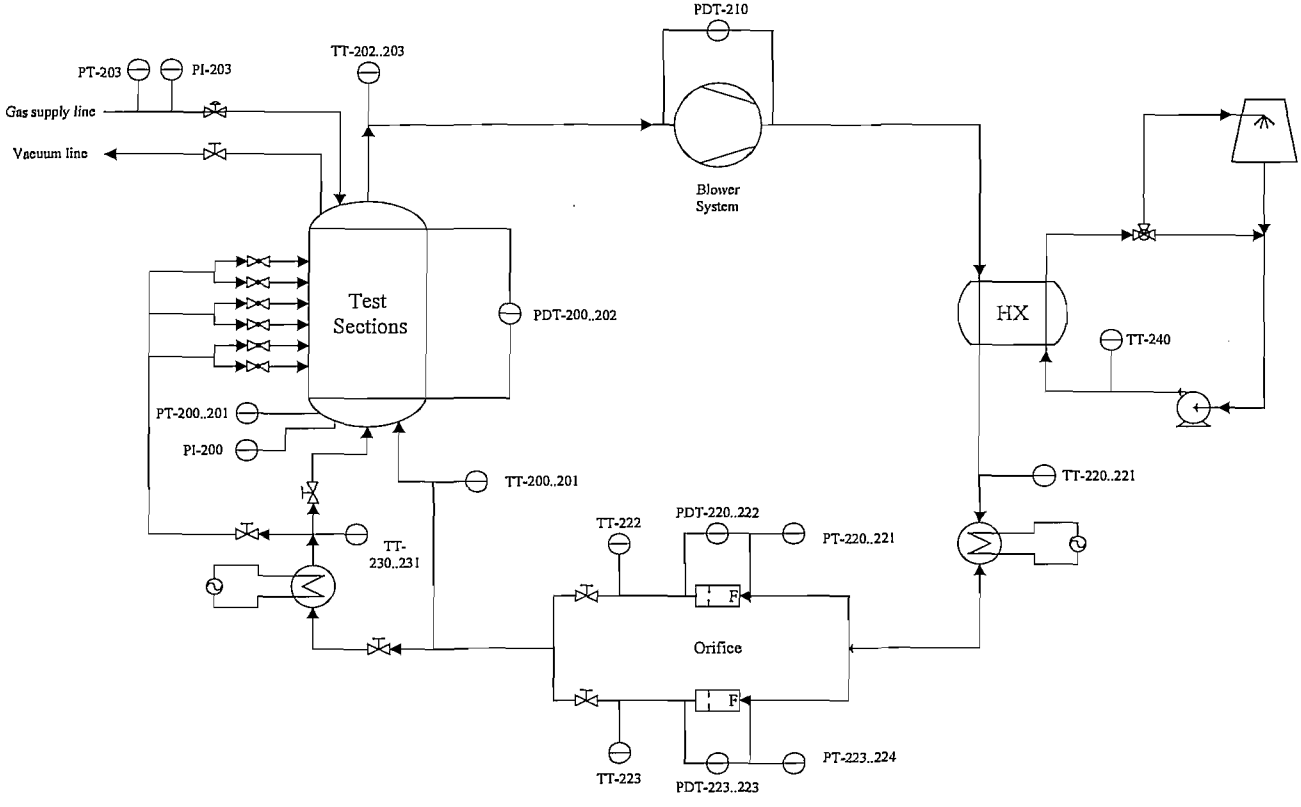

Figure A 1: Schematic layout of HPTU with instrumentation.

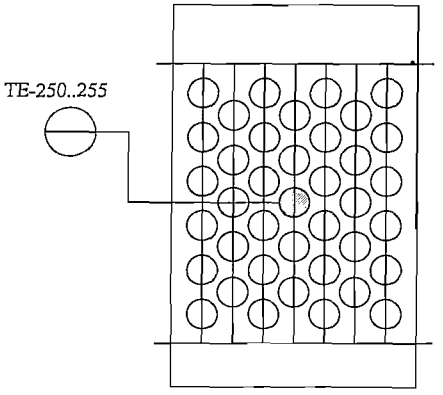

(a)

Figure A 2: Schematic layout of the CCTS.

Table A 1: Table of instruments for HPTU with reference to Figure A 1 and Figure A 2.

Instrument tag no.	Description	Model	Range	Uncertainty
PDT-200	Vessel pressure drop Low	Deltabar S	0-1 *kPa*	0.15%
PDT-201	Vessel pressure drop Med	Deltabar S	0-10 *kPa*	0.075%
PDT-202	Vessel pressure drop High	Deltabar S	0-50 *kPa*	0.075%
PDT-210	Blower pressure difference	Deltabar S	0-300 *kPa*	0.075%
PDT-220	Orifice 220 Pressure difference Low	Deltabar S	0-1 *kPa*	0.15%
PDT-221	Orifice 220 Pressure difference Med	Deltabar S	0-10 *kPa*	0.075%
PDT-222	Orifice 220 Pressure difference High	Deltabar S	0-50 *kPa*	0.075%
PDT-223	Orifice 221 Pressure difference Low	Deltabar S	0-1 *kPa*	0.15%
PDT-224	Orifice 221 Pressure difference Med	Deltabar S	0-10 *kPa*	0.075%
PDT-225	Orifice 221 Pressure difference High	Deltabar S	0-50 *kPa*	0.075%
PI-200	System pressure indicator		100-5500 *kPa*	
PI-203	Nitrogen supply pressure indicator		100-5500 *kPa*	
PT-200	System pressure Low	Unitrans	0-1600 *kPa*	1.6
PT-201	System pressure High	S10	0-6000 *kPa*	30
PT-203	Nitrogen supply pressure	S10	100-5500 *kPa*	30
PT-220	Orifice 220 pressure Low	Unitrans	0-1600 *kPa*	1.6
PT-221	Orifice 220 pressure High	S10	0-6000 *kPa*	30
PT-223	Orifice 221 pressure Low	Unitrans	0-1600 *kPa*	1.6
PT-224	Orifice 221 pressure High	S10	0-6000 *kPa*	30
TE-250..255	CCTS sphere surface temperature	TC Type T	0-100 *°C*	$0.004\|T\|$
TT-200	Vessel inlet temperature	PT100	0-100*°C*	$0.15 + 0.002\|T\|$
TT-201	Vessel inlet temperature	PT100	0-100*°C*	$0.15 + 0.002\|T\|$
TT-202	Vessel outlet temperature	PT100	0-100*°C*	$0.15 + 0.002\|T\|$
TT-203	Vessel outlet temperature	PT100	0-100*°C*	$0.15 + 0.002\|T\|$
TT-220	HX gas outlet temperature	PT100	0-100*°C*	$0.15 + 0.002\|T\|$
TT-221	HX gas outlet temperature	PT100	0-100*°C*	$0.15 + 0.002\|T\|$
TT-222	Orifice 220 temperature	PT100	0-100*°C*	$0.15 + 0.002\|T\|$
TT-223	Orifice 221 temperature	PT100	0-100*°C*	$0.15 + 0.002\|T\|$
TT-230	Braiding flow temperature	PT100	0-150*°C*	$0.15 + 0.002\|T\|$
TT-231	Braiding flow temperature	PT100	0-150*°C*	$0.15 + 0.002\|T\|$
TT-240	Cooled water temperature	PT100	0-100*°C*	$0.15 + 0.002\|T\|$

Appendix B

CFD code for the calculation of the heat loss through thermocouples acting as fins on the heated sphere.

File:CFD - THERMOCOUPLE HEAT LOSS.EES 6/8/2006 11:18:45 AM Page 1
EES Ver. 7.450: #0753: Mechanical & Materials Engineering, North-West University, Potchefstroom, South Africa

```
"!  CFD - simulation for flow through a packed bed

    T.A.Hoogenboezem
    26/01/2006

    v

Comments:

"!  Procedures

Procedure  Nusselt(Re, Pr, Pr_s : Nus)
  If [(Re > 1) and (Re <= 40)] Then
      C := 0.75
      m := 0.4
    Else
      If [(Re > 40) and (Re <= 1000)] Then
          C := 0.51
          m := 0.5
        Else
          If [(Re > 10^3) and (Re <= 200000)] Then
              C := 0.26
              m := 0.6
            Else
              If [(Re > 200000) and (Re <= 10^8)] Then
                  C := 0.076
                  m := 0.7
                Else
                  C := 1
                  m := 1
              EndIf
          EndIf
      EndIf
  EndIf
```

If [Pr <= 10] Then

n := 0.37

Else

n := 0.36

EndIf

$$Nus := C \cdot Re^{m} \cdot Pr^{n} \cdot \left[\frac{Pr}{Pr_s}\right]^{[1/4]}$$

End Nusselt

Geometry

$$A = \pi \cdot \frac{D^2}{4} \quad [m^2]$$

D = 0.001 [m]

L = 2 [m]

Grid

---

n = 50 *nodes*

$$\Delta x = \frac{L}{n}$$

$$\Delta L_i = i \cdot \Delta x \quad \text{for } i = 1 \text{ to } n$$

Boundary conditions

$$T_{inv} = \frac{T_{c,g} + T_{c,l}}{2} \quad [K]$$

$T_0 = T_s$

$T_{51} = T_{50}$

Properties

$$p = \frac{P_{core,g} + P_{core,l}}{2}$$

Pr = Pr ['Nitrogen', T = T_{inv}, P = p]

$$k_f = \frac{k\,['Nitrogen', T = T_{inv}, P = p\,]}{1000}$$

$$k = \frac{16.6 - \left[(16.6 - 12.6) \cdot \left(\frac{400 - T_{inv}}{400 - 200}\right)\right]}{1000}$$

$$Pr_{s,i} = Pr\,['Nitrogen', T = T_i, P = p\,] \quad \text{for } i = 1 \text{ to } n$$

Call $Nusselt[Re, Pr, Pr_{s,i} : Nus_i]$ for $i = 1$ to n

$$h_i = Nus_i \cdot \frac{k_f}{D} \quad \text{for } i = 1 \text{ to } n$$

$$c_i^2 = \frac{h_i \cdot D}{k \cdot A} \quad \text{for } i = 1 \text{ to } n$$

==========

Energy conservation

==========

$$a_{W,1} = 0$$

$$a_{E,1} = \frac{1}{\Delta x}$$

$$S_{p,1} = -c_1^2 \cdot \Delta x - \frac{2}{\Delta x}$$

$$S_{u,1} = c_1^2 \cdot \Delta x \cdot T_{inv} + 2 \cdot \frac{T_s}{\Delta x}$$

$$a_{W,50} = \frac{1}{\Delta x}$$

$$a_{E,50} = 0$$

$$S_{p,50} = -c_{50}^2 \cdot \Delta x$$

$$S_{u,50} = c_{50}^2 \cdot \Delta x \cdot T_{inv}$$

$$a_{W,i} = \frac{1}{\Delta x} \quad \text{for } i = 2 \text{ to } n-1$$

$$a_{E,i} = \frac{1}{\Delta x} \quad \text{for } i = 2 \text{ to } n-1$$

$$S_{p,i} = -c_i^2 \cdot \Delta x \quad \text{for } i = 2 \text{ to } n-1$$

$$S_{u,i} = c_i^2 \cdot \Delta x \cdot T_{inv} \quad \text{for } i = 2 \text{ to } n-1$$

$$a_{P,i} = a_{W,i} + a_{E,i} - S_{p,i} \quad \text{for } i = 1 \text{ to } n$$

$$a_{P,i} \cdot T_i = a_{W,i} \cdot T_{i-1} + a_{E,i} \cdot T_{i+1} + S_{u,i} \quad \text{for } i = 1 \text{ to } n$$

==========

Heat loss

==========

$$q_i = h_i \cdot \pi \cdot D \cdot \Delta x \cdot [T_i - T_{inv}] \quad \text{for } i = 1 \text{ to } n$$

File:CFD - THERMOCOUPLE HEAT LOSS.EES 6/8/2006 11:18:45 AM Page 4
EES Ver. 7.450: #0753: Mechanical & Materials Engineering, North-West University, Potchefstroom, South Africa

$$q_{loss} = \sum_{i=1}^{n} [q_i]$$

==========

Parametric table input

==========

Re = 1000 [-]

$p_{core,e}$ = 100 [kPa]

$p_{core,i}$ = 100 [kPa]

$T_{g,e}$ = 85 + 273.15 [K]

$T_{g,i}$ = 85 + 273.15 [K]

T_s = 85 + 273.15

SOLUTION

Unit Settings: [kJ]/[K]/[kPa]/[kg]/[degrees]

A = 7.854E-07 [m^2]	D = 0.001 [m]	Δx = 0.04 [m]
k = 0.01576 [kW/m K]	k_f = 0.00002976 [kW/m K]	L = 2 [m]
n = 50 [-]	p = 100 [kPa]	Pr = 0.7312 [-]
$p_{core,e}$ = 100 [kPa]	$p_{core,i}$ = 100 [kPa]	q_{loss} = 1.302E-13 [kW]
Re = 1000 [-]	$T_{g,e}$ = 358.2	$T_{g,i}$ = 358.2
T_{inv} = 358.2 [K]	T_s = 358.2 [K]	

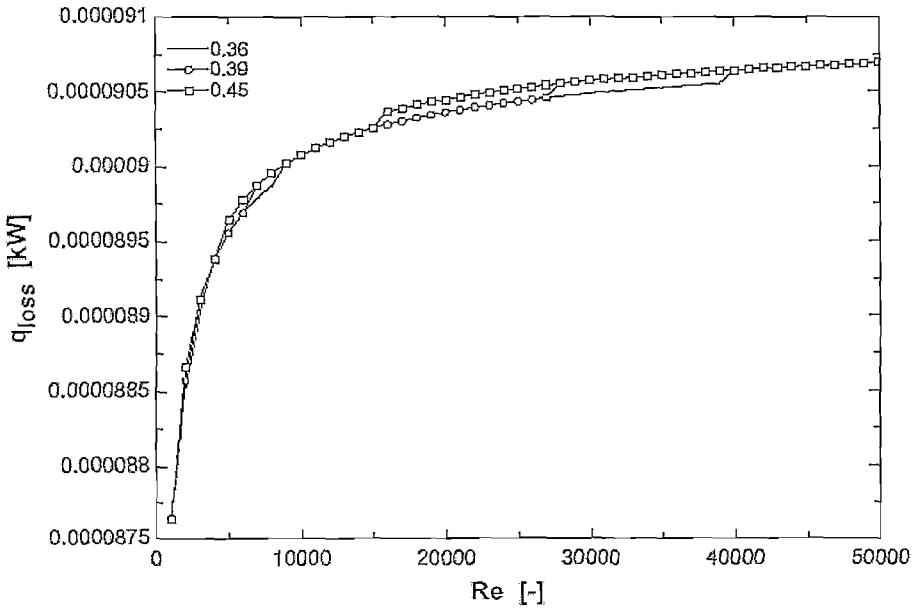

Appendix C

Average values of measured data for all test cases.

Table C 1 Fluid temperature data.

Test No.	Test Section	Reynolds number	TT-200 [°C]	TT-200 [°C]	T_f [°C]	σ_{TT-200} [°C]	σ_{TT-201} [°C]	σ_{Tf} [°C]
1.1.1	CCTS 0.36	1000	23.41	23.56	23.48	0.04	0.05	0.04
1.1.2		2000	21.83	21.95	23.48	0.04	0.03	0.03
1.1.3		3000	22.04	22.13	23.48	0.04	0.04	0.03
1.1.4		4000	22.18	22.30	23.48	0.03	0.04	0.03
1.1.5		5000	22.30	22.37	23.48	0.04	0.04	0.03
1.1.6		6000	22.42	22.46	23.48	0.04	0.06	0.04
1.1.7		7000	22.37	22.41	23.48	0.05	0.05	0.04
1.1.8		8000	22.31	22.41	23.48	0.04	0.04	0.03
1.1.9		9000	22.19	22.31	23.48	0.05	0.05	0.04
1.1.10		10000	22.06	22.23	23.48	0.03	0.04	0.03
1.1.11		20000	20.54	20.91	23.48	0.06	0.04	0.04
1.1.12		30000	20.51	20.90	23.48	0.06	0.04	0.04
1.1.13		40000	20.53	20.88	23.48	0.04	0.06	0.04
1.1.14		50000	20.56	20.90	23.48	0.03	0.04	0.03
1.2.1		1000	22.34	22.59	22.47	0.04	0.04	0.03
1.2.2		2000	21.41	21.77	22.47	0.05	0.04	0.04
1.2.3		3000	20.55	20.89	22.47	0.05	0.05	0.04
1.2.4		4000	20.38	20.72	22.47	0.03	0.04	0.03
1.2.5		5000	20.24	20.55	22.47	0.03	0.03	0.03
1.2.6		6000	19.96	20.34	22.47	0.03	0.07	0.04
1.2.7		7000	20.52	20.94	22.47	0.04	0.05	0.04
1.2.8		8000	20.65	21.02	22.47	0.04	0.04	0.03
1.2.9		9000	20.68	21.04	22.47	0.03	0.03	0.03
1.2.10		10000	20.72	21.05	22.47	0.04	0.04	0.03
1.2.11		20000	20.65	21.04	22.47	0.03	0.03	0.03
1.2.12		30000	20.52	21.00	22.47	0.08	0.05	0.05
1.2.13		40000	20.54	20.90	22.47	0.05	0.04	0.03
1.2.14		50000	20.55	20.90	22.47	0.03	0.04	0.03
2.1.1	CCTS 0.39	1000	25.82	26.15	25.98	0.04	0.04	0.03
2.1.2		2000	26.55	26.82	25.98	0.04	0.04	0.03
2.1.3		3000	26.57	26.82	25.98	0.05	0.04	0.03
2.1.4		4000	26.51	26.78	25.98	0.04	0.05	0.04

2.1.5		5000	22.41	22.70	25.98	0.04	0.04	0.04
2.1.6		6000	22.63	22.94	25.98	0.04	0.04	0.03
2.1.7		7000	22.85	23.01	25.98	0.05	0.04	0.03
2.1.8		8000	22.90	23.05	25.98	0.04	0.03	0.03
2.1.9		9000	22.97	23.10	25.98	0.04	0.05	0.04
2.1.10		10000	22.94	23.09	25.98	0.05	0.05	0.04
2.1.11		20000	22.78	23.03	25.98	0.04	0.04	0.03
2.1.12		30000	22.74	22.93	25.98	0.05	0.04	0.03
2.1.13		40000	22.72	22.93	25.98	0.05	0.03	0.04
2.1.14		50000	22.61	22.86	25.98	0.04	0.05	0.04
2.2.1		1000	24.72	25.01	24.87	0.06	0.06	0.05
2.2.2		2000	23.09	23.27	24.87	0.05	0.05	0.05
2.2.3		3000	22.01	22.20	24.87	0.05	0.05	0.05
2.2.4		4000	20.25	20.54	24.87	0.03	0.04	0.03
2.2.5		5000	19.34	19.62	24.87	0.06	0.04	0.04
2.2.6		6000	23.04	23.20	24.87	0.05	0.03	0.03
2.2.7		7000	23.07	23.28	24.87	0.04	0.05	0.03
2.2.8		8000	23.06	23.28	24.87	0.03	0.05	0.03
2.2.9		9000	22.97	23.17	24.87	0.04	0.03	0.03
2.2.10		10000	22.89	23.05	24.87	0.06	0.04	0.04
2.2.11		20000	22.79	22.93	24.87	0.04	0.03	0.03
2.2.12		30000	22.50	22.75	24.87	0.04	0.04	0.03
2.2.13		40000	22.79	22.93	24.87	0.04	0.03	0.03
2.2.14		50000	22.61	22.77	24.87	0.04	0.03	0.03
3.1.1	CCTS 0.45	1000	24.02	24.40	24.21	0.05	0.04	0.03
3.1.2		2000	24.67	25.04	24.21	0.04	0.04	0.03
3.1.3		3000	24.79	25.14	24.21	0.06	0.05	0.04
3.1.4		4000	24.84	25.25	24.21	0.03	0.04	0.03
3.1.5		5000	24.78	25.20	24.21	0.05	0.06	0.03
3.1.6		6000	24.78	25.15	24.21	0.04	0.04	0.03
3.1.7		7000	24.72	25.19	24.21	0.04	0.05	0.04
3.1.8		8000	24.76	25.14	24.21	0.04	0.04	0.04
3.1.9		9000	21.97	22.30	24.21	0.05	0.05	0.04
3.1.10		10000	22.08	22.43	24.21	0.04	0.05	0.03
3.1.11		20000	23.05	23.37	24.21	0.04	0.05	0.04
3.1.12		30000	23.03	23.30	24.21	0.04	0.05	0.04
3.1.13		40000	23.04	23.33	24.21	0.04	0.05	0.04
3.1.14		50000	23.22	23.52	24.21	0.06	0.04	0.04
3.2.1		1000	25.07	25.39	25.23	0.05	0.04	0.04

3.2.2		2000	24.44	24.73	25.23	0.06	0.06	0.05
3.2.3		3000	23.64	23.85	25.23	0.04	0.04	0.03
3.2.4		4000	23.38	23.59	25.23	0.03	0.03	0.03
3.2.5		5000	23.18	23.45	25.23	0.03	0.04	0.03
3.2.6		6000	23.09	23.41	25.23	0.04	0.03	0.03
3.2.7		7000	22.93	23.22	25.23	0.05	0.05	0.04
3.2.8		8000	22.97	23.30	25.23	0.03	0.05	0.03
3.2.9		9000	22.97	23.31	25.23	0.03	0.05	0.04
3.2.10		10000	23.07	23.42	25.23	0.04	0.04	0.03
3.2.11		20000	23.25	23.52	25.23	0.06	0.04	0.04
3.2.12		30000	23.18	23.46	25.23	0.04	0.04	0.03
3.2.13		40000	23.23	23.52	25.23	0.07	0.04	0.04
3.2.14		50000	23.15	23.45	25.23	0.05	0.05	0.04

Table C 2: Surface temperature data.

Test No.	Test Section	Reynolds number	TE-250 [°C]	TE-251 [°C]	TE-252 [°C]	TE-253 [°C]	TE-254 [°C]	T_s [°C]	Max TE difference form T_s	σ_{TE-250} [°C]	σ_{TE-251} [°C]	σ_{TE-252} [°C]	σ_{TE-253} [°C]	σ_{TE-254} [°C]	σ_{Ts} [°C]
1.1.1	CCTS 0.36	1000	75.65	75.14	77.75	72.94	79.36	76.17	3.23	0.14	0.18	0.12	0.03	0.13	0.0
1.1.2		2000	74.32	77.12	73.44	78.22	75.40	75.40	2.82	0.26	0.16	0.16	0.08	0.25	0.1
1.1.3		3000	73.90	77.47	74.22	77.08	75.10	75.10	2.37	0.32	0.17	0.25	0.06	0.31	0.1
1.1.4		4000	75.19	79.24	76.22	77.50	76.29	76.29	2.99	0.52	0.24	0.32	0.19	0.37	0.1
1.1.5		5000	74.63	79.08	76.38	76.50	75.82	75.82	3.32	0.41	0.15	0.26	0.05	0.28	0.1
1.1.6		6000	75.21	79.93	77.91	76.99	76.62	76.62	3.55	0.51	0.16	0.27	0.06	0.26	0.1
1.1.7		7000	74.76	79.99	78.46	76.93	76.62	76.62	3.66	0.66	0.43	0.67	0.21	0.42	0.2
1.1.8		8000	72.40	77.90	76.55	74.69	74.42	74.42	3.88	0.47	0.21	0.41	0.13	0.36	0.1
1.1.9		9000	73.24	79.25	78.24	75.91	75.68	75.68	3.93	0.77	0.24	0.31	0.13	0.33	0.1
1.1.10		10000	71.32	77.55	76.95	74.52	74.16	74.16	3.72	0.69	0.24	0.35	0.14	0.33	0.1
1.1.11		20000	66.22	72.75	76.79	72.43	71.71	71.71	5.49	1.40	0.27	0.36	0.08	0.42	0.3
1.1.12		30000	64.73	75.01	78.27	71.98	72.22	72.22	7.48	1.20	0.29	0.43	0.20	0.40	0.2
1.1.13		40000	63.61	74.60	80.03	71.82	72.40	72.40	8.78	1.18	0.27	0.48	0.12	0.37	0.2
1.1.14		50000	63.11	74.85	82.02	72.26	73.09	73.09	9.99	1.09	0.34	0.49	0.10	0.42	0.2
1.2.1		1000	70.35	73.01	68.49	74.60	71.53	71.53	3.08	0.18	0.17	0.17	0.14	0.22	0.0
1.2.2		2000	70.62	73.40	69.64	75.23	71.89	71.89	3.34	0.18	0.14	0.15	0.07	0.15	0.0
1.2.3		3000	72.72	76.44	72.68	77.50	74.30	74.30	3.21	0.38	0.16	0.20	0.10	0.24	0.1
1.2.4		4000	72.85	76.91	73.61	77.06	74.43	74.43	2.71	0.54	0.26	0.31	0.18	0.44	0.1
1.2.5		5000	70.69	74.96	72.20	74.15	72.22	72.22	3.12	0.57	0.18	0.24	0.08	0.34	0.1
1.2.6		6000	70.34	74.91	72.51	73.49	72.02	72.02	3.17	0.48	0.19	0.27	0.08	0.37	0.1
1.2.7		7000	72.09	77.20	75.06	75.55	74.03	74.03	3.77	0.64	0.19	0.27	0.10	0.42	0.1
1.2.8		8000	70.49	75.71	74.20	74.03	72.67	72.67	3.76	0.80	0.34	0.54	0.38	0.47	0.2
1.2.9		9000	70.89	76.49	75.34	74.69	73.44	73.44	3.66	0.71	0.32	0.46	0.23	0.37	0.2
1.2.10		10000	70.47	76.84	75.68	75.14	73.80	73.80	3.34	1.84	0.32	0.31	0.15	0.56	0.4
1.2.11		20000	66.23	74.57	76.16	72.83	71.91	71.91	5.69	1.35	0.27	0.41	0.13	0.42	0.3
1.2.12		30000	65.01	74.70	78.67	73.08	72.60	72.60	7.59	1.08	0.26	0.42	0.08	0.45	0.2
1.2.13		40000	64.51	75.47	81.07	73.37	73.48	73.48	8.97	0.91	0.29	0.51	0.10	0.44	0.2
1.2.14		50000	62.63	74.19	81.22	71.82	72.54	72.54	9.91	1.02	0.35	0.47	0.10	0.40	0.2
2.1.1	CCTS 0.39	1000	86.69	85.15	77.27	65.84	79.00	79.00	13.15	0.18	0.15	0.12	0.05	0.05	0.0
2.1.2		2000	90.84	89.34	81.84	68.64	82.91	82.91	14.27	0.34	0.27	0.29	0.26	0.19	0.1

2.1.3		3000	86.45	84.51	78.31	65.20	78.73	78.73	13.53	0.29	0.27	0.26	0.15	0.12	0.1
2.1.4		4000	85.07	82.78	77.37	63.89	77.32	77.32	13.43	0.39	0.27	0.31	0.21	0.15	0.1
2.1.5		5000	83.68	81.84	75.93	61.26	75.64	75.64	14.37	0.47	0.23	0.52	0.08	0.10	0.1
2.1.6		6000	81.62	79.39	74.34	59.69	73.70	73.70	14.01	0.48	0.29	0.49	0.13	0.17	0.1
2.1.7		7000	82.87	78.70	74.33	59.49	73.70	73.70	14.21	0.57	0.27	0.18	0.16	0.17	0.1
2.1.8		8000	82.78	78.72	74.56	59.50	73.68	73.68	14.18	0.62	0.54	0.30	0.16	0.16	0.1
2.1.9		9000	83.85	79.06	75.05	59.69	74.12	74.12	14.43	0.77	0.37	0.28	0.20	0.18	0.1
2.1.10		10000	84.77	79.77	75.91	60.10	74.81	74.81	14.71	0.75	0.35	0.28	0.22	0.20	0.1
2.1.11		20000	84.50	78.02	75.87	58.60	73.59	73.59	14.99	0.90	0.48	0.36	0.28	0.24	0.2
2.1.12		30000	87.16	80.13	78.52	59.36	75.43	75.43	16.06	0.86	0.54	0.35	0.21	0.25	0.2
2.1.13		40000	90.53	82.72	81.79	60.33	77.84	77.84	17.51	0.85	0.96	0.92	0.27	0.29	0.3
2.1.14		50000	86.81	79.25	79.46	57.60	74.52	74.52	16.92	0.81	0.86	1.01	0.31	0.23	0.3
2.2.1		1000	87.27	86.37	77.19	64.44	79.13	79.13	14.69	0.22	0.16	0.13	0.05	0.06	0.0
2.2.2		2000	85.18	84.55	75.78	62.08	77.15	77.15	15.07	0.22	0.18	0.18	0.07	0.08	0.0
2.2.3		3000	83.54	82.85	74.57	60.08	75.42	75.42	15.35	0.33	0.24	0.30	0.16	0.11	0.1
2.2.4		4000	83.21	82.38	74.41	58.76	74.77	74.77	16.00	0.39	0.23	0.52	0.16	0.14	0.1
2.2.5		5000	85.59	82.08	75.93	59.02	75.71	75.71	16.68	0.49	0.28	0.21	0.12	0.13	0.1
2.2.6		6000	92.10	88.02	82.30	64.25	81.62	81.62	17.37	0.64	0.32	0.24	0.12	0.17	0.1
2.2.7		7000	91.54	87.09	81.60	63.55	80.84	80.84	17.30	0.79	0.35	0.22	0.22	0.21	0.1
2.2.8		8000	92.12	87.28	81.68	63.15	80.93	80.93	17.78	0.76	0.41	0.27	0.21	0.22	0.1
2.2.9		9000	90.28	85.40	80.43	62.08	79.30	79.30	17.22	0.89	0.35	0.23	0.26	0.22	0.2
2.2.10		10000	88.92	83.82	79.18	61.03	78.01	78.01	16.98	0.81	0.35	0.26	0.27	0.20	0.2
2.2.11		20000	84.54	78.42	75.50	56.99	73.31	73.31	16.32	0.90	0.72	0.63	0.26	0.24	0.2
2.2.12		30000	87.94	80.84	78.41	58.36	75.63	75.63	17.28	0.78	0.79	0.70	0.23	0.31	0.2
2.2.13		40000	87.08	79.81	78.77	58.49	75.04	75.04	16.55	0.81	0.94	0.69	0.22	0.24	0.2
2.2.14		50000	86.13	78.84	78.84	57.28	74.09	74.09	16.80	0.84	0.86	0.85	0.23	0.24	0.3
3.1.1	CCTS 0.45	1000	77.90	79.77	70.89	81.69	77.14	77.14	6.24	0.26	0.25	0.20	0.16	0.19	0.1
3.1.2		2000	84.19	86.86	76.43	90.29	83.73	83.73	7.31	0.29	0.21	0.18	0.13	0.13	0.1
3.1.3		3000	81.79	85.18	74.40	88.99	81.64	81.64	7.35	0.32	0.21	0.20	0.08	0.09	0.1
3.1.4		4000	80.17	83.87	72.94	88.01	80.01	80.01	8.00	0.44	0.21	0.22	0.08	0.09	0.1
3.1.5		5000	81.05	85.09	73.64	89.75	80.82	80.82	8.93	0.55	0.32	0.34	0.26	0.32	0.1
3.1.6		6000	76.34	80.20	69.46	84.80	76.03	76.03	8.78	0.57	0.26	0.25	0.12	0.17	0.1
3.1.7		7000	79.89	84.14	72.50	89.53	79.55	79.55	9.99	0.59	0.27	0.22	0.08	0.10	0.1
3.1.8		8000	82.54	87.06	74.71	93.13	82.16	82.16	10.96	0.74	0.34	0.27	0.10	0.10	0.1
3.1.9		9000	74.78	77.39	65.98	82.80	73.12	73.12	9.69	0.72	0.32	0.24	0.07	0.06	0.1
3.1.10		10000	78.21	81.03	68.75	87.10	76.49	76.49	10.60	0.87	0.38	0.26	0.12	0.16	0.2
3.1.11		20000	74.63	79.03	66.35	86.91	74.26	74.26	12.66	1.14	0.52	0.36	0.14	0.17	0.2
3.1.12		30000	75.26	80.64	67.08	90.58	75.72	75.72	14.87	1.25	0.57	0.46	0.16	0.19	0.2
3.1.13		40000	74.87	80.45	66.19	91.37	75.40	75.40	15.97	1.02	0.70	0.44	0.18	0.22	0.2

3.1.14		50000	74.12	79.05	64.64	90.88	74.39	74.39	16.48	1.15	0.79	0.44	0.16	0.15	0.3
3.2.1		1000	82.88	83.08	73.59	85.78	80.74	80.74	7.15	0.24	0.16	0.16	0.08	0.10	0.0
3.2.2		2000	82.89	83.34	73.22	87.53	80.91	80.91	7.70	0.24	0.24	0.22	0.13	0.16	0.1
3.2.3		3000	81.38	82.42	71.68	87.18	79.58	79.58	7.90	0.35	0.21	0.20	0.12	0.15	0.1
3.2.4		4000	78.16	79.49	68.83	84.51	76.40	76.40	8.11	0.38	0.23	0.22	0.12	0.16	0.1
3.2.5		5000	79.47	80.93	69.67	86.59	77.50	77.50	9.08	0.52	0.21	0.22	0.08	0.08	0.1
3.2.6		6000	78.82	80.33	68.93	86.35	76.70	76.70	9.65	0.55	0.22	0.19	0.07	0.05	0.1
3.2.7		7000	80.89	82.02	70.21	87.89	78.14	78.14	9.75	0.62	0.22	0.21	0.07	0.07	0.1
3.2.8		8000	79.35	80.53	68.80	86.42	76.55	76.55	9.87	0.65	0.29	0.29	0.12	0.18	0.1
3.2.9		9000	81.28	82.67	70.42	89.12	78.50	78.50	10.63	0.83	0.35	0.29	0.14	0.17	0.2
3.2.10		10000	80.78	82.31	70.04	88.77	78.07	78.07	10.70	0.76	0.34	0.29	0.11	0.13	0.1
3.2.11		20000	77.09	79.92	67.31	88.33	75.58	75.58	12.76	1.02	0.53	0.39	0.14	0.18	0.2
3.2.12		30000	74.59	78.27	65.14	87.75	73.75	73.75	14.00	1.16	0.62	0.45	0.17	0.23	0.2
3.2.13		40000	75.67	80.61	66.47	91.88	75.86	75.86	16.02	1.07	0.70	0.46	0.13	0.16	0.2
3.2.14		50000	74.38	78.37	64.24	90.32	73.98	73.98	16.33	1.06	0.76	0.52	0.18	0.21	0.2

Table C 3: Fluid pressure data

Test No.	Test Section	Reynolds number	SCADA $p_{calc,f}$ $[kPa]$	$\sigma_{Pcalc,f}$ $[kPa]$
1.1.1	CCTS 0.36	1000	101.60	0.40
1.1.2		2000	202.41	0.31
1.1.3		3000	300.58	0.32
1.1.4		4000	399.82	0.37
1.1.5		5000	500.52	0.50
1.1.6		6000	599.69	0.43
1.1.7		7000	698.68	0.45
1.1.8		8000	799.54	0.59
1.1.9		9000	899.67	0.65
1.1.10		10000	996.66	0.55
1.1.11		20000	1996.81	1.90
1.1.12		30000	2998.54	2.72
1.1.13		40000	3991.58	2.60
1.1.14		50000	4998.41	2.84
1.2.1		1000	101.66	0.32
1.2.2		2000	202.89	0.35
1.2.3		3000	301.20	0.32
1.2.4		4000	403.23	0.41
1.2.5		5000	503.35	0.36
1.2.6		6000	605.64	0.50
1.2.7		7000	702.09	0.56
1.2.8		8000	802.17	0.50
1.2.9		9000	902.21	0.91
1.2.10		10000	1006.41	0.69
1.2.11		20000	2009.01	1.89
1.2.12		30000	2997.72	2.59
1.2.13		40000	4003.70	2.19
1.2.14		50000	4998.32	2.91
2.1.1	CCTS 0.39	1000	101.58	0.32
2.1.2		2000	200.22	0.52

2.1.3		3000	300.77	0.34
2.1.4		4000	399.92	0.39
2.1.5		5000	502.29	0.32
2.1.6		6000	601.16	0.34
2.1.7		7000	700.63	0.44
2.1.8		8000	799.43	0.49
2.1.9		9000	898.96	0.86
2.1.10		10000	999.64	0.89
2.1.11		20000	1992.28	1.71
2.1.12		30000	3005.42	3.01
2.1.13		40000	3997.53	1.94
2.1.14		50000	4990.32	2.81
2.2.1		1000	101.51	0.35
2.2.2		2000	201.89	0.30
2.2.3		3000	303.11	0.42
2.2.4		4000	403.41	0.50
2.2.5		5000	504.34	0.35
2.2.6		6000	601.23	0.36
2.2.7		7000	702.03	0.39
2.2.8		8000	803.09	0.50
2.2.9		9000	903.86	0.54
2.2.10		10000	1005.90	0.51
2.2.11		20000	2004.13	1.44
2.2.12		30000	3013.23	3.67
2.2.13		40000	4006.18	2.64
2.2.14		50000	4989.03	2.98
3.1.1	CCTS 0.45	1000	100.84	0.34
3.1.2		2000	201.76	0.47
3.1.3		3000	300.01	0.41
3.1.4		4000	399.89	0.36
3.1.5		5000	500.31	0.38
3.1.6		6000	598.94	0.55
3.1.7		7000	697.67	0.42
3.1.8		8000	798.68	0.60
3.1.9		9000	901.81	0.68
3.1.10		10000	1001.13	0.66
3.1.11		20000	1998.31	3.79
3.1.12		30000	2993.74	2.68
3.1.13		40000	4003.88	2.94

3.1.14		50000	4997.28	3.41
3.2.1		1000	101.03	0.39
3.2.2		2000	201.46	0.72
3.2.3		3000	301.14	0.31
3.2.4		4000	401.86	0.40
3.2.5		5000	500.79	0.52
3.2.6		6000	602.96	0.88
3.2.7		7000	701.04	0.56
3.2.8		8000	801.49	0.58
3.2.9		9000	900.53	0.74
3.2.10		10000	1001.28	0.54
3.2.11		20000	2002.38	2.80
3.2.12		30000	3001.51	2.18
3.2.13		40000	4008.39	4.63
3.2.14		50000	4998.03	2.99

Table C 4: Fluid property data.

Test No.	Test Section	Reynolds number	$\partial\lambda_f/\partial T_f$	$\partial\lambda_f/\partial p_f$	λ_f [W/m K]	$\Delta\lambda_f$ [W/m K]	$\partial\mu_f/\partial T_f$	$\partial\mu_f/\partial p_f$	μ_f [kg/m s]	$\Delta\mu_f$ [kg/m s]	$\partial\rho_f/\partial T_f$	$\partial\rho_f/\partial p_f$	ρ_f [kg/m^3]	$\Delta\rho_f$ [kg/m^3]
1.1.1	CCTS 0.36	1000	6.72E-05	3.40E-07	2.56E-02	3.36E-06	4.63E-08	1.56E-10	1.77E-05	2.31E-09	-3.85E-03	1.13E-02	1.14	5.67E-03
1.1.2		2000	6.72E-05	3.47E-07	2.56E-02	3.37E-06	4.63E-08	1.58E-10	1.77E-05	2.32E-09	-7.86E-03	1.14E-02	2.31	5.74E-03
1.1.3		3000	6.71E-05	3.52E-07	2.56E-02	3.36E-06	4.63E-08	1.59E-10	1.77E-05	2.31E-09	-1.17E-02	1.14E-02	3.42	1.70E-02
1.1.4		4000	6.70E-05	3.57E-07	2.56E-02	3.35E-06	4.62E-08	1.60E-10	1.77E-05	2.31E-09	-1.56E-02	1.14E-02	4.56	5.77E-03
1.1.5		5000	6.69E-05	3.63E-07	2.57E-02	3.36E-06	4.61E-08	1.61E-10	1.78E-05	2.31E-09	-1.96E-02	1.14E-02	5.72	1.15E-02
1.1.6		6000	6.67E-05	3.68E-07	2.57E-02	3.36E-06	4.61E-08	1.62E-10	1.78E-05	2.31E-09	-2.36E-02	1.14E-02	6.86	1.15E-02
1.1.7		7000	6.66E-05	3.73E-07	2.58E-02	3.35E-06	4.60E-08	1.63E-10	1.78E-05	2.31E-09	-2.76E-02	1.15E-02	8.01	1.15E-02
1.1.8		8000	6.65E-05	3.79E-07	2.58E-02	3.35E-06	4.60E-08	1.64E-10	1.78E-05	2.30E-09	-3.16E-02	1.15E-02	9.16	1.16E-02
1.1.9		9000	6.63E-05	3.84E-07	2.58E-02	3.34E-06	4.59E-08	1.65E-10	1.78E-05	2.30E-09	-3.57E-02	1.15E-02	10.30	1.17E-02
1.1.10		10000	6.62E-05	3.90E-07	2.59E-02	3.33E-06	4.58E-08	1.66E-10	1.78E-05	2.30E-09	-3.97E-02	1.15E-02	11.43	1.16E-02
1.1.11		20000	6.47E-05	4.46E-07	2.62E-02	3.34E-06	4.52E-08	1.77E-10	1.79E-05	2.29E-09	-8.44E-02	1.16E-02	23.61	2.81E-02
1.1.12		30000	6.27E-05	5.00E-07	2.67E-02	3.42E-06	4.45E-08	1.88E-10	1.81E-05	2.28E-09	-1.29E-01	1.18E-02	35.39	2.49E-02
1.1.13		40000	6.02E-05	5.54E-07	2.72E-02	3.34E-06	4.35E-08	1.98E-10	1.83E-05	2.24E-09	-1.74E-01	1.19E-02	47.07	3.79E-02
1.1.14		50000	5.74E-05	6.08E-07	2.78E-02	3.35E-06	4.25E-08	2.09E-10	1.85E-05	2.21E-09	-2.22E-01	1.21E-02	59.13	4.51E-02
1.2.1		1000	6.73E-05	3.41E-07	2.56E-02	3.37E-06	4.63E-08	1.57E-10	1.77E-05	2.32E-09	-3.93E-03	1.14E-02	1.15	5.72E-03
1.2.2		2000	6.73E-05	3.48E-07	2.55E-02	3.37E-06	4.63E-08	1.58E-10	1.77E-05	2.32E-09	-7.90E-03	1.15E-02	2.31	7.83E-03
1.2.3		3000	6.72E-05	3.54E-07	2.55E-02	3.37E-06	4.63E-08	1.60E-10	1.76E-05	2.32E-09	-1.19E-02	1.15E-02	3.45	1.71E-02
1.2.4		4000	6.71E-05	3.60E-07	2.55E-02	3.38E-06	4.63E-08	1.61E-10	1.77E-05	2.32E-09	-1.60E-02	1.15E-02	4.64	1.15E-02
1.2.5		5000	6.70E-05	3.65E-07	2.56E-02	3.37E-06	4.62E-08	1.62E-10	1.77E-05	2.32E-09	-2.00E-02	1.15E-02	5.80	1.16E-02
1.2.6		6000	6.69E-05	3.71E-07	2.56E-02	3.37E-06	4.62E-08	1.63E-10	1.77E-05	2.32E-09	-2.42E-02	1.15E-02	6.97	1.16E-02
1.2.7		7000	6.67E-05	3.76E-07	2.57E-02	3.36E-06	4.61E-08	1.64E-10	1.77E-05	2.31E-09	-2.80E-02	1.15E-02	8.08	1.16E-02
1.2.8		8000	6.66E-05	3.81E-07	2.57E-02	3.35E-06	4.60E-08	1.65E-10	1.77E-05	2.31E-09	-3.21E-02	1.15E-02	9.24	1.18E-02
1.2.9		9000	6.65E-05	3.86E-07	2.57E-02	3.35E-06	4.60E-08	1.66E-10	1.78E-05	2.31E-09	-3.63E-02	1.15E-02	10.41	1.17E-02
1.2.10		10000	6.63E-05	3.92E-07	2.58E-02	3.34E-06	4.59E-08	1.67E-10	1.78E-05	2.30E-09	-4.05E-02	1.15E-02	11.60	1.17E-02
1.2.11		20000	6.47E-05	4.46E-07	2.62E-02	3.34E-06	4.52E-08	1.77E-10	1.79E-05	2.29E-09	-8.50E-02	1.16E-02	23.77	2.89E-02
1.2.12		30000	6.27E-05	5.00E-07	2.67E-02	3.39E-06	4.44E-08	1.88E-10	1.81E-05	2.28E-09	-1.29E-01	1.18E-02	35.38	2.92E-02
1.2.13		40000	6.02E-05	5.54E-07	2.72E-02	3.25E-06	4.35E-08	1.98E-10	1.83E-05	2.22E-09	-1.75E-01	1.19E-02	47.23	3.82E-02
1.2.14		50000	5.74E-05	6.08E-10	2.78E-02	2.87E-06	4.25E-08	2.09E-13	1.85E-05	2.13E-09	-2.22E-01	1.21E-02	59.15	5.32E-02
2.1.1	CCTS 0.39	1000	6.70E-05	3.38E-07	2.58E-02	3.35E-06	4.61E-08	1.55E-10	1.79E-05	2.31E-09	-3.78E-03	1.13E-02	1.13	5.63E-03
2.1.2		2000	6.68E-05	3.42E-07	2.59E-02	3.35E-06	4.60E-08	1.56E-10	1.79E-05	2.30E-09	-7.52E-03	1.13E-02	2.24	5.65E-03
2.1.3		3000	6.67E-05	3.47E-07	2.59E-02	3.34E-06	4.60E-08	1.57E-10	1.79E-05	2.31E-09	-1.13E-02	1.13E-02	3.36	1.68E-02
2.1.4		4000	6.66E-05	3.52E-07	2.59E-02	3.34E-06	4.59E-08	1.58E-10	1.79E-05	2.30E-09	-1.52E-02	1.13E-02	4.49	5.68E-03

2.1.5		5000	6.68E-05	3.63E-07	2.57E-02	3.36E-06	4.61E-08	1.61E-10	1.78E-05	2.31E-09	-1.96E-02	1.14E-02	5.72	1.15E-0
2.1.6		6000	6.67E-05	3.68E-07	2.58E-02	3.35E-06	4.60E-08	1.62E-10	1.78E-05	2.31E-09	-2.36E-02	1.14E-02	6.87	1.15E-0
2.1.7		7000	6.66E-05	3.73E-07	2.58E-02	3.35E-06	4.60E-08	1.63E-10	1.78E-05	2.30E-09	-2.76E-02	1.14E-02	8.01	1.16E-0
2.1.8		8000	6.64E-05	3.78E-07	2.58E-02	3.34E-06	4.59E-08	1.64E-10	1.78E-05	2.30E-09	-3.16E-02	1.14E-02	9.16	1.16E-0
2.1.9		9000	6.63E-05	3.83E-07	2.59E-02	3.34E-06	4.59E-08	1.65E-10	1.78E-05	2.30E-09	-3.56E-02	1.15E-02	10.28	1.16E-0
2.1.10		10000	6.61E-05	3.89E-07	2.59E-02	3.33E-06	4.58E-08	1.66E-10	1.79E-05	2.30E-09	-3.96E-02	1.15E-02	11.43	1.20E-0
2.1.11		20000	6.46E-05	4.42E-07	2.63E-02	3.32E-06	4.51E-08	1.76E-10	1.80E-05	2.28E-09	-8.29E-02	1.16E-02	23.38	2.73E-0
2.1.12		30000	6.25E-05	4.96E-07	2.68E-02	3.47E-06	4.43E-08	1.86E-10	1.82E-05	2.29E-09	-1.27E-01	1.17E-02	35.13	3.14E-0
2.1.13		40000	6.02E-05	5.49E-07	2.73E-02	3.19E-06	4.35E-08	1.96E-10	1.84E-05	2.21E-09	-1.71E-01	1.18E-02	46.71	4.49E-0
2.1.14		50000	5.74E-05	6.02E-07	2.79E-02	3.33E-06	4.25E-08	2.06E-10	1.86E-05	2.20E-09	-2.18E-01	1.20E-02	58.61	5.83E-0
2.2.1		1000	6.71E-05	3.39E-07	2.57E-02	3.36E-06	4.62E-08	1.56E-10	1.78E-05	2.31E-09	-3.81E-03	1.13E-02	1.14	5.64E-0
2.2.2		2000	6.71E-05	3.46E-07	2.56E-02	3.36E-06	4.62E-08	1.57E-10	1.77E-05	2.31E-09	-7.76E-03	1.14E-02	2.29	5.71E-0
2.2.3		3000	6.71E-05	3.52E-07	2.56E-02	3.36E-06	4.63E-08	1.59E-10	1.77E-05	2.31E-09	-1.18E-02	1.15E-02	3.46	1.72E-0
2.2.4		4000	6.71E-05	3.60E-07	2.55E-02	3.38E-06	4.63E-08	1.61E-10	1.76E-05	2.32E-09	-1.60E-02	1.15E-02	4.63	1.15E-0
2.2.5		5000	6.71E-05	3.66E-07	2.55E-02	3.37E-06	4.63E-08	1.63E-10	1.76E-05	2.32E-09	-2.02E-02	1.16E-02	5.84	1.16E-0
2.2.6		6000	6.67E-05	3.67E-07	2.58E-02	3.35E-06	4.60E-08	1.61E-10	1.78E-05	2.31E-09	-2.36E-02	1.14E-02	6.87	1.15E-0
2.2.7		7000	6.65E-05	3.72E-07	2.58E-02	3.35E-06	4.60E-08	1.62E-10	1.78E-05	2.30E-09	-2.76E-02	1.14E-02	8.02	1.15E-0
2.2.8		8000	6.64E-05	3.78E-07	2.59E-02	3.34E-06	4.59E-08	1.63E-10	1.78E-05	2.30E-09	-3.17E-02	1.14E-02	9.18	1.16E-0
2.2.9		9000	6.63E-05	3.83E-07	2.59E-02	3.34E-06	4.58E-08	1.65E-10	1.79E-05	2.30E-09	-3.57E-02	1.15E-02	10.33	1.16E-0
2.2.10		10000	6.61E-05	3.89E-07	2.59E-02	3.33E-06	4.58E-08	1.66E-10	1.79E-05	2.30E-09	-3.99E-02	1.15E-02	11.51	1.33E-0
2.2.11		20000	6.45E-05	4.42E-07	2.63E-02	3.29E-06	4.51E-08	1.76E-10	1.80E-05	2.27E-09	-8.34E-02	1.16E-02	23.51	2.42E-0
2.2.12		30000	6.25E-05	4.97E-07	2.68E-02	3.62E-06	4.43E-08	1.86E-10	1.82E-05	2.32E-09	-1.27E-01	1.17E-02	35.23	3.50E-0
2.2.13		40000	6.01E-05	5.49E-07	2.73E-02	3.34E-06	4.34E-08	1.96E-10	1.84E-05	2.23E-09	-1.72E-01	1.18E-02	46.86	4.30E-0
2.2.14		50000	5.74E-05	6.02E-07	2.79E-02	3.38E-06	4.25E-08	2.06E-10	1.86E-05	2.21E-09	-2.18E-01	1.20E-02	58.61	5.86E-0
3.1.1	CCTS 0.45	1000	6.71E-05	3.39E-07	2.57E-02	3.36E-06	4.62E-08	1.56E-10	1.78E-05	2.31E-09	-3.79E-03	1.13E-02	1.13	5.66E-0
3.1.2		2000	6.70E-05	3.44E-07	2.58E-02	3.35E-06	4.61E-08	1.57E-10	1.78E-05	2.31E-09	-7.66E-03	1.13E-02	2.27	5.67E-0
3.1.3		3000	6.69E-05	3.49E-07	2.58E-02	3.35E-06	4.61E-08	1.57E-10	1.78E-05	2.31E-09	-1.14E-02	1.13E-02	3.39	1.70E-0
3.1.4		4000	6.67E-05	3.54E-07	2.58E-02	3.34E-06	4.60E-08	1.58E-10	1.79E-05	2.30E-09	-1.53E-02	1.13E-02	4.52	5.72E-0
3.1.5		5000	6.66E-05	3.60E-07	2.59E-02	3.35E-06	4.60E-08	1.59E-10	1.79E-05	2.30E-09	-1.92E-02	1.13E-02	5.66	1.14E-0
3.1.6		6000	6.65E-05	3.65E-07	2.59E-02	3.35E-06	4.59E-08	1.60E-10	1.79E-05	2.30E-09	-2.31E-02	1.13E-02	6.78	1.14E-0
3.1.7		7000	6.64E-05	3.70E-07	2.59E-02	3.34E-06	4.58E-08	1.61E-10	1.79E-05	2.30E-09	-2.70E-02	1.13E-02	7.92	1.14E-0
3.1.8		8000	6.63E-05	3.75E-07	2.60E-02	3.33E-06	4.58E-08	1.62E-10	1.79E-05	2.30E-09	-3.09E-02	1.13E-02	9.04	1.15E-0
3.1.9		9000	6.63E-05	3.85E-07	2.58E-02	3.34E-06	4.59E-08	1.65E-10	1.78E-05	2.30E-09	-3.58E-02	1.15E-02	10.33	1.18E-0
3.1.10		10000	6.62E-05	3.90E-07	2.59E-02	3.33E-06	4.58E-08	1.66E-10	1.78E-05	2.30E-09	-3.98E-02	1.15E-02	11.47	1.17E-0
3.1.11		20000	6.45E-05	4.41E-07	2.63E-02	3.63E-06	4.51E-08	1.76E-10	1.80E-05	2.35E-09	-8.27E-02	1.15E-02	23.38	3.24E-0
3.1.12		30000	6.25E-05	4.94E-07	2.68E-02	3.40E-06	4.43E-08	1.86E-10	1.82E-05	2.27E-09	-1.26E-01	1.17E-02	34.94	3.16E-0
3.1.13		40000	6.01E-05	5.48E-07	2.73E-02	3.41E-06	4.34E-08	1.96E-10	1.84E-05	2.25E-09	-1.71E-01	1.18E-02	46.72	6.33E-0
3.1.14		50000	5.74E-05	6.00E-07	2.79E-02	3.53E-06	4.24E-08	2.06E-10	1.86E-05	2.24E-09	-2.17E-01	1.20E-02	58.48	6.04E-0
3.2.1		1000	6.71E-05	3.38E-07	2.57E-02	3.36E-06	4.62E-08	1.55E-10	1.78E-05	2.31E-09	-3.82E-03	1.13E-02	1.13	5.67E-0

3.2.2		2000	6.70E-05	3.44E-07	2.57E-02	3.36E-06	4.61E-08	1.57E-10	1.78E-05	2.31E-09	-7.68E-03	1.13E-02	2.27	5.68E-0
3.2.3		3000	6.70E-05	3.50E-07	2.57E-02	3.35E-06	4.61E-08	1.58E-10	1.78E-05	2.31E-09	-1.16E-02	1.14E-02	3.42	1.71E-0
3.2.4		4000	6.69E-05	3.56E-07	2.57E-02	3.36E-06	4.61E-08	1.59E-10	1.78E-05	2.31E-09	-1.56E-02	1.14E-02	4.56	1.14E-0
3.2.5		5000	6.68E-05	3.62E-07	2.58E-02	3.36E-06	4.61E-08	1.60E-10	1.78E-05	2.31E-09	-1.95E-02	1.14E-02	5.71	1.14E-0
3.2.6		6000	6.67E-05	3.67E-07	2.58E-02	3.35E-06	4.60E-08	1.61E-10	1.78E-05	2.31E-09	-2.36E-02	1.14E-02	6.87	1.15E-0
3.2.7		7000	6.65E-05	3.73E-07	2.58E-02	3.35E-06	4.60E-08	1.63E-10	1.78E-05	2.30E-09	-2.75E-02	1.14E-02	8.01	1.15E-0
3.2.8		8000	6.64E-05	3.78E-07	2.59E-02	3.34E-06	4.59E-08	1.63E-10	1.78E-05	2.30E-09	-3.15E-02	1.14E-02	9.15	1.15E-0
3.2.9		9000	6.63E-05	3.83E-07	2.59E-02	3.34E-06	4.58E-08	1.64E-10	1.79E-05	2.30E-09	-3.55E-02	1.14E-02	10.29	1.16E-0
3.2.10		10000	6.61E-05	3.88E-07	2.59E-02	3.33E-06	4.58E-08	1.65E-10	1.79E-05	2.29E-09	-3.96E-02	1.14E-02	11.45	1.29E-0
3.2.11		20000	6.45E-05	4.41E-07	2.64E-02	3.45E-06	4.51E-08	1.75E-10	1.81E-05	2.31E-09	-8.30E-02	1.15E-02	23.46	2.55E-0
3.2.12		30000	6.25E-05	4.94E-07	2.68E-02	3.31E-06	4.43E-08	1.86E-10	1.82E-05	2.25E-09	-1.26E-01	1.17E-02	35.06	3.11E-0
3.2.13		40000	6.01E-05	5.48E-07	2.74E-02	3.93E-06	4.34E-08	1.96E-10	1.84E-05	2.35E-09	-1.71E-01	1.18E-02	46.75	5.41E-0
3.2.14		50000	5.74E-05	6.01E-07	2.79E-02	3.38E-06	4.24E-08	2.06E-10	1.86E-05	2.21E-09	-2.17E-01	1.20E-02	58.53	6.57E-0

Table C 5: Heat transfer, heat transfer coefficient and Nusselt number data.

Test No.	Test Section	Reynolds number	q_{elec} [W]	Δq_{elec} [W]	q_{rad} [W]	Δq_{rad} [W]	q_{conv} [W]	Δq_{conv} [W]	α [W/m2 K]	$\Delta\alpha$ [W/m2 K]	Nu [-]	ΔNu [-]	$\Delta Nu/Nu$ [%]
1.1.1	CCTS 0.36	1000	47.44	1.91	2.06	0.07	45.38	1.91	79.62	3.22	186.43	15.10	8.10
1.1.2		2000	78.07	2.89	2.07	0.07	76.00	2.89	129.00	4.80	302.90	22.55	7.44
1.1.3		3000	103.42	4.34	2.05	0.07	101.37	4.34	172.49	7.28	404.27	34.13	8.44
1.1.4		4000	130.18	7.05	2.10	0.07	128.08	7.05	212.97	11.59	498.26	54.22	10.88
1.1.5		5000	151.72	5.71	2.08	0.07	149.65	5.71	250.85	9.52	585.90	44.46	7.59
1.1.6		6000	176.73	4.59	2.11	0.07	174.62	4.59	288.40	7.60	672.49	35.47	5.27
1.1.7		7000	203.02	7.63	2.11	0.07	200.90	7.63	331.00	12.58	770.81	58.62	7.60
1.1.8		8000	214.32	7.84	2.01	0.07	212.31	7.84	364.03	13.44	846.55	62.86	7.43
1.1.9		9000	238.93	8.76	2.07	0.07	236.85	8.76	395.43	14.65	918.47	68.05	7.41
1.1.10		10000	247.47	8.20	2.00	0.07	245.47	8.20	420.71	14.11	976.04	65.47	6.71
1.1.11		20000	416.59	12.58	1.93	0.06	414.66	12.58	722.55	22.43	1655.52	102.81	6.21
1.1.12		30000	590.25	12.71	1.95	0.06	588.30	12.71	1013.22	22.83	2280.35	102.79	4.51
1.1.13		40000	769.87	9.24	1.96	0.06	767.91	9.24	1316.95	18.04	2906.87	79.70	2.74
1.1.14		50000	977.67	19.33	1.99	0.07	975.68	19.33	1650.79	34.33	3566.83	148.39	4.16
1.2.1		1000	46.98	1.91	1.87	0.06	45.12	1.91	84.68	3.47	198.80	16.28	8.19
1.2.2		2000	74.39	2.53	1.91	0.06	72.48	2.53	130.77	4.49	307.29	21.11	6.87
1.2.3		3000	104.04	4.46	2.05	0.07	101.99	4.46	171.70	7.40	403.86	34.83	8.62
1.2.4		4000	125.46	5.15	2.06	0.07	123.40	5.15	205.89	8.51	483.81	40.06	8.28
1.2.5		5000	146.77	5.87	1.96	0.06	144.81	5.87	250.42	10.09	587.84	47.42	8.07
1.2.6		6000	169.54	5.19	1.96	0.06	167.58	5.19	288.99	8.95	677.83	42.00	6.20
1.2.7		7000	195.29	6.88	2.04	0.07	193.25	6.88	323.96	11.52	757.64	53.90	7.11
1.2.8		8000	212.28	10.26	1.97	0.06	210.31	10.26	362.14	17.64	845.43	82.38	9.74
1.2.9		9000	230.96	7.59	2.00	0.07	228.96	7.59	388.39	12.94	905.32	60.34	6.67
1.2.10		10000	248.38	11.16	2.02	0.07	246.36	11.16	415.02	18.98	965.81	88.34	9.15
1.2.11		20000	412.71	9.08	1.93	0.06	410.78	9.08	714.52	16.51	1636.32	76.40	4.67
1.2.12		30000	592.21	21.69	1.97	0.06	590.25	21.69	1010.17	37.54	2273.26	170.63	7.51
1.2.13		40000	785.44	15.51	2.01	0.07	783.43	15.51	1316.43	27.15	2904.92	119.86	4.13
1.2.14		50000	966.50	17.58	1.97	0.06	964.53	17.58	1649.43	31.72	3563.90	137.11	3.85
2.1.1	CCTS 0.39	1000	30.29	1.30	2.12	0.07	28.17	1.31	50.52	2.19	117.52	10.18	8.66
2.1.2		2000	52.81	1.93	2.30	0.07	50.51	1.93	83.05	3.06	192.59	14.20	7.37
2.1.3		3000	62.79	2.53	2.09	0.07	60.70	2.53	106.69	4.33	247.07	20.05	8.12

2.1.4		4000	74.58	2.50	2.02	0.07	72.56	2.50	130.14	4.40	301.02	20.36	6.76
2.1.5		5000	91.10	2.67	2.06	0.07	89.03	2.67	151.73	4.51	354.19	21.06	5.95
2.1.6		6000	99.07	4.11	1.96	0.06	97.11	4.11	172.04	7.18	400.80	33.46	8.35
2.1.7		7000	111.81	2.94	1.96	0.06	109.85	2.94	194.72	5.21	452.80	24.24	5.35
2.1.8		8000	122.76	3.29	1.95	0.06	120.81	3.29	214.05	5.84	497.00	27.15	5.46
2.1.9		9000	134.65	3.81	1.97	0.06	132.68	3.81	233.03	6.71	540.19	31.10	5.76
2.1.10		10000	147.80	3.46	2.01	0.07	145.79	3.46	252.29	6.05	583.99	28.04	4.80
2.1.11		20000	246.65	5.59	1.95	0.06	244.70	5.59	430.29	10.08	980.67	45.96	4.69
2.1.12		30000	367.13	14.07	2.04	0.07	365.08	14.07	617.27	23.92	1382.13	107.12	7.75
2.1.13		40000	499.81	11.35	2.16	0.07	497.65	11.35	803.33	19.11	1764.68	83.99	4.76
2.1.14		50000	590.85	16.27	2.00	0.07	588.84	16.27	1008.93	28.75	2171.35	123.76	5.70
2.2.1		1000	30.02	1.33	2.17	0.07	27.86	1.33	48.92	2.17	114.12	10.14	8.88
2.2.2		2000	50.10	2.12	2.12	0.07	47.98	2.12	82.08	3.49	192.08	16.34	8.51
2.2.3		3000	65.32	2.82	2.06	0.07	63.26	2.82	108.31	4.70	253.84	22.03	8.68
2.2.4		4000	79.04	2.74	2.08	0.07	76.95	2.74	128.53	4.49	302.14	21.14	7.00
2.2.5		5000	95.29	4.44	2.15	0.07	93.13	4.44	149.84	7.01	352.60	32.99	9.36
2.2.6		6000	115.48	4.71	2.34	0.08	113.13	4.71	174.52	7.17	406.22	33.39	8.22
2.2.7		7000	130.24	4.73	2.30	0.08	127.94	4.74	199.69	7.33	464.07	34.07	7.34
2.2.8		8000	141.64	3.37	2.31	0.08	139.34	3.37	216.83	5.27	503.17	24.47	4.86
2.2.9		9000	147.99	3.60	2.23	0.07	145.76	3.60	232.70	5.80	539.32	26.89	4.99
2.2.10		10000	157.80	4.43	2.17	0.07	155.63	4.44	253.51	7.25	586.81	33.56	5.72
2.2.11		20000	250.00	6.92	1.94	0.06	248.06	6.92	438.21	12.47	998.64	56.84	5.69
2.2.12		30000	373.09	6.85	2.06	0.07	371.03	6.85	622.34	12.11	1393.97	54.27	3.89
2.2.13		40000	478.82	16.23	2.02	0.07	476.80	16.23	811.39	28.05	1781.94	123.20	6.91
2.2.14		50000	584.70	14.99	1.98	0.07	582.72	14.99	1005.98	26.76	2165.24	115.20	5.32
3.1.1	CCTS 0.45	1000	24.59	1.22	2.09	0.07	22.51	1.22	41.09	2.05	96.02	9.62	10.01
3.1.2		2000	41.59	2.00	2.40	0.08	39.18	2.00	62.45	3.01	145.50	14.04	9.65
3.1.3		3000	51.96	1.91	2.29	0.07	49.67	1.92	81.05	3.01	188.54	14.00	7.42
3.1.4		4000	62.66	2.07	2.20	0.07	60.45	2.07	100.80	3.36	234.11	15.63	6.68
3.1.5		5000	73.87	3.41	2.25	0.07	71.62	3.41	116.99	5.43	271.38	25.19	9.28
3.1.6		6000	78.80	2.90	2.01	0.07	76.79	2.90	136.45	5.07	316.10	23.50	7.43
3.1.7		7000	93.06	4.40	2.18	0.07	90.87	4.40	150.71	7.17	348.65	33.16	9.51
3.1.8		8000	109.24	5.18	2.32	0.08	106.93	5.18	168.83	8.06	390.02	37.22	9.54
3.1.9		9000	101.09	3.56	1.95	0.06	99.14	3.56	175.34	6.24	407.37	29.00	7.12
3.1.10		10000	114.93	4.03	2.11	0.07	112.82	4.03	187.36	6.65	434.51	30.83	7.10
3.1.11		20000	184.86	8.60	1.97	0.07	182.89	8.60	320.20	15.04	729.17	68.50	9.39
3.1.12		30000	263.10	7.26	2.05	0.07	261.05	7.26	442.68	12.59	990.66	56.83	5.74
3.1.13		40000	339.82	7.77	2.03	0.07	337.79	7.77	575.45	13.67	1262.93	60.03	4.75
3.1.14		50000	404.72	10.02	1.98	0.07	402.74	10.02	701.36	18.06	1507.22	77.63	5.15

3.2.1		1000	24.78	1.17	2.24	0.07	22.54	1.17	39.47	1.88	91.99	8.75	9.51
3.2.2		2000	37.82	1.50	2.26	0.07	35.56	1.50	59.37	2.36	138.43	11.11	8.02
3.2.3		3000	51.96	1.91	2.22	0.07	49.73	1.92	82.28	3.05	192.00	14.50	7.55
3.2.4		4000	59.28	2.31	2.07	0.07	57.21	2.31	99.07	3.89	231.02	18.12	7.84
3.2.5		5000	71.91	2.59	2.13	0.07	69.78	2.60	117.34	4.27	273.37	19.89	7.27
3.2.6		6000	79.50	2.09	2.09	0.07	77.41	2.09	131.51	3.51	306.00	16.31	5.33
3.2.7		7000	91.65	2.98	2.17	0.07	89.48	2.98	147.17	4.83	342.11	22.46	6.57
3.2.8		8000	98.35	3.91	2.09	0.07	96.26	3.91	162.81	6.52	377.84	30.29	8.02
3.2.9		9000	109.53	4.02	2.19	0.07	107.35	4.02	174.96	6.49	405.44	30.08	7.42
3.2.10		10000	118.87	5.12	2.16	0.07	116.71	5.12	191.72	8.32	443.51	38.48	8.68
3.2.11		20000	191.67	5.94	2.03	0.07	189.64	5.94	324.73	10.27	739.10	46.73	6.32
3.2.12		30000	256.07	10.80	1.95	0.06	254.12	10.80	448.99	19.18	1004.27	86.16	8.58
3.2.13		40000	340.80	6.43	2.05	0.07	338.75	6.43	574.17	11.47	1259.49	50.34	4.00
3.2.14		50000	400.92	10.68	1.96	0.06	398.96	10.68	699.43	19.24	1503.27	82.72	5.50

Table C 6: Mass flow and Reynolds number data.

Test No.	Test Section	Reynolds number	Δp [kPa]	C	ε	$\frac{\Delta\varepsilon}{\varepsilon}$	$\frac{\Delta p_{Unc}}{\Delta p}$	$\frac{\Delta\rho_1}{\rho_1}$	$\frac{\Delta\dot{m}}{\dot{m}}$	$\dot{m}$ [kg/s]	Re_0 [-]	ΔRe_0 [-]	$\Delta Re_0/Re_0$ [-]
1.1.1	CCTS 0.36	1000	0.23	0.613	1.00	5.71E-05	0.003	0.005	0.01	0.03	999.95	21.06	2.11
1.1.2		2000	0.46	0.999	0.05	5.67E-05	0.002	0.002	0.01	0.05	2001.53	41.00	2.05
1.1.3		3000	0.70	0.999	0.08	5.85E-05	0.002	0.002	0.01	0.08	3002.90	61.38	2.04
1.1.4		4000	0.94	0.999	0.11	5.86E-05	0.002	0.001	0.01	0.11	4003.25	81.43	2.03
1.1.5		5000	1.18	0.999	0.13	5.84E-05	0.005	0.002	0.01	0.13	5004.33	104.31	2.08
1.1.6		6000	1.42	0.999	0.16	5.86E-05	0.004	0.002	0.01	0.16	6006.85	124.40	2.07
1.1.7		7000	1.66	0.999	0.19	5.86E-05	0.004	0.001	0.01	0.19	7007.27	144.71	2.07
1.1.8		8000	1.90	0.999	0.21	5.87E-05	0.004	0.001	0.01	0.21	8009.56	164.93	2.06
1.1.9		9000	2.14	0.999	0.24	5.88E-05	0.003	0.001	0.01	0.24	9009.93	183.65	2.04
1.1.10		10000	2.38	0.999	0.27	5.90E-05	0.003	0.001	0.01	0.27	10010.17	204.66	2.04
1.1.11		20000	4.69	0.999	0.54	5.59E-05	0.003	0.001	0.01	0.54	20007.67	408.52	2.04
1.1.12		30000	7.26	0.999	0.82	5.73E-05	0.002	0.001	0.01	0.82	30098.81	610.96	2.03
1.1.13		40000	9.87	0.999	1.10	5.82E-05	0.003	0.001	0.01	1.10	39946.20	818.27	2.05
1.1.14		50000	12.69	0.999	1.39	5.92E-05	0.002	0.001	0.01	1.39	50038.92	1017.12	2.03
1.2.1		1000	0.23	0.999	0.03	5.62E-05	0.003	0.005	0.01	0.03	999.75	21.02	2.10
1.2.2		2000	0.46	0.999	0.05	5.71E-05	0.002	0.003	0.01	0.05	2000.28	41.30	2.06
1.2.3		3000	0.69	0.999	0.08	5.71E-05	0.002	0.002	0.01	0.08	3002.64	61.20	2.04
1.2.4		4000	0.92	0.999	0.11	5.66E-05	0.003	0.002	0.01	0.11	4003.37	82.09	2.05
1.2.5		5000	1.15	0.999	0.13	5.67E-05	0.005	0.002	0.01	0.13	5003.38	104.68	2.09
1.2.6		6000	1.38	0.999	0.16	5.64E-05	0.005	0.002	0.01	0.16	6003.46	125.21	2.09
1.2.7		7000	1.63	0.999	0.19	5.74E-05	0.004	0.001	0.01	0.19	7006.49	144.91	2.07
1.2.8		8000	1.86	0.999	0.21	5.74E-05	0.004	0.001	0.01	0.21	8007.06	164.80	2.06
1.2.9		9000	2.10	0.999	0.24	5.75E-05	0.004	0.001	0.01	0.24	9008.21	185.64	2.06
1.2.10		10000	2.34	0.999	0.27	5.73E-05	0.003	0.001	0.01	0.27	10016.49	204.05	2.04
1.2.11		20000	4.67	0.999	0.54	5.53E-05	0.002	0.001	0.01	0.54	20021.78	406.90	2.03
1.2.12		30000	7.25	0.999	0.82	5.72E-05	0.002	0.001	0.01	0.82	30070.47	610.53	2.03
1.2.13		40000	9.90	0.999	1.10	5.81E-05	0.003	0.001	0.01	1.10	40056.76	816.53	2.04
1.2.14		50000	12.69	0.999	1.39	5.91E-05	0.002	0.001	0.01	1.39	50047.69	1017.94	2.03
2.1.1	CCTS 0.39	1000	0.24	0.999	0.03	5.86E-05	0.003	0.005	0.01	0.03	998.87	21.01	2.10
2.1.2		2000	0.48	0.999	0.05	6.04E-05	0.003	0.003	0.01	0.05	1997.62	41.04	2.05

2.1.3		3000	0.73	0.999	0.08	6.09E-05	0.002	0.002	0.01	0.08	2998.13	61.21	2.04
2.1.4		4000	0.97	0.999	0.11	6.09E-05	0.002	0.001	0.01	0.11	3999.18	81.37	2.03
2.1.5		5000	1.18	0.999	0.13	5.85E-05	0.005	0.002	0.01	0.13	5003.80	104.72	2.09
2.1.6		6000	1.42	0.999	0.16	5.88E-05	0.005	0.002	0.01	0.16	6004.07	125.11	2.08
2.1.7		7000	1.66	0.999	0.19	5.92E-05	0.004	0.001	0.01	0.19	7005.00	145.09	2.07
2.1.8		8000	1.90	0.999	0.21	5.92E-05	0.003	0.001	0.01	0.21	8006.69	163.85	2.05
2.1.9		9000	2.15	0.999	0.24	5.97E-05	0.003	0.001	0.01	0.24	9008.74	184.22	2.04
2.1.10		10000	2.40	0.999	0.27	5.98E-05	0.003	0.001	0.01	0.27	10009.15	204.64	2.04
2.1.11		20000	4.80	0.999	0.54	5.88E-05	0.002	0.001	0.01	0.54	20023.57	406.88	2.03
2.1.12		30000	7.38	0.999	0.82	6.04E-05	0.002	0.001	0.01	0.82	30067.21	610.55	2.03
2.1.13		40000	10.08	0.999	1.10	6.24E-05	0.003	0.001	0.01	1.10	39994.13	816.54	2.04
2.1.14		50000	12.94	0.999	1.40	6.42E-05	0.002	0.001	0.01	1.40	50060.84	1018.53	2.03
2.2.1		1000	0.23	0.999	0.03	5.77E-05	0.003	0.005	0.01	0.03	998.12	21.07	2.11
2.2.2		2000	0.46	0.999	0.05	5.72E-05	0.002	0.002	0.01	0.05	1998.04	40.96	2.05
2.2.3		3000	0.69	0.999	0.08	5.72E-05	0.003	0.002	0.01	0.08	2999.33	61.44	2.05
2.2.4		4000	0.91	0.999	0.11	5.67E-05	0.002	0.002	0.01	0.11	4000.42	81.92	2.05
2.2.5		5000	1.13	0.999	0.13	5.61E-05	0.005	0.002	0.01	0.13	5002.31	104.49	2.09
2.2.6		6000	1.42	0.999	0.16	5.89E-05	0.005	0.002	0.01	0.16	6008.19	125.61	2.09
2.2.7		7000	1.66	0.999	0.19	5.90E-05	0.004	0.001	0.01	0.19	7007.78	144.77	2.07
2.2.8		8000	1.90	0.999	0.21	5.91E-05	0.003	0.001	0.01	0.21	8008.12	163.79	2.05
2.2.9		9000	2.14	0.999	0.24	5.92E-05	0.004	0.001	0.01	0.24	9008.63	184.94	2.05
2.2.10		10000	2.38	0.999	0.27	5.90E-05	0.004	0.001	0.01	0.27	10006.35	206.54	2.06
2.2.11		20000	4.75	0.999	0.54	5.79E-05	0.002	0.001	0.01	0.54	19987.42	405.99	2.03
2.2.12		30000	7.31	0.999	0.82	5.97E-05	0.002	0.001	0.01	0.82	29993.42	609.19	2.03
2.2.13		40000	10.09	0.999	1.11	6.22E-05	0.003	0.001	0.01	1.11	40070.24	816.56	2.04
2.2.14		50000	12.88	0.999	1.39	6.39E-05	0.002	0.001	0.01	1.39	49948.83	1015.85	2.03
3.1.1	CCTS 0.45	1000	0.23	0.999	0.03	5.86E-05	0.002	0.005	0.01	0.03	998.92	20.97	2.10
3.1.2		2000	0.47	0.999	0.05	5.86E-05	0.002	0.002	0.01	0.05	1998.06	40.90	2.05
3.1.3		3000	0.72	0.999	0.08	5.98E-05	0.003	0.002	0.01	0.08	2998.22	61.35	2.05
3.1.4		4000	0.96	0.999	0.11	6.01E-05	0.002	0.001	0.01	0.11	3998.74	81.47	2.04
3.1.5		5000	1.20	0.999	0.13	6.01E-05	0.005	0.002	0.01	0.13	5001.59	104.03	2.08
3.1.6		6000	1.45	0.999	0.16	6.04E-05	0.004	0.002	0.01	0.16	6000.40	124.45	2.07
3.1.7		7000	1.69	0.999	0.19	6.05E-05	0.004	0.001	0.01	0.19	6999.88	145.04	2.07
3.1.8		8000	1.94	0.999	0.22	6.08E-05	0.003	0.001	0.01	0.22	8000.86	164.12	2.05
3.1.9		9000	2.13	0.999	0.24	5.89E-05	0.004	0.001	0.01	0.24	9003.28	185.01	2.05
3.1.10		10000	2.33	0.999	0.27	5.81E-05	0.003	0.001	0.01	0.27	9912.20	202.27	2.04
3.1.11		20000	4.79	0.999	0.54	5.86E-05	0.003	0.001	0.01	0.54	20002.09	408.70	2.04
3.1.12		30000	7.40	0.999	0.82	6.08E-05	0.003	0.001	0.01	0.82	30010.29	613.85	2.05
3.1.13		40000	10.03	0.999	1.10	6.20E-05	0.003	0.001	0.01	1.10	39866.42	815.67	2.05

3.1.14		50000	12.97	0.999	1.40	6.44E-05	0.003	0.001	0.01	1.40	49991.43	1020.94	2.04
3.2.1		1000	0.23	0.999	0.03	5.85E-05	0.002	0.005	0.01	0.03	998.40	20.88	2.09
3.2.2		2000	0.47	0.999	0.05	5.87E-05	0.002	0.002	0.01	0.05	1998.98	40.88	2.04
3.2.3		3000	0.71	0.999	0.08	5.87E-05	0.002	0.002	0.01	0.08	3000.15	61.18	2.04
3.2.4		4000	0.94	0.999	0.11	5.89E-05	0.002	0.003	0.01	0.11	4000.63	81.99	2.05
3.2.5		5000	1.18	0.999	0.13	5.89E-05	0.004	0.002	0.01	0.13	4999.01	103.74	2.08
3.2.6		6000	1.42	0.999	0.16	5.87E-05	0.004	0.002	0.01	0.16	5996.88	123.89	2.07
3.2.7		7000	1.66	0.999	0.19	5.91E-05	0.004	0.001	0.01	0.19	7002.67	144.48	2.06
3.2.8		8000	1.91	0.999	0.21	5.93E-05	0.003	0.001	0.01	0.21	8004.57	164.18	2.05
3.2.9		9000	2.15	0.999	0.24	5.95E-05	0.003	0.001	0.01	0.24	9003.63	184.06	2.04
3.2.10		10000	2.39	0.999	0.27	5.96E-05	0.003	0.001	0.01	0.27	10009.00	203.95	2.04
3.2.11		20000	4.79	0.999	0.54	5.83E-05	0.002	0.001	0.01	0.54	20008.95	406.49	2.03
3.2.12		30000	7.39	0.999	0.82	6.05E-05	0.002	0.001	0.01	0.82	30023.78	609.66	2.03
3.2.13		40000	9.99	0.999	1.10	6.17E-05	0.004	0.001	0.01	1.10	39787.72	817.10	2.05
3.2.14		50000	12.97	0.999	1.40	6.43E-05	0.003	0.001	0.01	1.40	50024.87	1022.00	2.04

Appendix D

The properties of the nitrogen were obtained by fitting curves through REFPROP[1] data. The following fluid properties were used:

1) Density
2) Conductivity
3) Viscosity
4) Specific heat

These properties were obtained for different temperatures (10 °C, 15 °C, 20 °C, 25 °C, 30 °C, 35 °C, 40 °C) and different pressures (100 kPa, 200 kPa, 300 kPa, 400 kPa, 500 kPa, 600 kPa, 700 kPa, 800 kPa, 900 kPa, 1000 kPa, 2000 kPa, 3000 kPa, 4000 kPa, 5000 kPa) across the applicable range.

For each of these temperatures a plot as function of pressure was drawn and then a third or second order polynomial trend line derived for each temperature. The coefficients of the trend lines were then plotted as function of temperature. For each of the coefficients a third order polynomial trend line as function of temperature was derived. This resulted in the following equations for the fluid properties named above:

Viscosity [μ]

$$\mu \text{ [kg/m s]} = \left(b2_3 T^3 + b2_2 T^2 + b2_1 T + b2_0\right) p^2 + \left(b1_3 T^3 + b1_2 T^2 + b1_1 T + b1_0\right) p + \left(b0_3 T^3 + b0_2 T^2 + b0_1 T + b0_0\right)$$

where

$b2_3$ = -2.31556E-21

$b2_2$ = 5.91776E-19

$b2_1$ = -7.83363E-17

$b2_0$ = 6.5815E-15

[1] REFPROP – Reference Fluid Thermodynamic and Transport Properties, NIST Standard Reference database 23, Version 7.

$b1_3$ = -6.22222E-18

$b1_2$ = 1.96619E-15

$b1_1$ = -5.86961E-13

$b1_0$ = 1.67993E-10

$b0_3$ = 0

$b0_2$ = -3.25714E-11

$b0_1$ = 4.785E-8

$b0_0$ = 1.66207E-5

$T[^\circ C]$ = Temperature

$p[kPa]$ = Static pressure

Conductivity [k]

$$k\ [\mathrm{W/m\ K}] = \left(b2_3 T^3 + b2_2 T^2 + b2_1 T + b2_0\right) p^2 + \left(b1_3 T^3 + b1_2 T^2 + b1_1 T + b1_0\right) p + \left(b0_3 T^3 + b0_2 T^2 + b0_1 T + b0_0\right)$$

where

$b2_3$ = -6.75556E-18

$b2_2$ = 1.65848E-15

$b2_1$ = -2.60956E-13

$b2_0$ = 3.18278E-11

$b1_3$ = 2.44444E-15

$b1_2$ = 1.94952E-12

$b1_1$ = -1.11385E-9

$b1_0$ = 3.59872E-7

$b0_3$ = 1.11111E-10

$b0_2$ = -5.12857E-8

$b0_1$ = 6.95408E-5

$b0_0$ = 2.39847E-2

$T[^{\circ}C]$ = Temperature

$p[kPa]$ = Static pressure

Specific heat (Cp)

$$c_p \text{ [kJ/kg K]} = \left(b2_3T^3 + b2_2T^2 + b2_1T + b2_0\right)p^2 + \left(b1_3T^3 + b1_2T^2 + b1_1T + b1_0\right)p + \left(b0_3T^3 + b0_2T^2 + b0_1T + b0_0\right)$$

where

$b2_3$ = -3.85978E-16

$b2_2$ = 6.77637E-14

$b2_1$ = -4.71685E-12

$b2_0$ = 5.15349E-11

$b1_3$ = -4.37778E-12

$b1_2$ = 1.13067E-9

$b1_1$ = -1.82351E-7

$b1_0$ = 2.04783E-5

$b0_3$ = 2.22222E-9

$b0_2$ = 9.52381E-9

$b0_1$ = 1.28968E-5

$b0_0$ = 1.03927

$T[^{\circ}C]$ = Temperature

$p[kPa]$ = Static pressure

Density (ρ)

$$\rho \text{ [kg/m}^3\text{]} = \left(b3_3T^3 + b3_2T^2 + b3_1T + b3_0\right)p^3 + \left(b2_3T^3 + b2_2T^2 + b2_1T + b2_0\right)p^2 + \left(b1_3T^3 + b1_2T^2 + b1_1T + b1_0\right)p + \left(b0_3T^3 + b0_2T^2 + b0_1T + b0_0\right)$$

Where

$b3_3 =$ 3.4e-19

$b3_2 =$ -2.32257e-16

$b3_1 =$ 4.59236e-14

$b3_0 =$ -3.73572e-12

$b2_3 =$ -7.74489e-14

$b2_2 =$ 1.67423e-11

$b2_1 =$ -1.76353e-9

$b2_0 =$ 5.78174e-8

$b1_3 =$ -4.22222e-10

$b1_2 =$ 1.58476e-7

$b1_1 =$ -4.50004e-5

$b1_0 =$ 1.23325e-2

$b0_3 =$ -1.90620e-9

$b0_2 =$ 2.79035e-7

$b0_1 =$ -1.78122e-5

$b0_0 =$ 4.19341e-4

$T[^{\circ}C]$ = Temperature

$p[kPa]$ = Static pressure